DOKUZ EYLÜL UNIVERSITY
GRADUATE SCHOOL OF NATURAL AND APPLIED SCIENCES

MODAL PARAMETER ESTIMATION OF WIND TURBINES BASED ON p-LSCF METHOD AND THEIR DAMAGE IDENTIFICATION

by
Veysel YURTSEVEN

March, 2023
İZMİR

MODAL PARAMETER ESTIMATION OF WIND TURBINES BASED ON p-LSCF METHOD AND THEIR DAMAGE IDENTIFICATION

A Thesis Submitted to the
Graduate School of Natural and Applied Sciences of Dokuz Eylül Universty in Partial Fulfillment of the Requirements for the Degree of Master of Science in Civil Engineering Structure Program

by
Veysel YURTSEVEN

March, 2023
İZMİR

M.Sc THESIS EXAMINATION RESULT FORM

We have read the thesis entitled **"MODAL PARAMETER ESTIMATION OF WIND TURBINES BASED ON p-LSCF METHOD AND THEIR DAMAGE IDENTIFICATION"** completed by **VEYSEL YURTSEVEN** under supervision of **PROF. DR. ÖZGÜR ÖZÇELİK** and we certify that in our opinion it is fully adequate, in scope and in quality, as a thesis fort he degree of Master of Science.

Prof. Dr. Özgür ÖZÇELİK

Supervisor

---	---
Prof. Dr. O. Özgür EĞİLMEZ	Doç. Dr. Sadık Can GİRGİN
Jury Member	Jury Member

Prof. Dr. Okan FISTIKOĞLU

Director
Graduated School of Natural and Applied Sciences

ACKNOWLEDGEMENTS

First of all, I would like to thank my esteemed advisor, Prof. Dr. Özgür ÖZÇELİK, who encouraged me against all kinds of difficulties during the working process, enabled me to look at events from a different perspective with his experience and knowledge, and provided me with all kinds of support.

I would like to thank to my valuable instructors Assoc. Prof. Dr. Serkan GÜNEL, Civil Engineers Dr. Umut YÜCEL and Civil Engineers Dr. Erkan DURMAZGEZER. Thanks to their knowledge and experience, this thesis was created.

I would like to thank to my dear friends Civil Engineers (M.Sc) Onur ÖZTÜRKOĞLU and (M.Sc) Yaşar TANER for helps to conduct our experiments.

I would like to thank to I am grateful to my family for their continued love, support and guidance. Whenever I needed them, they didn`t leave me alone. They never spared their support and gave me every opportunity to become an engineer.

Structural health monitoring studies on wind turbine were performed by the financial support of the Scientific and Technological Council of Turkey (TÜBİTAK) under the grant #120M218 between the years 2021-2023, so I would like to express my thanks to TÜBİTAK for their support. I would like to thank Dost Enerji A.Ş. for permission to use one of the wind turbines to the research team of this project to establish a long-term monitoring system. I would also like to thank the friendly energy electrician Turan DOĞAN for his support in the field work.

Veysel YURTSEVEN

MODAL PARAMETER ESTIMATION OF WIND TURBINES BASED ON p-LSCF METHOD AND THEIR DAMAGE IDENTIFICATION

ABSTRACT

Wind energy has increasing its importance among renewable energy sources in recent times and has become a better variant of conventional energy sources due to its high energy production capacity and return of investment cost in a short time. The share of relatively large wind turbines, which can produce more energy in a short time, is rapidly increasing in the renewable energy market. Being able to define the dynamic properties of turbines accurately and consistently is very important in terms of keeping these structures operational throughout their economic life and even serving more than their expected life. In this study, one of the wind turbine with a production capacity of 2.5MW, that is currently operational in Urla/İzmir, has been examined. While the turbine was in operation, vibration data were collected by means of the data acquisition system, which was designed to be distributed over the turbine tower along the tower height. These vibration data were processed by using the p-LSCF method, which is one of the operational modal analysis methods, and the dynamic properties of the structure were determined. Furthermore, the effects of environmental effects such as wind speed, wind direction and temperature on the predicted dynamic featues of the tower were investigated.

Keywords: Operational modal analysis, data acquisition system design, data processing, wind turbine.

RÜZGAR TÜRBİNİ YAPILARININ p-LSCF YÖNTEMİNE BAĞLI MODAL PARAMETRELERİNİN VE HASARLARININ TAHMİNİ

ÖZ

Rüzgar enerjisi, yüksek enerji üretim kapasitesi ve yatırım maliyetinin kısa zamanda geri dönmesi sebepleriyle son yıllarda yenilenebilir enerji kaynakları arasında önemini arttırmış ve konvansiyonel enerji kaynaklarına daha iyi bir alternatif haline gelmiştir. Yenilenebilir enerji piyasasında kısa zamanda daha çok enerji üretebilen görece büyük rüzgar türbinlerinin payı hızla artmaktadır. Türbinlerin dinamik özelliklerini doğru ve tutarlı bir biçimde tanımlayabilmek, bu yapıların ekonomik ömürleri boyunca çalışır durumda kalabilmesi ve hatta planlanan ömürlerinden daha fazla hizmet verebilmesi bakımından oldukça önemlidir. Bu çalışmada Urla/İzmir'de hâlihazırda operasyonel olan 2.5MW üretim kapasitesi bir rüzgâr türbini incelenmiştir. Türbin kulesi üzerinden kule yüksekliği boyunca dağıtılmış şekilde tasarlanan veri toplama sitemi aracılığı ile türbin çalışır durumdayken titreşim verileri toplanmıştır. Bu titreşim verileri operasyonel modal analiz yöntemlerinden biri olan p-LSCF yöntemi kullanılarak işlenmiş ve yapının dinamik özellikleri belirlenmiştir. Buna ek olarak rüzgâr hızı, rüzgâr yönü ve sıcaklık gibi çevresel faktörlerin kulenin tahmin edilen dinamik özelliklerine etkisi araştırılmıştır**.**

Anahtar Kelimeler: Operasyonel modal analiz, veri toplama sistemi tasarımı, veri işleme, rüzgar türbini.

CONTENTS

Page

M.Sc THESIS EXAMINATION RESULT FORM ii
ACKNOWLEDGEMENTS iii
ABSTRACT iv
ÖZ v
CONTENTS vi
LIST OF FIGURES viii
LIST OF TABLES xi

CHAPTER 1 - INTRODUCTION 1

1.1 Motivation and Objectives 1
1.2 Organization of the Thesis 3

CHAPTER 2 - SYSTEM AND DAMAGE IDENTIFICATION: THEORETICAL BACKGROUNDS 4

2.1 System Identifications 4
2.2 Damage Identifications 5
2.3 Operational Modal Analysis (OMA) Method (only output) 6
2.3.1 Enhanced Frequency Domain Decomposition (EFDD) Method 10
2.3.2 Least Square Complex Frequency (LSCF) Method 12
2.3.2.1 Common-Denominator Transfer Function Model 13
2.3.2.2 Linearity in the Parameters 14
2.3.2.3 Reduced Normal Equations 15
2.3.2.4 Fast Implementation of the Reduced Normal Equations 16
2.3.2.5 Solving the Reduced Normal Equations 18
2.3.3 Poly Least Square Complex Frequency (p-LSCF) Method 18
2.3.3.1 Right matrix-fraction model 19
2.3.3.2 Equation error formulation 20
2.3.3.3 Reduced normal equations 22

CHAPTER 3 - MACEC: The MATLAB Toolbox for Experimental and Operational Modal Analysis 26

3.1 MACEC 26

3.1.1 MACEC Grafical User Interface 26

CHAPTER 4- WIND TURBINE STRUCTURE AND TEST SETUP 34

4.1 Features of Wind Turbine 34

4.2 Equipments Used in Test Setups 36

CHAPTER 5 - EXPERIMENTAL RESULTS 43

5.1 Wind Turbine Test Results (Collected and SCADA Data from The Wind Turbine) 43

5.2 Experimental Wind Turbine Modal Parameter Obtained by p-LSCF Methods 47

5.3 Damage Scenorios 71

CHAPTER 6 - CONCLUSIONS 75

REFERENCES 77

LIST OF FIGURES

Page

Figure 3. 1 MACEC main window 27

Figure 3. 2 Define or Edit measurement grid window 27

Figure 3. 3 Define/Edit beam or surfaces window 28

Figure 3. 4 Uploading the data file and converting the data to the appropriate format 28

Figure 3. 5 Entering the sampling frequency 29

Figure 3. 6 Conversion of measured data 29

Figure 3. 7 Preprocess mcsignal object 30

Figure 3. 8 Channel specifications window 30

Figure 3. 9 PSD+ estimation window 31

Figure 3. 10 p-LSCF method window 32

Figure 3. 11 Stabilization plot window 32

Figure 3. 12 Mode shape animation window 33

Figure 4. 1 (a) The monitored wind turbine and, (b) farm general view 35

Figure 4. 2 Tower geometry (flipped – right is top) 35

Figure 4. 3 Components of the Data Acquisition System 38

Figure 4. 4 Assembly of the system components in the laboratory 38

Figure 4. 5 Attachment of the accelerometers 39

Figure 4. 6 Schema representing the scada system 41

Figure 4. 7 Data colection loop works on instrial pc in turbine 42

Figure 4. 8 Network configuration of data acquisition system 42

Figure 5. 1 Temperature, humidity, wind speed and rotor speeds of 80 data sets collected from the Scada system are shown in (a), (b), (c) and (d) respectively 45

Figure 5. 2 Vibration data x direction-time graph from data acquisition system on 04.11.2022 at 04:31 am 46

Figure 5.3 It shows the stabilization diagrams obtained by using (a) the y direction data on Agust 2 at 06:00 am, (b) the y direction data on Agust 11 at 00:38 am, (c) the x direction data on October 14 at 00:58 am, (d) the y direction data on October 14 at 00:58 50

Figure 5. 4 Analysis and frequency (a) x-direction, (b) y- direction 52

Figure 5. 5 The vibration data in the x direction collected from accelerometers at four different levels (Level 2-3-4-5) were found to be frequency values using the p-LSCF method. The frequency values of the first, second, and third modes are shown in (a), (b), and (c) respectively 54

Figure 5. 6 The vibration data in the y direction collected from accelerometers at four different levels (Level 2-3-4-5) were found to be frequency values using the p-LSCF method. The frequency values of the first, second, and third modes are shown in (a), (b), and (c) respectively 55

Figure 5. 7 The values of the first three modes obteined by the p-LSCF method using the x-direction data, corresponding to the frequencies and variable humidity ratios are shown in (a), (b), and (c) respectively 57

Figure 5.8 The values of the first three modes obteined by the p-LSCF method using the x-direction data, corresponding to the frequencies and variable humidity ratios are shown in (a), (b), and (c) respectively 59

Figure 5. 9 The values of the first three modes obteined by the p-LSCF method using the x-direction data, corresponding to the frequencies and variable wind speed are shown in (a), (b), and (c) respectively..... 60

Figure 5. 10 The values of the first three modes obteined by the p-LSCF method using the y-direction data, corresponding to the frequencies and variable wind speed are shown in (a), (b), and (c) respectively..... 62

Figure 5. 11 The values of the first three modes obteined by the p-LSCF method using the x-direction data, corresponding to the frequencies and variable rotor speed are shown in (a), (b), and (c) respectively..... 63

Figure 5. 12 The values of the first three modes obteined by the p-LSCF method using the y-direction data, corresponding to the frequencies and variable rotor speed are shown in (a), (b), and (c) respectively..... 65

Figure 5.13 80 analyses for x and y directions respectively (a) and (b), obtained from the damping ratio. The average damping ratio for the x direction was 1.9394 and for the y direction it was 1.8245. 66

Figure 5.14 The temperature changes corresponding to the damping rates (a) x direction and (b) y direction 67

Figure 5.15 The humidity changes corresponding to the damping rates (a) x direction and (b) y direction 68

Figure 5.16 The wind speed changes corresponding to the damping rates (a) x direction and (b) y direction 69

Figure 5.17 The rotor speed changes corresponding to the damping rates (a) x direction and (b) y direction 70

Figure 5.18 Mode figures for (a) Mode 1, (b) Mode 2 and (c) Mode 3 obtained using data collected at 06:15 pm on October 19, 2022..... 70

Figure 5.19 Mode figures for (a) Mode 1, (b) Mode 2 and (c) Mode 3 obtained using data collected at 23:50 pm on November 26, 2022..... 71

Figure 5.20 Eartquake record x direction..... 72

LIST OF TABLES

Page

Table 4. 1 Properties of wind turbine 34

Table 4. 2 Material properties (S355) 35

Table 4. 3 Soil properties 36

Table 4. 4 Components of the Data Acquisition System 37

Table 4. 5 Specifications of accelerometers 39

Table 5. 1 The monthly averages of scada data 47

Table 5. 2 Mode frequencies 51

Table 5. 3 Mode shapes obtained using earthquake data 73

Table 5. 4 Analysis reasults of earthquakes 74

CHAPTER 1
INTRODUCTION

1.1 Motivation and Objectives

The usage of fossil and fossil-derived fuels causes serious and irreversible damage to the ecosystem. With the advancement of technology, energy consumption has gained momentum. Most of this required energy is provided from fossil and fossil-derived fuels. One of the most important consequences of the use of fossil fuels, which are limited resources, is the emission of greenhouse gases that cause global warming to the atmosphere. In this context, the demand of renewable energy sources is increasing gradually. Wind energy, which is among the renewable energy sources, has gained importance due to factors such as high efficiency and short amortization periods when compared with traditional energy production methods.

Installed wind power in the world has increased nearly four and a half times in the last twelve years (World Wind Energy Association [WWEA], 2021). while this capacity in our country has increased by 4.7 times (Turkish Wind Power Plants Association [TWPPA], 2022). This increase in capacity of wind turbines in our country has made it a subject that needs to be researched and developed.

Structural behavior of wind turbines under environmental and operational effects has been investigated. As a result of these researches, standards such as RISØ (Danish Technical University [DTU], 2002) and GL (Germanischer Lloyd [GL], 2010) have been established. As a thesis proposal, it aims to change the modal parameters and damage identification of an actively operating wind turbine under operational and environmental effects by using the p-LSCF (Poly Least Square Complex Frequency) method. Understanding the effects of these environmental factors on modal parameters will form a significant part of structural health monitoring and will also controbute to understanding the complex dynamic structure of the wind turbine.

The main objectives within the scope of the thesis can be listed as follows (a little more detail should be given) First, long-term dynamic data will be collected from an actively operating wind turbine with a permanent structural monitoring system

consisting of various sensors (accelerometer, thermocouple, relative humidity-meter, temperature-meter), Dynamic data collected synchronously will be used in modal parameter estimation, statistical and correlation analysis with operational modal analysis methods. This will provide important insights into how modal parameters change and how they affect against operational/environmental factors.

Wind turbine structures are being designed larger and higher gradually to increase their energy generation capacity. Determining the modal parameters on a long scale with the p-LSCF method will make valuable contributions to future designs.

In case of long-term observation, it also provides the opportunity to examine the earthquake response of the turbine structure. With the increasing demand, seismic zones have started to be used as wind power plants. Earthquake effect has become an important factor in wind turbine designs.

Within this study, a 2.5 MW capacity wind turbine installed in Urla/İzmir, operated by Dost Energy, will be examined (shown in Figure 3.1). Due to the climatic conditions of the region where it is established, the wind speed and direction are constantly changing throughout the year. In addition, these changes will provide significant stimulation of the tower and wing structure, making it easier to collect valuable data for determining modal parameters. The turbine structure is 90m high. It is a horizontal-axis pitch regulated wind turbine and has three blades. The tower is a circular steel tower bolted to a concrete foundation. In the top section, there is the generator and engine section. Table 3.1 contains some technical specifications of the turbine. A long-term monitoring system has been granted by Dost Enerji (operating company) to install a long-term monitoring system on one of the turbines. By its location, the Wind Turbine is 2 km away from the Güzelbahçe fault, ensuring that it is in a high earthquake zone (Emre et al., 2005). The proximity of the tower to this fault line is an important issue in terms of examining its response to possible earthquake effects.

1.2 Organization of the Thesis

Within the scope of this thesis, it consists of a total of six chapters prepared as follows.

- In Chapter One, an introduction has been made about why wind turbine structures are researched. Preliminary information was given about the subjects to be researched and examined within the scope of the thesis.

- In Chapter Two, operational analysis methods are explained and their theoretical backgrounds are examined in general. Information is given about the studies on damage and system identification.

- In Chapter Three, within the scope of the study, information was given about the MATLAB MACEC toolbox, where operational modal analyzes were made.

- In Chapter Four, the wind turbine features and test equipment features and installation methods, which are the subject of the thesis, are mentioned.

- In Chapter Five, the obtained modal properties of the wind turbine, which were examined under operational and environmental operating conditions at different times, are presented comparatively.

- In Chapter Six, in the light of the analyzes obtained from the vibration and SCADA data obtained from the wind turbine, the results regarding the estimation of the modal parameters and the damage are discussed.

CHAPTER 2
SYSTEM AND DAMAGE IDENTIFICATION: THEORETICAL BACKGROUNDS

2.1 System Identifications

Determining the dynamic parameters of the structure by using experimental measurements and presenting mathematical models is briefly referred to as System identification. Damping rate, mode shapes, frequency and period are dynamic parameters. These dynamic parameters change according to the type of system, geometric and material properties. Recently, system identification methods have become effective and common especially for examining the current state of civil engineering structures. In addition, they are important tools that can be used for the verification of numerical FE models created under certain assumptions (Rainieri & Fabbrocino 2014).

The first of the system identification methods used in the vibration-based SHM (Structure Health Monitoring) subheading is input-output and the second is only-output methods. (Moaveni, 2007). Input-output methods are known as EMA (Experimental Modal Analysis) methods, and in order to use these methods, they require measuring the reaction of the structure along with the impulse acting on the system. However, when only output methods are used, there is no need to measure the excitation affecting the system. Input-output methods are used in many fields, such as automotive/mechanical, civil and aerospace engineering. In the case of large structures, input-output methods can be classified as a difficult and expensive task due to effects such as the required measurement difficulties. Therefore, it can be said that input-output methods are more convenience for small systems. Considering the large dimensions of civil engineering structures, it would be wise to use only output methods, namely operational modal analysis (OMA) methods, as the measurement of input effects would be costly and inconvenient. In addition, the characteristically random and noise content of loads acting on civil engineering structures will complicate the measurement/recording processes (Rainieri & Fabbrocino 2014).

2.2 Damage Identifications

The effect of damage on a can be divided into two groups as linear and non-linear. Linear damage is defined as a structure that behaves elastically at the beginning of damage and maintains the same property afterwards. Modal parameters change as a result of changes in the shape of the structure and/or material strength. A relationship can be established between the modal parameters and these geometric and strength changes, and the relationships are expressed by linear equations of motion. Two different methods are followed as model-based and model-based linear methods.

An example of a non-linear damage class is the formation of a fatigue fracture in a structural member loaded under normal operating vibration. Most of the studies in the literature are about linear damage.(Maciej Serda et al. 1993).

Many researchers have studied changes in the dynamic behavior of a structure using non-destructive damage assessment (NDE) methods. These NDE methods are briefly divided into 4 levels as a result of studies. these 4 levels are explained below. (Stubbs et al. 2000).

- Level 1: This method only covers the identification of damage in the event of damage (Vandiver 1975, Begg et al.; 1976, Loland & Dodds 1976; Crohas & Lepert 1982).

- Level 2: This method captures both the location of the damage and the location of the damage if damage occurs. (Pandey et al. 1991).

- Level 3: This method includes determining the presence of damage, determining the location of the damage and determining the severity of the damage. (Stubbs et al. 2000).

- Level 4: In addition to the parameters covered by level 3, this method also includes the evaluation of the effect of damage on the structure.

The impact of damage on the structure can be interpreted as the main potential indicator of building safety. Although there are various methods for determining structural damage, examples of level 4 NDE methods continue to be researched and developed.

The number of studies examining the change in modal frequencies for damage detection of the structure is quite high. It was thought that the alters in the modal features of the building directly caused a change in the vibration frequencies, and accordingly, studies were carried out to form the basis of damage detection and building health monitoring methods. It requires either very precise measurements or large damage levels to be able to estimate damage according to the frequency change occurring in the structure.

2.3 Operational Modal Analysis (OMA) Method (only output)

OMA methods are used in many engineering disciplines to define modal parameters. In civil engineering, OMA methods are used in the analysis of structures of various sizes such as bridges, tall buildings, railway bridges, wind turbines, dams, stadiums. (Rainieri & Fabbrocino 2014).

The modal features of a structure are not established exclusively by measuring the reactions of that structure under ambient or operating stimulation. This feature makes OMA extremely effective and powerful for modal analysis of large and hard-to-reach structures. Wind turbines can be given as examples of structures where the excitation forces are not easy to measure. (Tcherniak, Chauhan, & Hansen 2011).

OMA is used under 3 basic assumptions: a) Linearity: The response of the structural system to specific load combinations is equivalent to the output against the same load combinations; b) Stationarity: The modal parameters of the structure does not alter over time, the modal parameters of the structural system (damping rate, frequency, etc.) are considered constant regardless of time; c) Observability: All sensors layout in the structure are placed at the points where the most accurate/quality data can be

obtained, and it is assumed that the mode shapes or displacements are not zero (nodes) at these placed points (Rainieri & Fabbrocino, 2014).

On the other hand, Long-term measurements can define the modal properties of the structure (frequency, vibration levels or damping rate) by taking into account the relationship with the external effects that the structure is exposed to during its service life. In the case of wind turbines, experimental modal analysis methods (input-output methods) or methods that require measurement of input are not applied, since the drives caused by wind and/or earthquake or other effects cannot be measured or predicted precisely. Furthermore, when there is an unknown external stimulus, they treat this stimulus as noise. For this reason, the use of OMA methods (Zhang, Brinker & Andersen 2005) in determining the modal parameters of wind turbines gives more effective results.

Wind turbines have been studied operationally and experimentally by many researchers. Studies were carried out on the vibration response of the 37 m long steel-supported tower structure using 2 different finite element models. Firstly, 3D quadratic shell finite elements are defined in the Greek Seismic code, and the elastic spectrum is analyzed using standard normal superposition procedures. Secondly, Response History analysis (RHA) was performed and the masses positioned along the height were assumed as multiple degrees of freedom and 6 different artificial earthquake acceleration records were created and applied to the structure (Bazeos et al. 2002).

Studies have been ongoing since the 1990s to understand the complex behavior of starting wind turbines, for the first time operational modal analysis (OMA) methods were developed using only-output test on a 110 m high turbine (Carne & James 2010).

The operational wind turbine dynamic parameters are estimated under the operative wind load by using the only output method using the vibration responses of the 3MW wind turbine in operation and using the professional aeroelastic code as reference. (Tcherniak et al. 2010).

A wind turbine located in Colorado USA, which can produce 600 Kw of power, was first evaluated with the Experimental Modal Analysis (EMA) approach for the parking situation and then examined with the OMA method, considering only the parking situation scenario. (Manzato et al. 2010).

Acceleration data were collected from a wind turbine with model number Micon 65/13M operated by the US Department of Energy/Sandia National Laboratories (SNL). Speed and direction parameters were evaluated for the parked/operating tower and modal parameters were obtained using OMA methods (Allemang et al. 2014).

The idea of classification depending on the time of observation of wind turbine structures has been adopted and two different classifications have been made; the short-term scale, observation of vibrations caused by rotational motion because of the nature of the turbine tower. The long-term scale, observation that the parameters constituting the load (e.g. wind, temperature and humidity, etc.) are constantly changing, and that these parameters affect the structural behavior (Bogoevska et al. 2017). In various studies OMA methods in wind onshore turbine structures have been taken into consideration and different concepts and new measurement techniques have been obtained (Chauhan et al. 2011; Hansen et al. 2006; Ozbek & Rixen 2011).

In more recent studies, long-term scale observation has been proposed to examine the change in defined dynamic parameters and the focus of automated SHM schemes has been accepted as long-term scale observation (Devriendt et al. 2014; Hansen et al. 2006; Maes et al. 2016; Proulx 2015).

When we want to study wind turbines dynamically, the main challenge is that the dynamic properties of the structure change with time (time-variable systems). Since the wind, earthquake and wave forces (for marine structures) that the structure is exposed to change randomly, it causes difficulties in obtaining the modal parameters on the structure and creates uncertainty (Devriendt et al., 2014). For this reason, classical OMA methods (SSI-Data, EFDD, NExT-ERA etc.) do not give appropriate results in the determination of modal parameters of wind turbine structures. It is a

mandatory prerequisite for these structures that the unknown or unidentified excitation is WN (White Noise) and OMA methods operating under this assumption do not give reliable results (Devriendt et al., 2014).

Due to the disadvantages of classical OMA methods, new identification algorithms have been developed and the p-LSCF (poly-reference least squares complex frequency-domain estimator) method has been developed (Peeters et al, 2004). With this method, it is possible to obtain clearer stabilization diagrams and accurate estimation of physical mode shapes.

In this thesis, it is aimed to determine the modal parameters of the turbine tower using the poly-reference least squares complex frequency method (Guillaume et al., 2003). This method is a frequency domain method and provides high precision estimation of modal parameters of systems. Continuously incoming data from the turbine in certain packets will be read simultaneously, and first, frequency, damping and mass participation rates and stabilization diagrams will be created, and then mode shape estimations will be made. At the same time, the obtained modal parameters will be used in the fitting of the turbine numerical model scope of the TUBITAK project.

The p-LCSF method is mathematically very similar to the LSCF (Least Squares Complex Frequency) method and even relies on the mathematical infrastructure of the LSCF method.(Peeters et al., 2004). The LSCF method needs the inputs that affect the structure and the response data corresponding to these inputs (input-output is a method). With the p-LSCF method to be used within the scope of the project, modal parameters will be determined using only output data without the need for input data affecting the structure. This system can also be used as an output-only or input-output as needed (Culla & W. D'Ambrogio, 2012.).

p-LSCF method occurred to find the initial values of the iterative maximum likelihood method. The method approximates a model called the common denominator transfer function model. It has been shown that modal parameters can be estimated effectively because obtaining "initial values" can be done quickly (Guillaume et al.,

1998). Unlike classical OMA methods, the p-LSCF method, which uses net stabilization diagrams, is a method used to get information about the dynamic properties of the structure and to estimate its modal parameters.

2.3.1 Enhanced Frequency Domain Decomposition (EFDD) Method

The EFDD method is one of the classical frequency domain methods, it is defined as an improved version of the classical peak picking process. It has a negative side such that it does not give very effective results when capturing modes that are close to each other. In addition, it produces unclear results in the damping ratio estimations. (Brinckner et al., 2001). In this method, modal parameters are not obtained by selecting the peaks of the power spectral density functions (PSD). Functions obtained from the only-output data are created, spectral matrices are created, and then analysis is performed by singular values decomposing (SVD) into spectral matrices.

The discrete Inverse-Fourier transform is applied to the auto-PSD functions and converted to the time domain. After these processes, damping rates and natural vibration frequencies are determined. Optionally, Welch-Bartlett method can be used to obtain auto-PSD functions. (Manolakis et al., 2000).

The relation between input and measured output in Equation 2.1 is represented below (Bendat & Piersol, 2010).

$$G_{yy}(j\omega) = \hat{H}_o(j\omega)G_{xx}(j\omega)\ H(j\omega)^T \tag{2.1}$$

$G_{xx}(j\omega)$ = Input signal power spectral density function

$G_{yy}(j\omega)$ = Output signal PSD function

$H(j\omega)$ = Frequency Response Function (FRF)

"-" = complex conjuge, "T" = transpose

Equation 2.1 can be rewritten as a residual form as in Equation 2.2.

$$H(j\omega) = \sum_{k=1}^{n} \frac{R_k}{j\omega - \lambda_k} + \frac{\hat{R}_k}{j\omega - \hat{\lambda}_k} \tag{2.2}$$

n = Mode number

λ_k = Polar function

R_k = Residual function

$$R_k = \phi_k \, \gamma_k^T \tag{2.3}$$

ϕ_k = Mode number

γ_k^T = Modal participation vector

Accepting the input signal contains white noise.

$$G_{yy}(j\omega) = \sum_{k=1}^{n} \sum_{s=1}^{n} \left[\frac{R_k}{j\omega - \lambda_k} + \frac{\hat{R}_k}{j\omega - \hat{\lambda}_k} \right] xC \left[\frac{R_k}{j\omega - \lambda_s} + \frac{\hat{R}_k}{j\omega - \hat{\lambda}_s} \right]^H \tag{2.4}$$

"H" = complex conjugate and transpose

As in equation 2.5, the output PSD function can be written as polar and residual.

$$G_{yy}(j\omega) = \sum_{k=1}^{n} \frac{A_k}{j\omega - \lambda_k} + \frac{\hat{A}_k}{j\omega - \hat{\lambda}_k} + \frac{B_k}{-j\omega - \lambda_k} + \frac{\hat{A}_k}{-j\omega - \hat{\lambda}_k} \tag{2.5}$$

$$A_k = \frac{R_k C \, \widehat{R_k^T}}{2a_k} \tag{2.6}$$

"A_k" = output k. residual matrix

The fundamentel step in identifying an EFDD method is predicting the PSD matrix. An output signal at discrete frequencies noted $\omega=\omega_i$ is produced by the matrix SVD. For PSD function estimation is written as shown in Equation 2.7

$$G_{yy}(j\omega) = U_i S_i \mathrm{U}_i^H \tag{2.7}$$

U_i = Singular values matrix

S_i = Scalar singular values diagonal matrix

2.3.2 Least Square Complex Frequency (LSCF) Method

In conventional EMA, the main approach to FD (Frequency Domain) mode identification is grounded on parametric transfer function models represented by rational fractional polynomials (RFPs). SISO (Single Input Single Output), SIMO (Single Input Multi Output) and MIMO (Multi Input Multi Output) performances of the RFP system were developed in the 1980s grounded on the least places system (Richardson and Formenti 1982; Schwarz and Richardson 1999; Shih etal. 1988). ML (Maximum Likelihood) estimators has been developed to measure noise in traditional system identification methods. In the late 1990s, the MLFD system using FRF measures for modal demarcation was proposed (Guillaume et al. 1998). MLFD is a typical nonlinear estimator and should be enforced as an iterative process. A complex least- places frequence- sphere estimation (LSCF) system was presented to solve original values for the iterative MLFD system (Guillaume et al. 1998).

It be set up that these" original values" handed sufficiently accurate modal parameters with much lower computational trouble. Still, LSCF grounded on common denominator models or fractional descriptions of scalar matrices has two major downsides: The first one mode shapes and modal distribution portions are delicate to gain used by SVD to reduce the residuals to a rank of one matrix. The second one poles that are close together are inaptly displayed as one pole. Lately, a polyreference interpretation of the LSCF system grounded on the correct matrix fractional model was developed (Guillaume 2003).

The Least-Squares Complex Frequency-domain (LSCF) estimator can be thought of as the well-known Least-Squares Complex Exponential (LSCE) estimator in the frequency domain. Producing "fast-stabilizing" stabilization charts is a significant

benefit of the LSCF estimator. A "poly-reference or polyMAX" estimator of the LSCF estimator will be developed in this contribution (Guillaume 2003). The derivative and basic numerical properties of the LSCF estimator are described below.

2.3.2.1 Common-Denominator Transfer Function Model

The relationship between input *i* ($i = 1,\ldots, N_i$) and measured output output *o* ($o = 1,\ldots, N_o$) in Equation 2.8 is represented below, common-denominator transfer function is $\hat{A}_k$

$$\hat{H}_k(\omega) = [\hat{N}_k(\omega)][d(\omega)]^{-1} \tag{2.8}$$

For $k = 1,\ldots,N_o N_i$ (where $k = (o\text{-}1)\, N_i + i$) and with

$$N_i(\omega) = \sum_{j=0}^{n} \Omega_j\,(\omega) B_{kj} \tag{2.9}$$

The numerator polynomial between output *o* and input *i* and

$$d(\omega) = \sum_{j=0}^{n} \Omega_j\,(\omega) A_j \tag{2.10}$$

Equation 2.10 representa the common-denominator polynomial. The coefficients A_j and B_{kj} are the coefficients to be calculated. All these coefficients are sorted each other in one column vector $\theta = \alpha^T, \ldots, \beta^T_{N_o N_i} \left[\beta^T_1, \ldots, \beta^T_{N_o N_i}, \alpha^T\right]^T$ with

$$\beta_0 = \begin{pmatrix} \beta_{k0} \\ \beta_{k1} \\ \ldots \\ \beta_{kn} \end{pmatrix}, \alpha = \begin{pmatrix} A_0 \\ A_1 \\ \ldots \\ A_n \end{pmatrix} \tag{2.11}$$

There are several choices for polynomial basis functions $\Omega_j(\omega)$.

2.3.2.2 Linearity in the Parameters

İnitiating from measured FRFs, $H_k(\omega_k)$ ($with\ k = 1, \dots, N_o N_i\ and\ f = 1, \dots, N_f$), determines of the transfer-function parameterts calculated by reduced according to the nonlinear least-squares (NLS) cost function, which depends on the parameter vector θ.

$$l_{NLS}(\theta) = \sum_{k=1}^{N_o N_i} \sum_{k=1}^{N_f} |\varepsilon_k^{NLS}(\omega_f, \theta)|^2 \tag{2.12}$$

where the (weighted) NLS equation error, $\varepsilon_k^{NLS}(\omega_f, \theta)$, is specified as

$$\varepsilon_k^{NLS}(\omega_f, \theta) = W_k(\omega_f)\left(\frac{N_k(\omega_f, \beta_k)}{d(\omega_f, \alpha)} - H_k(\omega_f)\right) \tag{2.13}$$

with $W_k(\omega_f)$ an random weighting functions. The consistency of the estimation can be improved as follows

$$W_k(\omega_f) = \frac{1}{\sqrt{\text{var}\,\{H_k(\omega_f)\}}} \tag{2.14}$$

thus the measured FRFs are included in the assessment. If the FRFs have small variance, they make a significant contribution to the weighting function.

by multiplying $\varepsilon_k^{NLS}(\omega_f, \theta)$ with $d(\omega, \alpha)$, an equation error is calculated that is linear parameters

$$\begin{aligned} \varepsilon_k^{NLS}(\omega_f, \theta) &= d(\omega_f, \theta) * \varepsilon_k^{NLS}(\omega_f, \theta) \\ &= W_k(\omega_f)(N_k(\omega_f, \beta_k) - d(\omega_f, \alpha)H_k(\omega_f)) \\ &= W_k(\omega_f)\sum_{j=0}^{n}(\Omega_j(\omega_f)B_{kj} - \Omega_j(\omega_f)A_j H_k(\omega_f)) \end{aligned} \tag{2.15}$$

with

$$\varepsilon_k^{LS}(\theta) = \begin{pmatrix} \varepsilon_k^{LS}(\omega_1, \theta) \\ \varepsilon_k^{LS}(\omega_2, \theta) \\ \dots \\ \varepsilon_k^{LS}\left(\omega_{N_f}, \theta\right) \end{pmatrix} = (X_k \quad Y_k) \cdot \begin{pmatrix} \beta_k \\ \alpha \end{pmatrix} = \mathbf{J_k} \cdot \begin{pmatrix} \beta_k \\ \alpha \end{pmatrix} \tag{2.16}$$

$$X_k = \begin{pmatrix} W_k(\omega_1)(\Omega_o(\omega_1) \dots \Omega_n(\omega_1)) \\ \dots \\ W_k\left(\omega_{N_f}\right)(\Omega_o\left(\omega_{N_f}\right) \dots \Omega_n\left(\omega_{N_f}\right)) \end{pmatrix} \tag{2.17}$$

$$Y_k = \begin{pmatrix} -\omega_k(\omega_1)(\Omega_o(\omega_1) \dots \Omega_p(\omega_1))\, \widehat{H}_o(\omega_1) \\ \dots \\ -\omega_k\left(\omega_{N_f}\right)(\Omega_o\left(\omega_{N_f}\right) \dots \Omega_p\left(\omega_{N_f}\right))\, \widehat{H}_o\left(\omega_{N_f}\right) \end{pmatrix} \tag{2.18}$$

2.3.2.3 Reduced Normal Equations

The (weighted) linear least-squares approximations are found by reducing

$$\begin{aligned} l_{LS}(\theta) &= \sum_{k=1}^{N_o N_i} \sum_{k=1}^{N_f} |\varepsilon_k^{LS}(\omega_f, \theta)|^2 \\ &= \sum_{k=1}^{N_o N_i} \mathrm{Re}(\left(\varepsilon_k^{LS}(\theta)\right)^H . \varepsilon_k^{LS}(\theta)) \end{aligned} \tag{2.19}$$

With $R_k = Re(X_k^H\, X_k)$, $S_k = Re(X_k^H\, Y_k)$ and $T_k = Re(Y_k^H\, Y_k)$. cost function (2.12) is equivalent to

$$l_{LS}(\theta) = \theta^T \mathrm{Re}(\mathrm{J^T J}).\, \theta \tag{2.20}$$

with J the so-called Jacobian matrix,

$$\mathrm{J} = \begin{pmatrix} X_1 & 0 & \dots & 0 & Y_1 \\ 1 & X_2 & \dots & 0 & Y_2 \\ \dots & \dots & \dots & \dots & \dots \\ 0 & 0 & \dots & X_{N_o N_i} & Y_{N_o N_i} \end{pmatrix} \tag{2.21}$$

The cost function approaches the value of the minimum with the following operation

$$\frac{\partial}{\partial \beta_k} l_{LS}(\theta) = 2(R_k \beta_k \ + \ S_k \alpha) = 0, k = 1, \dots., N_o N_i \tag{2.22}$$

$$\boldsymbol{\frac{\partial}{\partial \alpha} l_{LS}(\theta) = 2 \sum_{k=1}^{N_o N_i} \left(S_k^T \beta_k \ + \ T_k \alpha \right) = 0} \tag{2.23}$$

Substitution of (2.43), $\beta_k \ = -R_k^{-1} S_k \, \alpha$, in (2.44) yields

$$(2 \sum_{k=1}^{N_o N_i} (T_k - S_k^T R_k^{-1} S_k)). \alpha = \mathrm{M}. \alpha = 0 \tag{2.24}$$

With $\mathrm{M} = 2 \sum_{k=1}^{N_o N_i} (T_k - S_k^T R_k^{-1} S_k)$. Equations (2.22) and (2.23) are the so-called normal equations,

$$2 \begin{pmatrix} \mathrm{R}_1 & 0 & \dots & \mathrm{S}_1 \\ 1 & \mathrm{R}_2 & \dots & \mathrm{S}_2 \\ \dots & \dots & \dots & \dots \\ S_1^T & S_2^T & \dots & \sum_{k=1}^{N_o N_i} \mathrm{T}_k \end{pmatrix} . \begin{pmatrix} \beta_1 \\ \beta_2 \\ \dots \\ \beta_{N_o N_i} \\ \alpha \end{pmatrix} = 2\mathrm{Re}(\mathrm{J}^{\mathrm{H}}\mathrm{J}). \theta = 0 \tag{2.25}$$

2.3.2.4 Fast Implementation of the Reduced Normal Equations

Examining the matrices $R_k = Re(X_k^H \, X_k)$, $S_k = Re(X_k^H \, Y_k)$ and $T_k = Re(Y_k^H \, Y_k)$ in more details reveals that the entries of these matrices equal

$$R_k(r, s) = \mathrm{Re}[\sum_{f=1}^{N_f} (|W_k(\omega_k)|^2 . \Omega_{r-1}^H(\omega_f) . \Omega_{s-1}(\omega_f))]$$

$$S_k(r,s) = -\mathrm{Re}[\sum_{f=1}^{N_f}(|W_k(\omega_k)|^2 H_k(\omega_f)\Omega_{r-1}^H(\omega_f).\Omega_{s-1}(\omega_f))] \quad (2.26)$$

$$T_k(r,s) = \mathrm{Re}[\sum_{f=1}^{N_f}(|W_k(\omega_k)H_k(\omega_f)|^2\Omega_{r-1}^H(\omega_f).\Omega_{s-1}(\omega_f))]$$

As $\Omega_j(\omega_f) = \exp(-\mathrm{i}\omega_f T_s.j)$ (i.e. $\omega_f = f.\Delta w, f = 1,\dots,N_f$ with $\Delta\omega = 2\pi/NT_s$) then the new formulation;

$$R_k(r,s) = \mathrm{Re}[\sum_{f=1}^{N_f}(|W_k(\omega_k)|^2.e^{i2\pi(r-s)f/N})]$$

$$S_k(r,s) = -\mathrm{Re}[\sum_{f=1}^{N_f}(|W_k(\omega_k)|^2 H_k(\omega_f)e^{i2\pi(r-s)f/N})] \quad (2.27)$$

$$T_k(r,s) = \mathrm{Re}[\sum_{f=1}^{N_f}(|W_k(\omega_k)H_k(\omega_f)|^2 e^{i2\pi(r-s)f/N})]$$

It can be verified that the above matrices have a Toeplitz structure, i.e. entry *(r,s)* only depends on (r - s) .

$$\mathrm{S}_k = \begin{pmatrix} \mathrm{s}_k(0) & \mathrm{s}_k(-1) & \dots & \mathrm{s}_k(-n) \\ \mathrm{s}_k(1) & \mathrm{s}_k(0) & \dots & \dots \\ \dots & \dots & \dots & \mathrm{s}_k(-1) \\ \mathrm{s}_k(n) & \dots & \mathrm{s}_k(1) & \mathrm{s}_k(0) \end{pmatrix} \quad (2.28)$$

With $\mathrm{s}_k(r) = -\mathrm{Re}[\sum_{f=1}^{N_f}(|W_k(\omega_k)|^2 H_k(\omega_f)e^{\frac{i2\pi(r-s)f}{N}})]$

For symmetric Toeplitz matrices (such as R_k and T_k) only the first column has to be computed.

2.3.2.5 Solving the Reduced Normal Equations

In order to solve the transfer function easily, a limitation should be made to reduce the number of parameters and not include the absolute solution where the coefficients are zero. This limitation can be done by setting any of the coefficients to be non-zero. So the reduced normal equations transform as follows

$$\mathbf{A.x = b} \tag{2.29}$$

with

$$\begin{aligned}\mathbf{A} &= \mathbf{M}(1{:}n,\ 1{:}n)\\ \mathrm{b} &= -\mathbf{M}(1{:}n,\ n{+}1)\end{aligned} \tag{2.30}$$

The least-squares estimate of α is given by

$$\widehat{\boldsymbol{\alpha}}_{\mathrm{LS}} = \begin{Bmatrix}\mathbf{x}\\ 1\end{Bmatrix} \tag{2.31}$$

with $\mathbf{x} = \mathbf{A}^{-1}.\mathbf{b}$.

2.3.3 Poly Least Square Complex Frequency (p-LSCF) Method

The commercial name of the method is “PolyMAX”. Principally, a stabilization diagram including the frequency damping ratio and the addition ratios is created, thus the mode shapes are determined in a second least squares step according to the operater's stable pole choosing. One of the particular advantages of the technique is that the system poles and participation factors are defined very stable as a function of the identyfied system order, and this is used to obtain net stabilization diagrams (Peeters et al., 2004).

Initially, LSCF method was presented to solve first values for the iterative maximum likelihood method (Guillaume, Verboven, & Vanlanduit 1998). LSCF estimation method approximately finds the common denominator transfer function

model. The importance of initial values in obtaining the correct modal parameters has been confirmed by many studies in a short time (Van der Auweraer et al., 2005; Guillaume et al., 1998; Verboven, 2002). The most important advantage of the p-LSCF method can be interpreted as obtaining net stabilization diagrams compared to the methods used for other model parameter estimation (Heylen et al., 1997). The multiple reference version of the LSCF method, "PolyMAX", is called the right matrix-fraction model. The basis advantage of the multi-reference method is that the SVD step can be omitted to separate residues and closely spaced poles are not confused. Polyreference method consists of 3 steps, respectively right matrix-fraction model, equation error formulation and reduced normal equations.

2.3.3.1 Right matrix-fraction model

p-LSCF needs FRFs as base data and generates the right fraction matrix model:

$$[H(\omega)] = [B(\omega)][A(\omega)]^{-1} \tag{2.32}$$

Where $H(\omega) \in \mathbb{C}^{lxm}$ is the FRF matrix including the FRFs between all m input and all l outputs; $B(\omega) \in \mathbb{C}^{lxm}$ is the numerator matrix polynomial and $A(\omega) \in \mathbb{C}^{lxm}$ is the denominator matrix polynomial. Each row of the right matrix-fraction model (2.32) can be written as:

$$\forall o = 1,2,\dots,l :< H_o(\omega) >=< B_o(\omega) > [A(\omega)]^{-1} \tag{2.33}$$

with

$$\begin{aligned} < B_o(\omega) > &= \sum_{r=0}^{p} \Omega_r(\omega) < \beta_{or} > \\ < [A(\omega)] > &= \sum_{r=0}^{p} \Omega_r(\omega)[\alpha_r] \end{aligned} \tag{2.34}$$

The $\Omega_r(\omega)$ are the basis functions of the input and output vectors. The polymax method uses a frequency-domain model derived from a discrete-time model. that is, the basis function is given in equation 2.35.

(with Δt the sampling rate and p is the polynomial order):

$$\Omega_r(\omega) = e^{j\omega\Delta tr} \tag{2.35}$$

The polynomial coefficients $\beta_{or} \in \mathbb{R}^{1xm}$ and $\alpha_r \in \mathbb{R}^{mxm}$ are assembled in following matrices:

$$\beta_0 = \begin{pmatrix} \beta_{o0} \\ \beta_{o1} \\ \dots \\ \beta_{op} \end{pmatrix} \in \mathbb{R}^{(p+1)xm} \ (\forall o = 1,2,\dots,l),$$

$$\alpha = \begin{pmatrix} \alpha_0 \\ \alpha_1 \\ \dots \\ \alpha_p \end{pmatrix} \in \mathbb{R}^{m(p+1)xm} \ , \tag{2.36}$$

$$\theta = \begin{pmatrix} \beta_1 \\ \beta_2 \\ \dots \\ \beta_l \\ \alpha \end{pmatrix} \in \mathbb{R}^{(l+m)(p+1)xm}$$

The FRF equation model given in Equation 2.32 is written in terms of the coefficients of the $\mathrm{H}(\omega_k, \theta)$ function. This method can be written by generating more complex coefficients. More detailed studies have been done on the common denominator LSCF operation (Verboven., 2002).

2.3.3.2 Equation error formulation

The important key in this section is to find all the model coefficients θ originating from the FRFs $\hat{\mathrm{H}}(\omega_k, \theta)$ measurements, where $\hat{\bullet}$ represents a measured quantity and $\omega_k(1,2,\dots.,N_f)$ are the discrite frequencies at which FRF measurements are

obtainable. The coefficients θ can be defined by decreasing the following non-linear least-squares (NLS) equation errors $\varepsilon_o^{NLS}(\omega_k, \theta) \in \mathbb{C}^{1x3}$:

$$\begin{aligned} \varepsilon_o^{NLS}(\omega_k, \theta) &= \omega_o(\omega_k)\left(H_o(\omega_k, \theta) - \widehat{H}_o(\omega_k, \theta)\right) \\ &= \omega_o(\omega_k)(B_o(\omega_k, \beta_o)A^{-1}(\omega_k, \alpha) - \widehat{H}_o(\omega_k)\ ) \end{aligned} \tag{2.37}$$

where the scalar weighting function $\omega_o(\omega_k)$ is acquainted. These frequency- and output-dependent weighting function take into account the differences in outputs within the collected data. The equation errors from all outputs and on the frequency line are summed up in the following equation and introduced cost function;

$$l^{NLS}(\theta) = \sum_{o}^{l} \sum_{k=1}^{N_f} tr\{\ (\varepsilon_o^{NLS}(\omega_k, \theta))^H\ \varepsilon_o^{NLS}(\omega_k, \theta)\ \} \tag{2.38}$$

where $\bullet^H$ represents the complex conjugate transpose (Hermitian) of a matrix and tr$\{\bullet\}$ is the trace of a matrix. The notation 'trace' is reduced to calculating the square 2-norm of the row vector of $\varepsilon_o^{NLS}(\omega_k, \theta)$. By setting the derivative (2.38) of the unknown θ coefficients equal to zero, the cost function is reduced to its minimum value. It is clear that when Equation 2.37 is used for error, a non-linear equation will occur. The Equation 2.37 can be written linearly as follows, where $\varepsilon_o^{LS}(\omega_k, \theta) \in \mathbb{C}^{1xm}$ that are linear in the parameters:

$$\begin{aligned} \varepsilon_o^{LS}(\omega_k, \theta) &= \omega_o(\omega_k)\big(B_o\big(\omega_{k,}\beta_o\big) - \widehat{H}_o(\omega_k)\, A\big(\omega_{k,}\alpha\big)\ \big) \\ &= \omega_o(\omega_k) \textstyle\sum_{r=0}^{p}(\Omega_r(\omega_k)\beta_{or} - \Omega_r(\omega_k)\beta_{or}\widehat{H}_o(\omega_k)\ \alpha_r) \end{aligned} \tag{2.39}$$

All the formed lines are collected in a single matrix ($E_o^{LS}(\theta) \in \mathbb{C}^{N_f x m}$)and written as

$$E_o^{LS}(\theta) = \begin{pmatrix} \varepsilon_o^{LS}(\omega_1, \theta) \\ \varepsilon_o^{LS}(\omega_2, \theta) \\ \dots \\ \varepsilon_o^{LS}\left(\omega_{N_f}, \theta\right) \end{pmatrix} = (X_O \quad Y_O) \begin{pmatrix} \beta_o \\ \alpha \end{pmatrix} \tag{2.40}$$

with:

$$X_O = \begin{pmatrix} \omega_o(\omega_1)(\Omega_o(\omega_1) \dots \Omega_p(\omega_1)) \\ \dots \\ \omega_o\left(\omega_{N_f}\right)(\Omega_o\left(\omega_{N_f}\right) \dots \Omega_p\left(\omega_{N_f}\right)) \end{pmatrix} \in \mathbb{C}^{N_f x(p+1)} \tag{2.41}$$

$$Y_O = \begin{pmatrix} -\omega_o(\omega_1)(\Omega_o(\omega_1) \dots \Omega_p(\omega_1)) \otimes \widehat{H}_o(\omega_1) \\ \dots \\ -\omega_o\left(\omega_{N_f}\right)(\Omega_o\left(\omega_{N_f}\right) \dots \Omega_p\left(\omega_{N_f}\right)) \otimes \widehat{H}_o\left(\omega_{N_f}\right) \end{pmatrix} \in \mathbb{C}^{N_f xm(p+1)} \tag{2.42}$$

where $\otimes$ indicates the Kronecker product.

2.3.3.3 Reduced normal equations

As in Equation 2.38, the cost function can be formulated in its linearized equation errors basis:

$$l^{LS}(\theta) = \sum_{o=1}^{l} \sum_{k=1}^{N_f} tr\{ (\varepsilon_o^{LS}(\omega_k, \theta))^H \varepsilon_o^{LS}(\omega_k, \theta) \} \tag{2.43}$$

Descending this cost function cause of a weighted linear least squares problem. Presentation the matrix symbolization of (2.40), (2.41) and (2.42), the cost function can be written as:

$$\begin{aligned} l^{LS}(\theta) &= \sum_{o=1}^{l} tr\{ (E_o^{LS}(\theta))^H E_o^{LS}(\theta) \} \\ &= \sum_{o=1}^{l} tr\left\{ (\beta_o^T \quad \alpha^T) \begin{pmatrix} X_o^H \\ Y_o^H \end{pmatrix} (X_o \quad Y_o) \begin{pmatrix} \beta_o \\ \alpha \end{pmatrix} \right\} \\ &= tr\{ \theta^T J^H J \theta \} \end{aligned} \tag{2.44}$$

where $J \in \mathbb{C}^{lN_f x(l+m)(p+1)}$ is supposed Jacobian matrix given by:

$$J = \begin{pmatrix} X_1 & 0 & \dots & 0 & Y_1 \\ 1 & X_2 & \dots & 0 & Y_2 \\ \dots & \dots & \dots & \dots & \dots \\ 0 & 0 & \dots & X_l & Y_l \end{pmatrix} \tag{2.45}$$

At this rate real-valued coefficients θ , it can be represent the $J^H J$ can be transformed its real part $Re(J^H J) \in \mathbb{R}^{(l+1)(p+1)x(l+m)(p+1)}$ and the cost function (2.44) turns:

$$l^{LS}(\theta) = tr\{\, \theta^T \, Re(J^H J) \; \theta \,\} \tag{2.46}$$

$$Re(J^H J) = \begin{pmatrix} R_1 & 0 & \dots & 0 & S_1 \\ 0 & R_2 & \dots & 0 & S_2 \\ \dots & \dots & \dots & \dots & \dots \\ 0 & 0 & \dots & R_l & S_l \\ S_1^T & S_2^T & \dots & S_l^T & \sum_{o=1}^{l} S_o \end{pmatrix} \in \mathbb{R}^{(l+m)(p+1)x(l+m)(p+1)} \tag{2.47}$$

$$\begin{aligned} R_o &= Re(X_o^H \, X_o) \in \mathbb{R}^{(p+1)x(p+1)} \\ S_o &= Re(X_o^H \, Y_o) \in \mathbb{R}^{(p+1)xm(p+1)} \\ T_o &= Re(Y_o^H \, Y_o) \in \mathbb{R}^{m(p+1)xm(p+1)} \end{aligned} \tag{2.48}$$

The cost function (2.46) is reduced by putting its derivatives with respect to the unidentified polynomial coefficients θ equal to zero:

$$\begin{aligned} \frac{\partial l^{LS}(\theta)}{\partial \beta_o} &= 2(R_o \beta_o \; + \; S_o \alpha) = 0, \forall_o = 1, \dots., l \\ \frac{\partial l^{LS}(\theta)}{\partial \alpha} &= 2 \sum_{o=1}^{l} (S_o^T \beta_o \; + \; T_o \alpha) = 0 \end{aligned} \tag{2.49}$$

These equations which can be written using (2.47) and (2.36), the new equations that occurs is called the normal equations:

$$2Re(J^H J)\theta = 0 \tag{2.50}$$

Firstly, α coefficients are needed to draw the stabilization diagram. α coefficients are calculated after obtaining the polarity and modal participation factors. then the β_o coefficients from equation 2.49 are found.

$$\beta_o = -R_o^{-1} S_o \alpha \tag{2.51}$$

yielding the alleged reduced normal equations:

$$\left\{ 2 \sum_{o=1}^{l} (T_o - S_o^T R_o^{-1} S_o) \right\} \alpha = 0$$
$$M\alpha = 0 \tag{2.52}$$

where $M \in \mathbb{R}^{m(p+1)xm(p+1)}$ is determined in above equation. This equation can be figured out for the denominator polynomial α in a least-squares perceive. The zero condition (α=0) of the parameters is eliminated to avoid meaningless solutions. (Peeters & Van der Auweraer, 2005). While determining the dynamic properties by using real data collected under operational operating conditions, keeping the model order high will give more effective results.

As a result of these processes, a stabilization diagram is created and stable physical modes are marked and separated from unstable modes (Peeters & Van der Auweraer, 2004). Poles with a certain rating criterion are compared sequentially and if they are within the tolerance level, they are marked as stable. Determining the order of the model, which is a typical system identification problem, is solved by using the stabilization diagram. It is easier to select the stable poles from the stabilization diagram compared to the Polymax with stochastic subspace identification method (Peeters & Van der Auweraer, 2005). The poles λ_i and the modal participation factors $< l_i^T >$ (in case of FRFs) or operational reference factors $< g_i >$ (in case of spectra) are detected from the denominator polynomial (2.52) by computing the eigenvalue decomposition of its companion matrix (Heylen et al., 1997).

A p^{th} order right matrix-fraction model gives *pm* poles. The PolyMAX stabilization diagram can be correctly constructed if the least squares problem (2.52) for the maximum order of models p_{max} is formulated. The stabilization diagram is interpreted to give the pole and its corresponding operational reference factors. The mode shapes can be found later from (2.43):

$$S_{yy}^{+}(j\omega) = \sum_{i=1}^{n} \frac{\{v_i\}<g_i>}{j\omega-\lambda_i} + \frac{\{v_i^*\}<g_i^*>}{j\omega-\lambda_i^*} + \frac{LR}{j\omega} + j\omega UR \qquad (2.53)$$

in which LR,UR $\in \mathbb{R}^{lxm}$, separately the lower and upper residuals, have been introduced to model the affect of the out-of-band modes in the considered frequency band.

Mode shapes $\{v_i\}$ and the lower and upper residuals are unknowns in (2.53). These unknowns can be easily found by solving them in the linear least-squares base, this level is called least- squares frequency-domain (LSFD) method (Peeters & Van der Auweraer, 2005).

CHAPTER 3
MACEC: The MATLAB Toolbox for Experimental and Operational Modal Analysis

3.1 MACEC

MACEC is a toolbox that provides a good user interface in MATLAB for estimating modal parameters of structures. MACEC has been developed by many researchers and includes some of the system identification methods (SSI (Stochastic Subspace Identification), CSI (Combined Subspace Identification), EFDD and p-LSCF). One of the system identification methods it contains is p-LSCF, so the MACEC toolbox was preferred in this study (Peeters & De Roeck 1999; Reynders & Roeck 2008; Reynders, Pintelon, & De Roeck 2008; Reynders 2012, 2021; Reynders et al. 2010, 2016). Thanks to this toolbox, the modal parameters of the structure, namely damping rates, mode shapes and structural frequencies, can be calculated using vibration records.

MACEC creates an interface where you can visually interpret the modal parameters, making the program more understandable and easier. The program has a graphical user interface (GUI) but can also be used standalone via MATLAB without a GUI.

3.1.1 MACEC Grafical User Interface

To use MACEC, MATLAB must be open first. When you type “macec” in the MACEC command window and press the “Enter” key, the MACEC main window shown in the Figure 3.1 opens.

First of all, it is necessary to describe to MACEC the structure you will examine. this recipe Grid and Beam/surfaces files are created, respectively shown in Figure 3.2 and 3.3. In Figure 3.2, the point that will come to each level is defined and these points are numbered from 1 to 7. Points 1,2 and 3 represent the ground level, point 4 represents the 20th meter, point 5 represents the 40th meter, point 6 represents the 60th meter and point 7 represents the 80th meter.

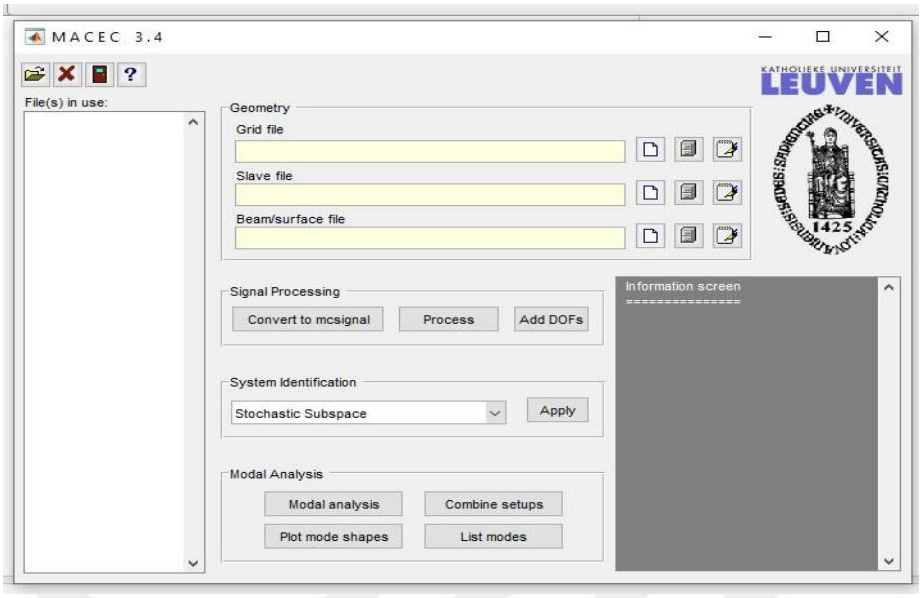


Figure 3. 1 MACEC main window

In Figure 3.3, the relation of the points to each level is defined, so as it can be understood from Figure 3.3, points 1-2, 1-3, 1-4, 4-5, 5-6 and 6-7 form a surface with each other. In this way, the geometric locations of the acceleration data we will receive along the tower are defined to MACEC.

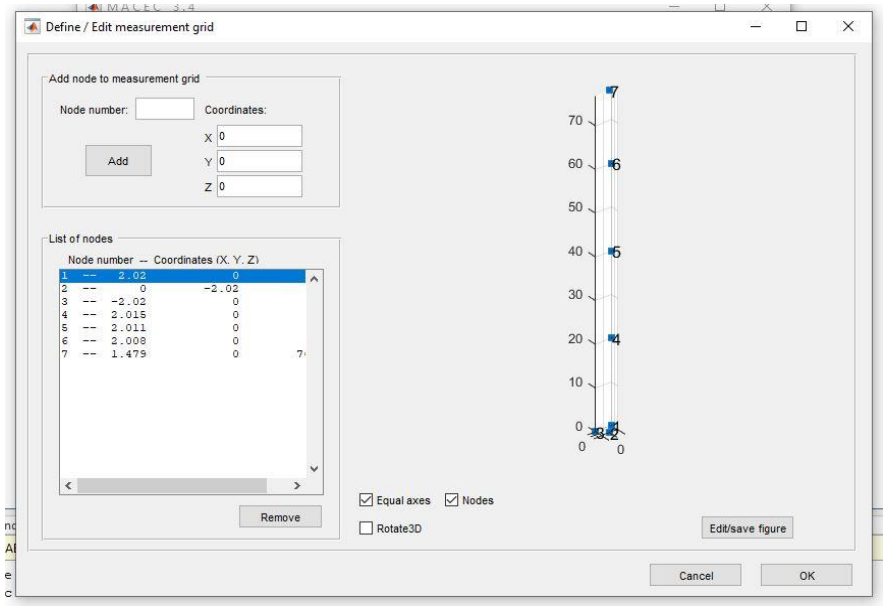


Figure 3. 2 Define or Edit measurement grid window

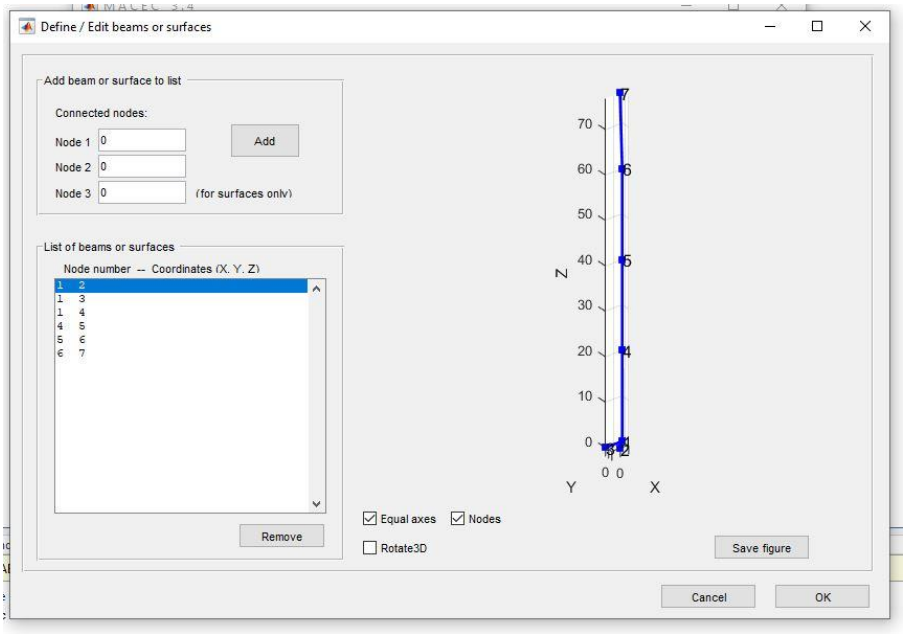


Figure 3. 3 Define/Edit beam or surfaces window

On the Main window shown in Figure 3.4, the file icon in the upper right corner is pressed and "the .mat" file, which is one of the desired formats, is read into the main window. This ".mat" file contains vibration data collected from various levels (level1, 2, 3 and 4) of the turbine.

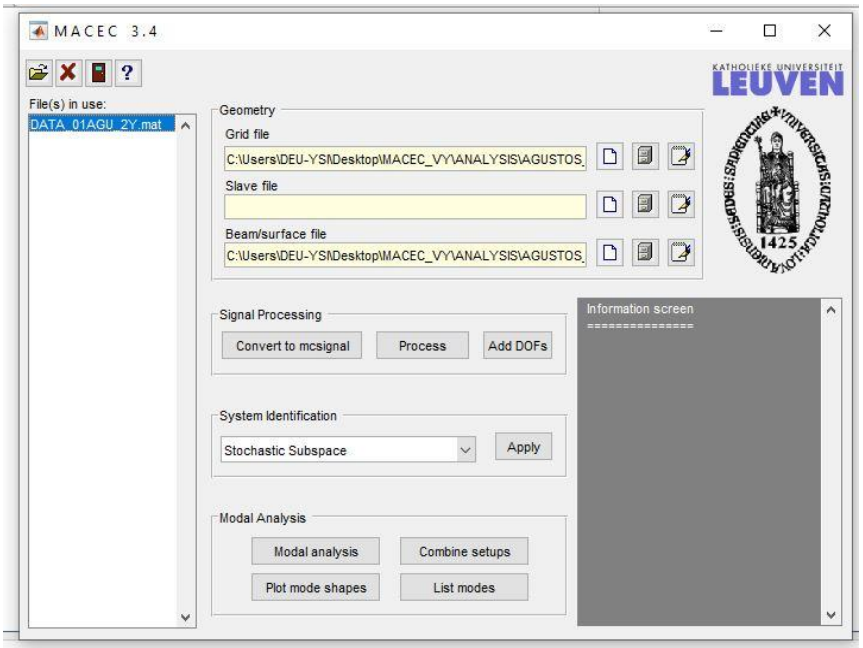


Figure 3. 4 Uploading the data file and converting the data to the appropriate format

The "convert to mcsignal" button in the signal processing menu is pressed and the sampling frequency tab shown in Figure 3.5 is opened. The sampling frequency is entered as 256 Hz and the "ok" button is pressed. The file "_conv.mat" is created.

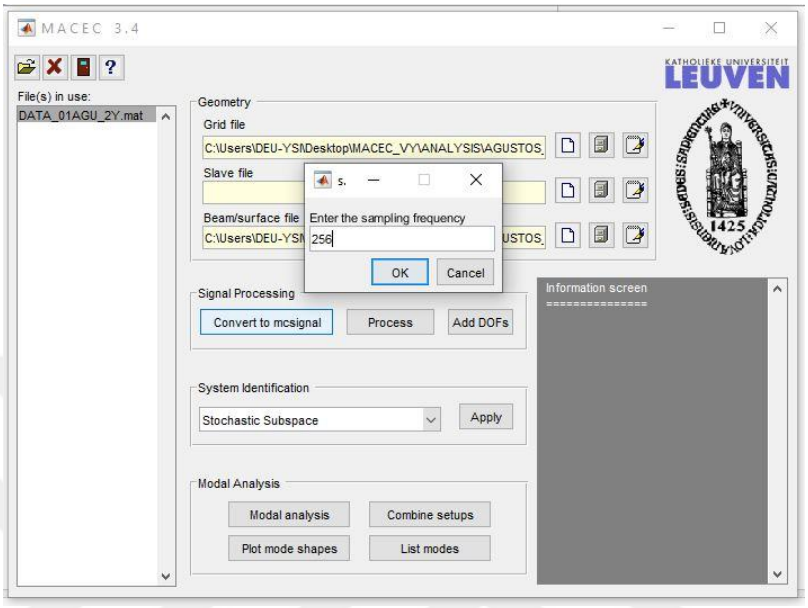


Figure 3. 5 Entering the sampling frequency

Select file "_conv.mat", click the "Proces" button and the conversion of measured data window shown in Figure 3.6 opens. In this window, the naming, data type, measurement unit classification and sensitivity properties of the collected data are set.

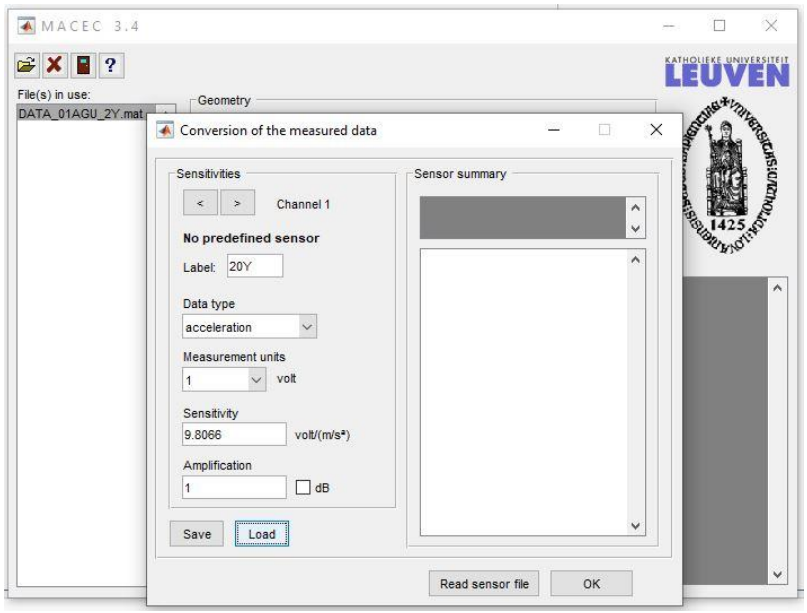


Figure 3. 6 Conversion of measured data

After naming the data, select file "_proc.mat", the data is processed in the mcsignal preprocessing window (shown in Figure 3.7) and the "ok" button is pressed. The file "_proc.mat" is created.

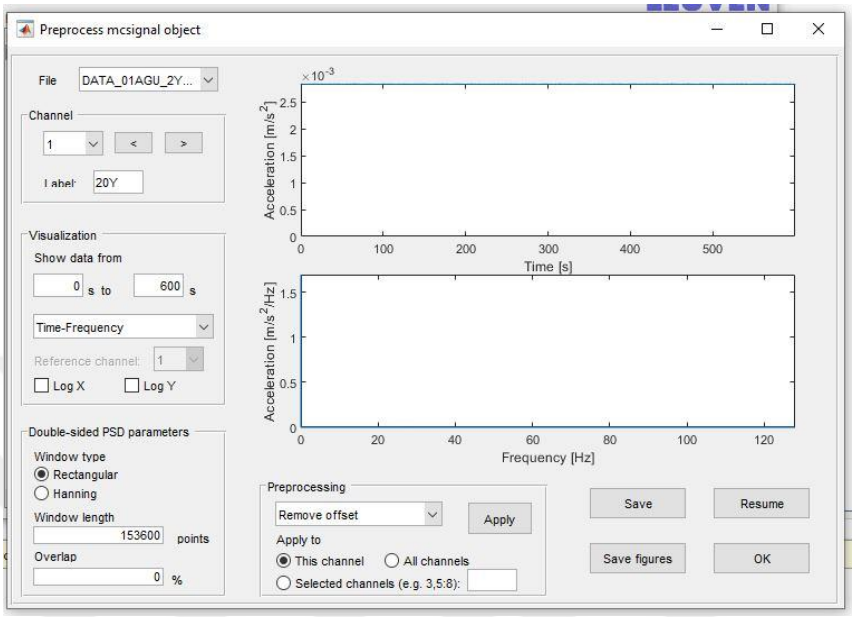


Figure 3. 7 Preprocess mcsignal object

In the main window shown in Figure 3.1, the "Add DOFs" button is pressed and the "Channel properties window" given in Figure 3.8 is opened. Directions and points are assigned to each channel in this window.

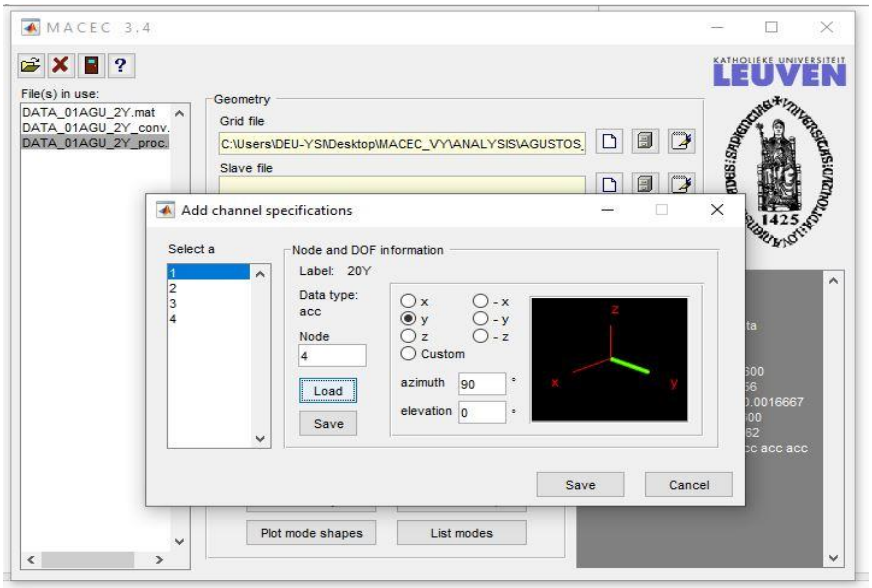


Figure 3. 8 Channel specifications window

Select file "_proc.mat", "p-LSCF" is selected from the system definition section in the main window and the "Apply" button on the right is pressed, and the PSD+ prediction window shown in Figure 3.9 opens. The periodogram method section is selected, the parameters are set to 40 and 2, the "calculate and show estimates" key is pressed, then the "ok" key is pressed. The p-LSCF method window opens see in Figure 3.10. Since the analysis type is only the output method, "stochastic" is selected, the reference intervals represent the desired channels and are adjusted up to 1:4, the frequency range is 0-128 Hz and the polynomial degree is adjusted from 1 to 200 and the "Calculate" button is pressed. The file "_pLSCF.mat" is created.

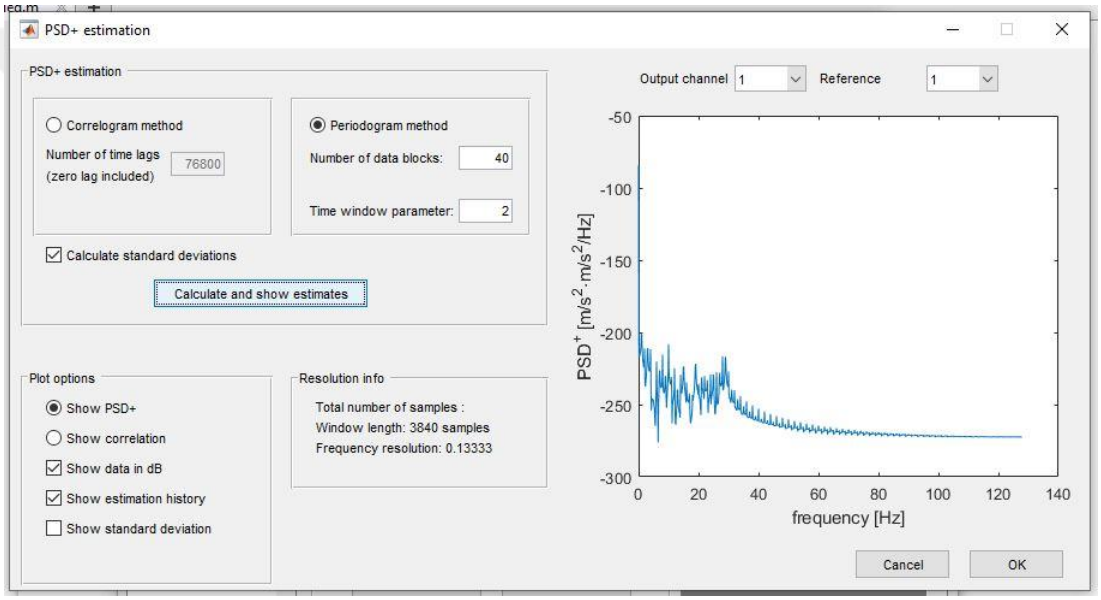


Figure 3. 9 PSD+ estimation window

The file "_pLSCF.mat" is created. The resulting "_pLSCF.mat" file is selected and the "modal analysis" button is pressed in the modal analysis section of the main window (Figure 3.1) and the stablization plot window given in Figure 3.11 is opened. In the stabilization plot window, the stabilization criteria are set as given in the figure, these criteria are adjusted to give the most optimum result by comparing the results obtained by making a series of trials.

Now a stabilization chart has been obtained using the p-LSCF method, plus rounded signs on this chart represent (Figure 3.11) the frequencies of the relevant modes. At this stage, the program asks you to select stable points.

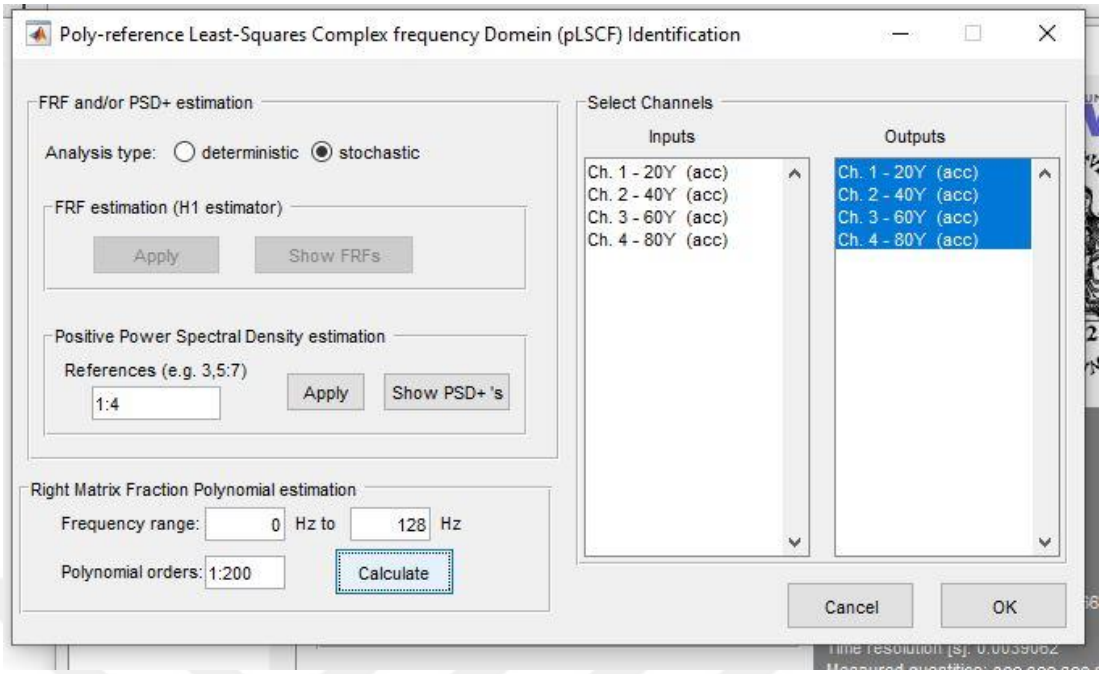


Figure 3. 10 p-LSCF method window

Stable points are selected and the "ok" button is pressed, then the "plot mode shapes" button is pressed in the modal analysis section in the main window (Figure 3.1), and the mode shape animation window opens (Figure 3.12). A display of the relevant mode shape is presented from this window.

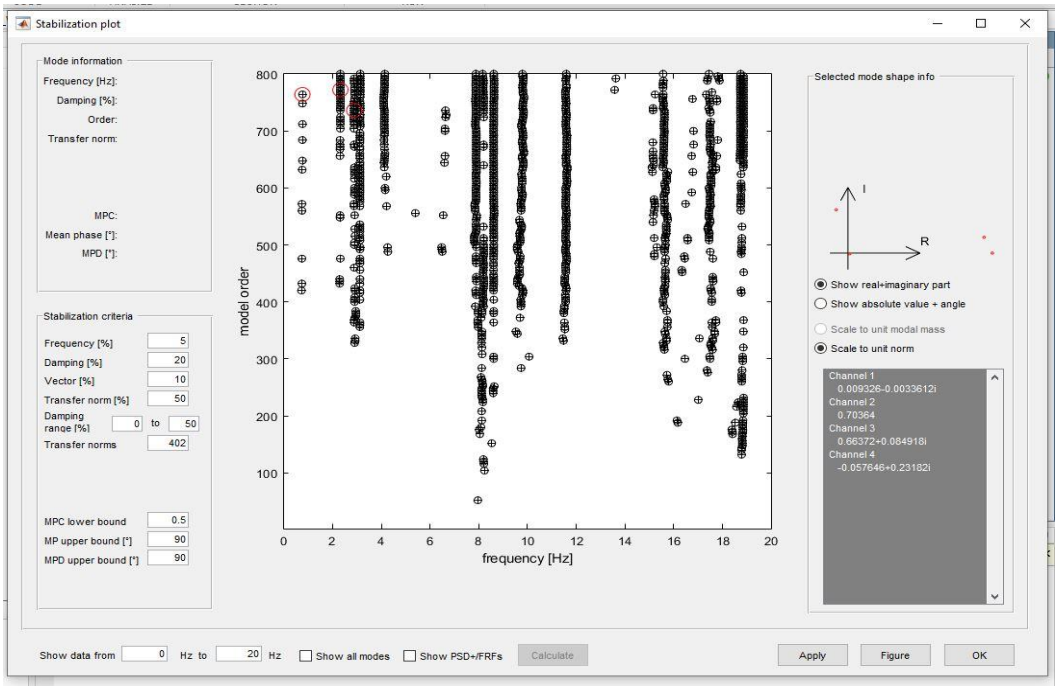


Figure 3. 11 Stabilization plot window

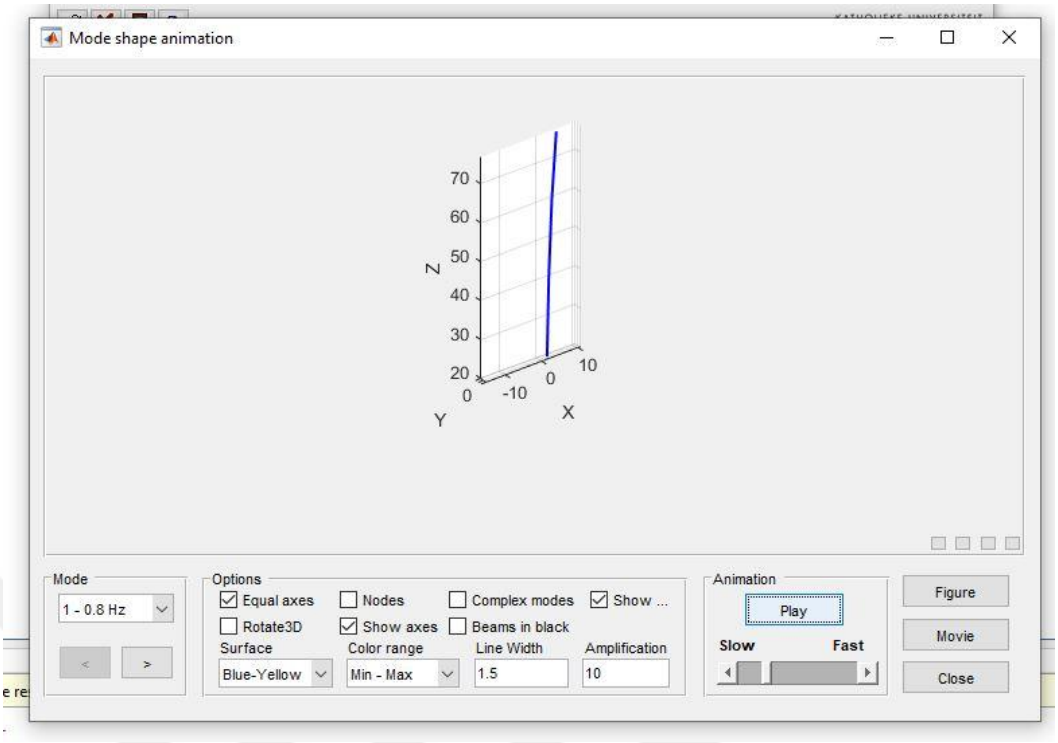


Figure 3. 12 Mode shape animation window

CHAPTER 4
WIND TURBINE STRUCTURE AND TEST SETUP

This thesis includes some parts of a project supported by TÜBİTAK 1001/Project No:120M218. In this thesis, a part of a comprehensive and large project such as establishing a data acquisition system, conducting laboratory tests, field studies, creating a three-dimensional turbine model, using the LabVIEW program to process the collected data and MATLAB for operational modal analysis tools is explained. Many researchers and scholars took part in the project. Each team member contributed significantly to the study.

4.1 Features of Wind Turbine

In the study, a wind turbine with a capacity of 2.5 MW (Figure 1) operated by a local energy company in Urla/İzmir was examined. The turbine has 3 blades and horizontal axes and the hub elevation of the turbine is 90 meters. The turbine tower has the form of a thin-walled steel cylinder, which is fixed to the reinforced concrete foundation system with bolts. At the top of the turbine tower are nacelles, hubs and blades. Various features of the wind turbine are listed in Table 4.1.

Table 4. 1 Properties of wind turbine

Properties	Value
Rated power	2.5MW
Rated wind speed	13 m/sn
Cut-in wind speed	3 m/sn
Cut-off wind speed	25 m/sn
Rotor speed	9,6-16 rpm
Rotor diameter	90 m
Tower height	80 m
Hub height	90 m
Nacelle mass	91 ton
Rotor mass	55 ton



(a) (b)

Figure 4. 1 (a) The monitored wind turbine and, (b) farm general view

The turbine tower consists of 4 sections connected to each other by bolts. The thickness and diameter of each section decreases along with height (Figure 4.2). The material properties of the tower are given in Table 4.2.

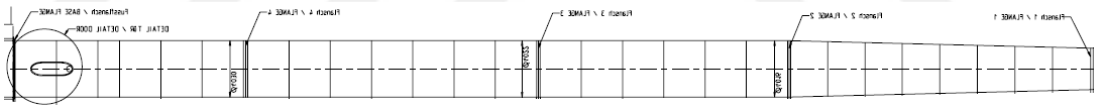


Figure 4.2 Tower geometry (flipped – right is top)

Table 4. 2 Material properties (S355)

Properties	Value
Yield strength	355 MPa
Tensile strength	510-630 MPa
Modulus of elasticity	210 GPa
Shear modulus	81 GPa
Density	7850 kg/m^3
Poisson ratio	0,30

The wind turbine sits on a relatively rigid ground. Some of the ground features found in the ground survey report conducted in December 2008 are introduced in Table 4.3.

Table 4. 3 Soil properties

Properties	Value
Bearing capacity	3 kg/cm^2
Coefficient of soil reaction	15000 t/m^3
Primary wave speed	399-910 m/s
Secondary wave speed	173-267 m/s

4.2 Equipments Used in Test Setups

The turbine tower height is 80 meters and there are horizontal platforms that can be walked on every 20 meters. These levels are named according to their height from the ground as follows; Level 1: 0 meters (base), Level 2: 20 meters, Level 3: 40 meters, Level 4: 60 meters, Level 5: 80 meters (top of the tower).

Information about the components of the system set upped along the tower height and the introduction of the general features of the system are given in Table 4.4. The sensors and data collection system components are used to collect data from the above-mentioned levels are listed as follows (Figure 4.3):

- Level 1 (0-meter): One triaxial accelerometer, three uniaxial accelerometers, and one temperature/humidity sensor are on this floor. To collect data from the sensors, two NI 9239 and one NI 9203 module modules is connected to a cDAQ-9185 chassis. In addition to these, industrial box PC, PoE switch, power supply, UPS and P2P antenna are on the foundation level.

- Level 2 (20-meter): Two uniaxial accelerometers are on this floor. To collect data from the sensors, a NI 9239 module is connected to a cDAQ-9185 chassis.

- Level 3 (40 meter): Two uniaxial accelerometers and one temperature/humidity sensor are on this floor. To collect data from the sensors, a NI 9239 module is connected to a cDAQ-9185 chassis.

- Level 4 (60-meter): Two uniaxial accelerometers are on this floor. To collect data from the sensors a NI 9239 module is connected to a cDAQ-9185 chassis.

- Level 5 (80-meter): Two uniaxial accelerometers and one temperature/humidity sensor are on this floor. To collect data from the sensors, a NI 9239 is connected to a cDAQ-9185 chassis.

Table 4. 4 Components of the Data Acquisition System

Device	**Description**
Uniaxial Accelerometer	Measures acceleration
Triaxial Accelerometer	Measures acceleration
Temperature and Relative Humidity Sensor	Measures temperature and relative humidity
NI 9239 Analog Input Module	Converts continuous-time and continuous-amplitude analog signals to discrete-time and discrete-amplitude digital signals
NI cDAQ-9185 Chassis	Controls timing, synchronization, and data transfer (at most four modules can be attached)
NI PS-16 Industrial Power Supply	Provides power for all system in the tower
P2P Wireless Antenna	Transfers data from the switchyard to the turbine tower
Industrial Box PC	Runs Labview codes to operate the system and controls data streaming
Workstation	Runs various codes for analyses
NAS	Backs up all collected data
UPS	Prevents system shutdown in case of power failure
Industrial Ethernet Switch	Allows devices to communicate with each other
Splitter	Separates data signals from power signals

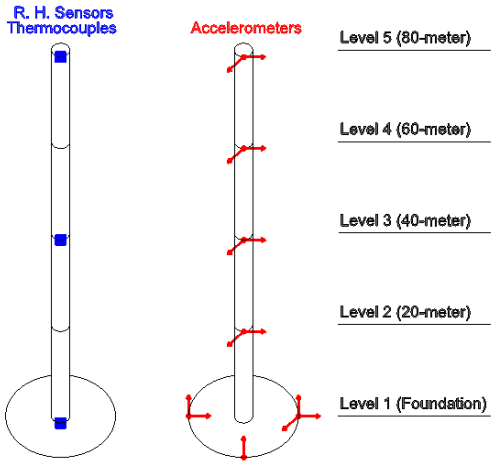


Figure 4.3 Components of the Data Acquisition System

The data acquisition system was assembled and tested in the laboratory before it was placed in the turbine. System elements assembled in the laboratory are shown in Figure 5 with their brief descriptions.

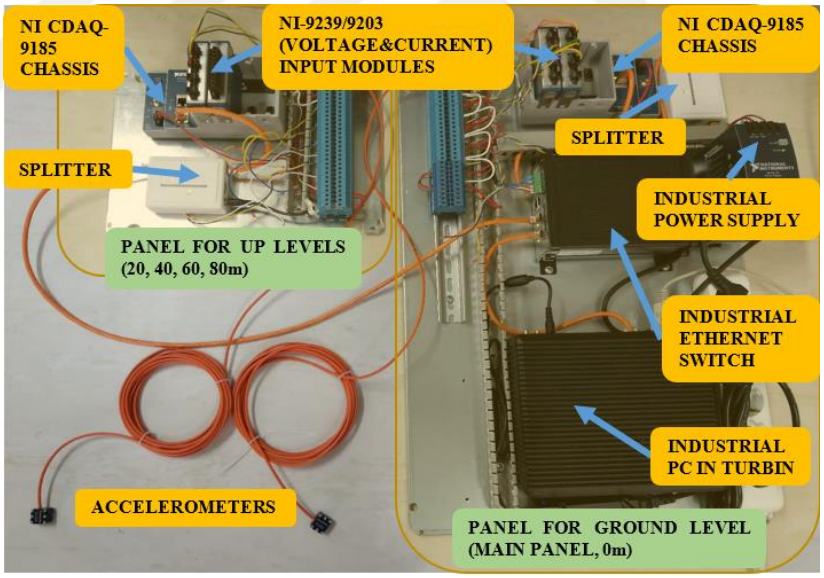


Figure 4.4 Assembly of the system components in the laboratory

In the system, NI 9185 cDAQ chassis are used to collect data synchronously on each level. Compatible inputs to the modules are provided by these chassis. The 8-port industrial switch, specifically manufactured for this project, enable all devices in the turbine tower to communicate with each other. At the same time, both data flow and energy flow is provided through the switch with PoE cables.

One triaxial and three uniaxial accelerometers at foundation level and at each level (e.g., 20, 40, 60 and 80 m) along the tower, two uniaxial accelerometers are placed perpendicular to each other. Some technical specifications of accelerometers are shown in Table 4.5.

Table 4. 5 Specifications of accelerometers

Uniaxial/Triaxial Accelerometer		
Acc. Range	(g)	±5
Sensitivity	(mV/g)	540
Frequency Range	(Hz)	700
Noise	(µg/√Hz)	0.1
Bias Temperature	(mg/°C)	17
Shock Survivability	(g)	2500
Operating Voltage	(V)	5-20

Since proper placement of the accelerometers along the horizontal and vertical directions is a critical issue in order to obtain the acceleration data correctly, they were placed with a spirit level as shown in Figure 4.5 and the position of the accelerometers relative to each other is measured with a laser meter and set as 20 m. It may be seen in Figure 4.5 that the accelerometers are attached by using strong magnets attached to the tower turbine wall. Temperature and humidity meters have been installed at three different levels (0, 40, 80 m) on the inner part of the tower.

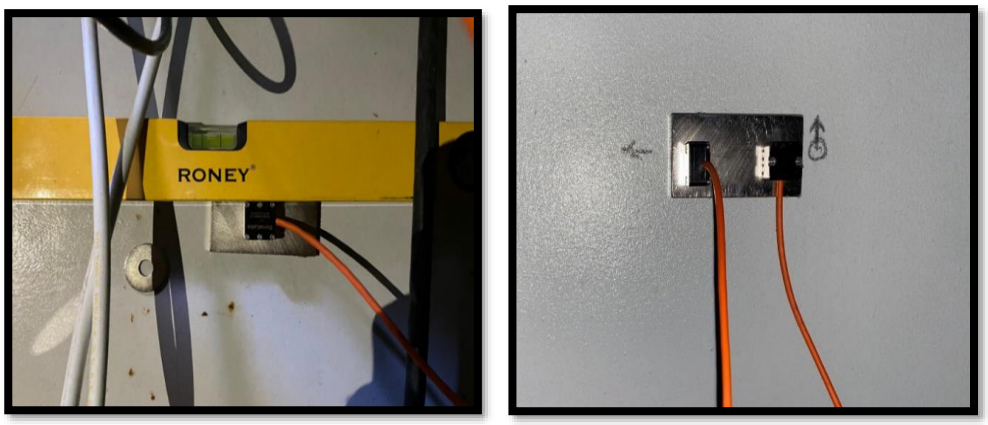


Figure 4. 5 Attachment of the accelerometers

In addition, rotor speed, nacelle direction, pitch angle, actual power, outside temperature values are instantly transferred to the workstation on the campus from the SCADA system. The data collected from the switchyard where the SCADA system is located and from the turbine where the data acquisition system is installed are transferred to the workstation located in the campus. Communication and lossless data transfers between these three points are provided by a custom code developed using LabVIEW for this project.

The energy required to keep the system operational is provided by the company operating the wind turbine as 220 V at the basic level, and since high voltage transmission from the tower is not allowed due to safety procedures, energy will be carried to the entire system using ethernet cables. These PoE CAT6 cables will not only transfer data but also stream data. With this method, in-tower cabling is kept to a minimum. PoE CAT6 cables connected to the switch transfer energy to all levels. General energy supply and data flow chart is given in Figure 4.6.

The labVIEW cycle used to flow the data collected in the turbine and transfer it to the workstation on the campus is shown in Figure 4.7. The cycle can be briefly explained in 8 main stages. Choosing the channel in 1 step, determining the sampling rate in the 2nd step, determining the channel number in the 3rd step, entering the loop execution rate for the CPU control in the 4th step, reading and storing the incoming data in the 5th step, since 200 samples are collected in 1 second, the time of data collection is recorded instantly for every 0.005 second in the 6th step, data will be collected in packets of 20 minutes in the 7th step and the case structure writes the incoming data as tdms file in desired periods in the 8th step.

As can be seen in the data collection system network layout (Figure 4.8), the scada and vibration data collected on the industrial PC in the turbine are transferred to the workstation on the campus via TCP (Transmission Control Protocol) protocol.

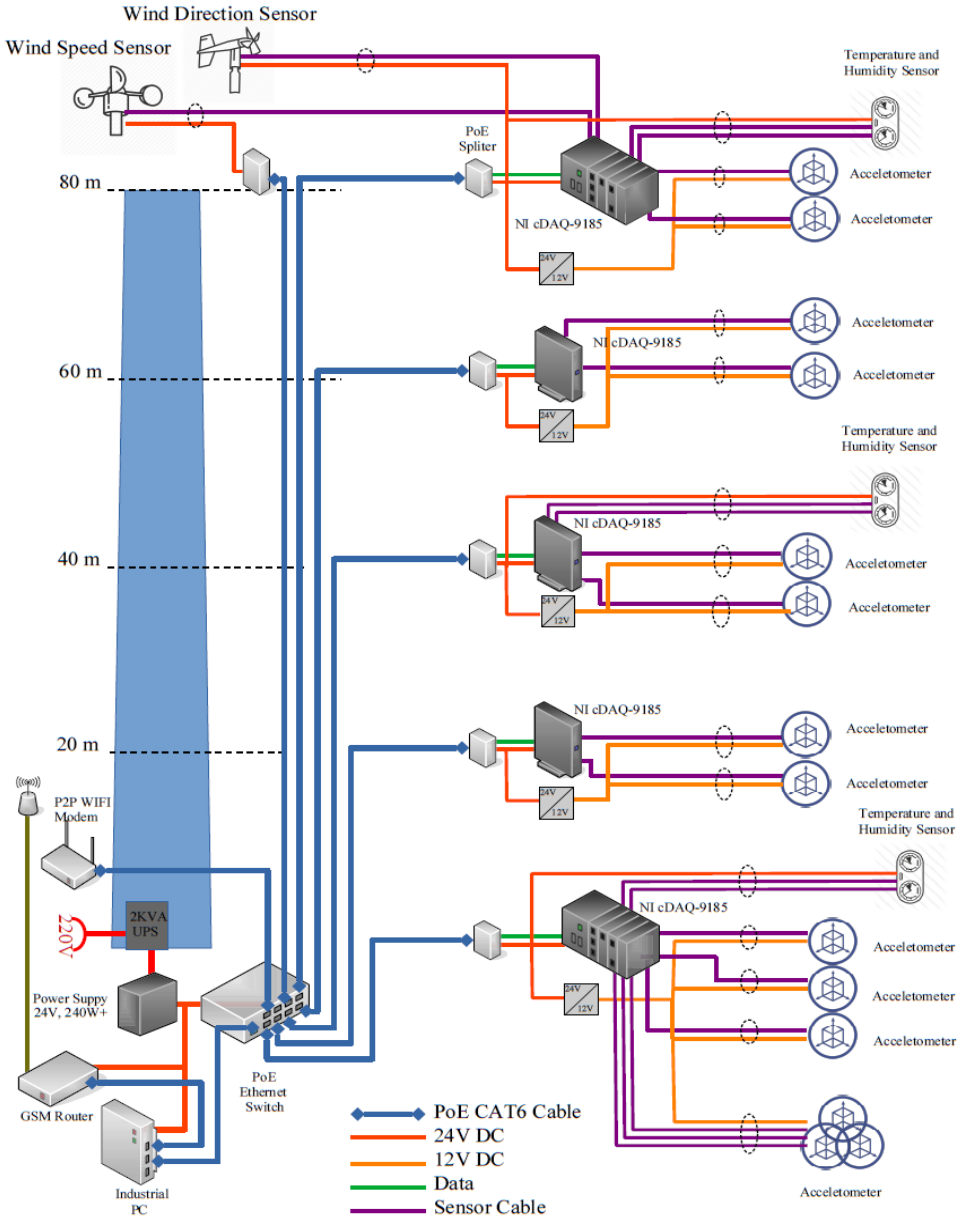


Figure 4.6 Schema representing the scada system

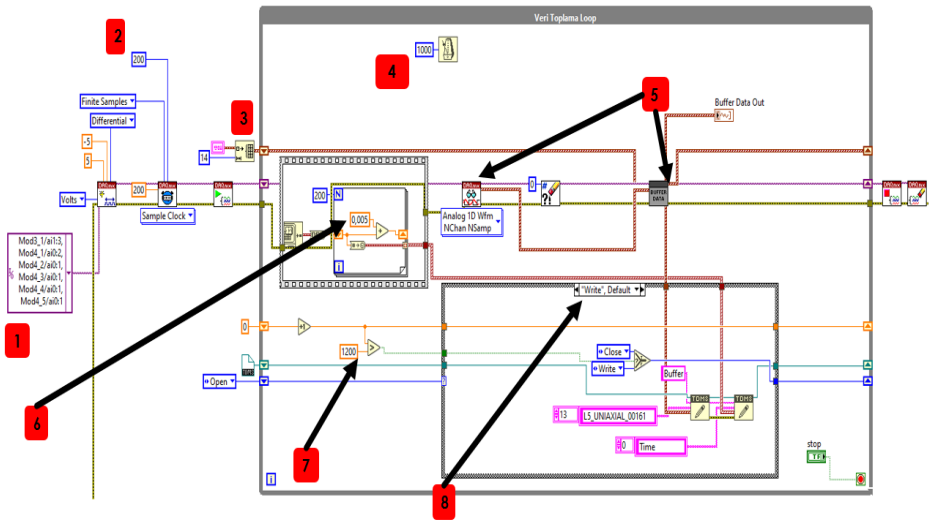


Figure 4. 7 Data colection loop works on instrial pc in turbine

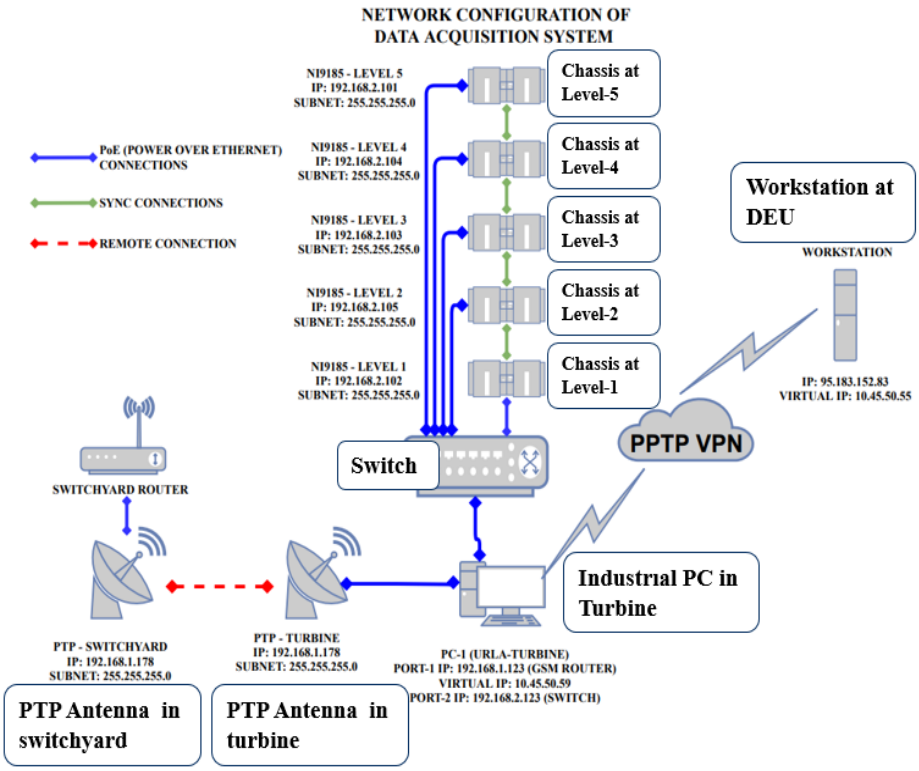


Figure 4. 8 Network configuration of data acquisition system

CHAPTER 5
EXPERIMENTAL RESULTS

5.1 Wind Turbine Test Results (Collected and SCADA Data from The Wind Turbine)

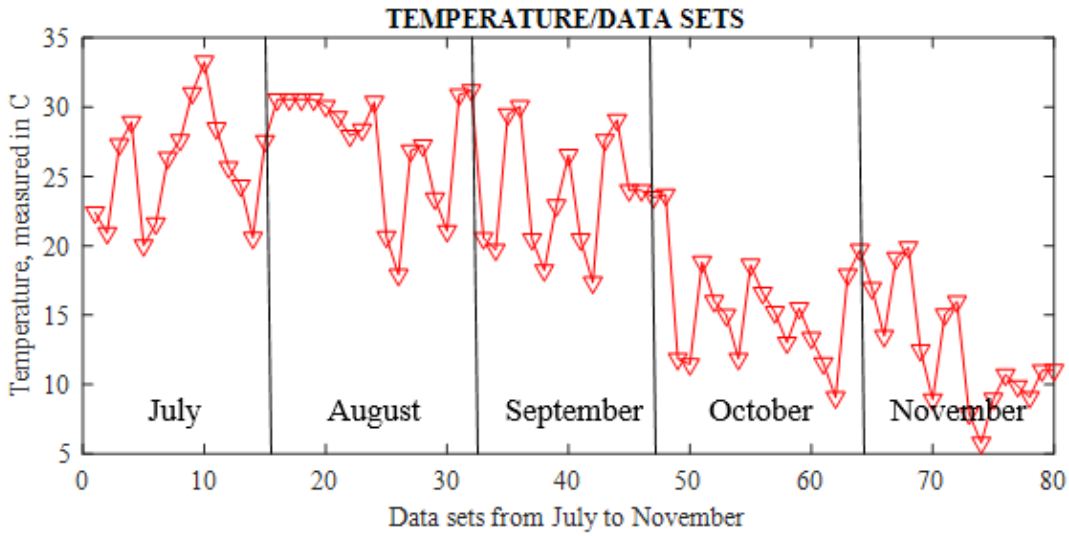
LabVIEW software has been developed for the data acquisition system and the data from the turbine's existing SCADA system (wind speed, wind direction, temperature, rotor speed, nacelle direction and pitch angle) to be synchronously collected and transferred to the university campus. The collected data were processed by p-LSCF method, which is an OMA method in the MACEC (Peeters & De Roeck 1999; Reynders & Roeck 2008; Reynders, Pintelon, & De Roeck 2008; Reynders 2012, 2021; Reynders et al. 2010, 2016) software, and dynamic characterization of the structure was performed. The effect of different operational and environmental conditions on modal parameters was interpreted.

The data received from both the scada system and the data acquisition system were recorded in the data storage system in 10-minute packages. Figure 5.1 (a) The temperature time graph is shown, the temperature data recorded from July to November, the average temperatures are normal considering the seasonal conditions of the region. When the moisture data shown in Figure 5.1 (b) were examined, it was observed that the humidity rate varied between 15.0 and 80.0 percent. An expected linear relationship was observed between wind speed (Figure 5.1 (c)) and rotor speed (Figure 5.1 (d)).

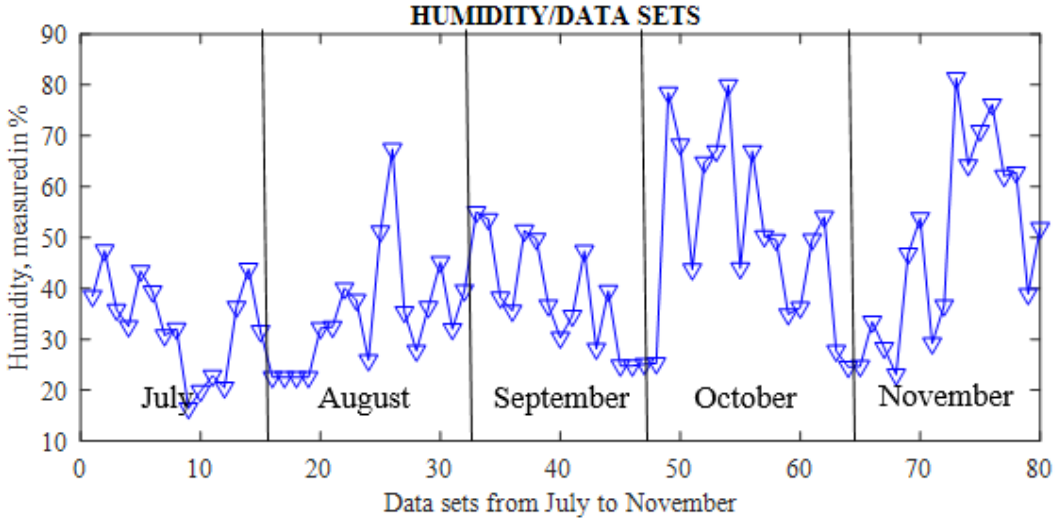
As can be seen from Figure 5.1 (a), a significant decrease was observed in temperature values from July to November. It can be said that this temperature change is at the seasonally expected levels and the measurements are made in a healthy way. It is understood that there is an increase in the humidity rates shown in Figure 5.1 (b) despite the temperature values.

There is an increase in average wind speeds from July to November as shown in Figure 5.1 (c). In Figure 5.1 (d), it is seen that rotor speeds vary between 10 and 15

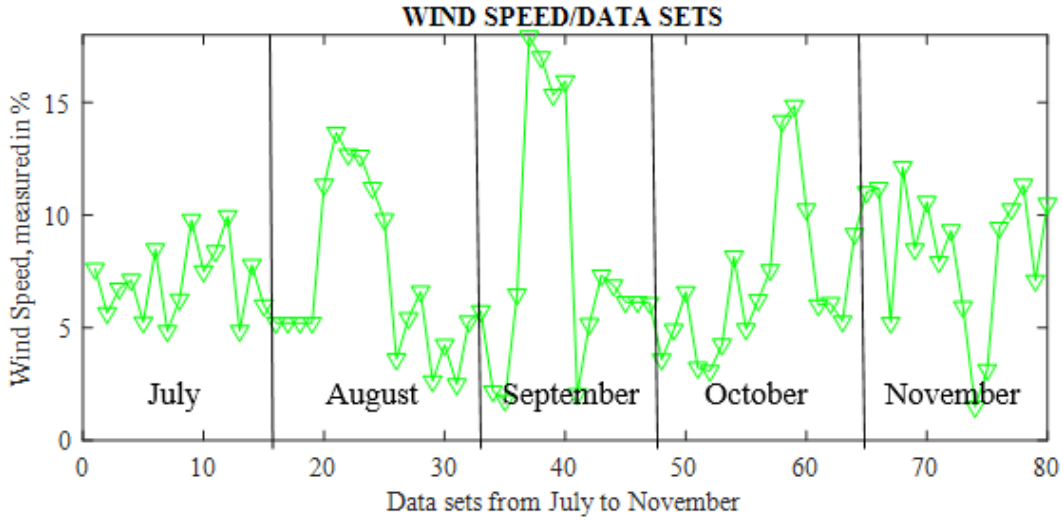
rpm. Especially at the end of August and the beginning of October, the values of approximately 0 rpm can be interpreted as cases where the turbine does not work. The turbine under study does not operate under 3 m/sec wind speed. It can be done by comparing the wind speed and rotor speed figures. In regions under 3 m's wind speed, rotor speeds are generally close to zero.



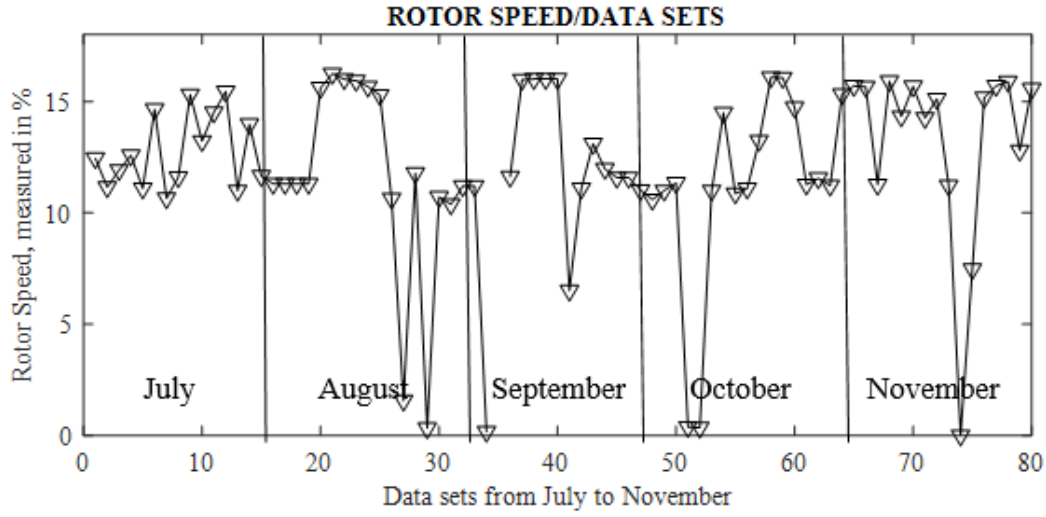
(a)



(b)



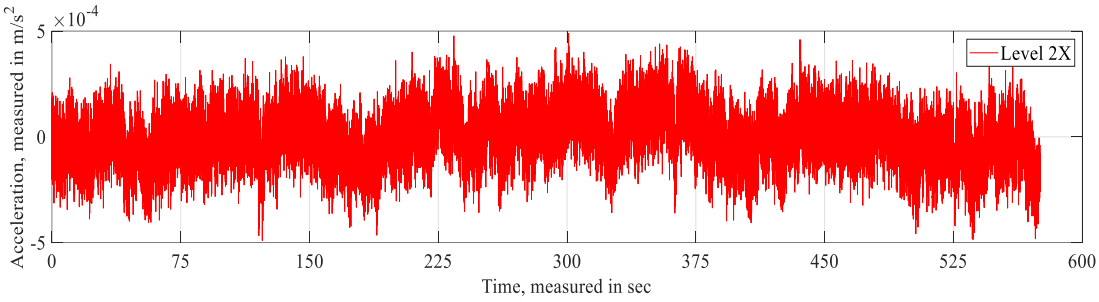
(c)



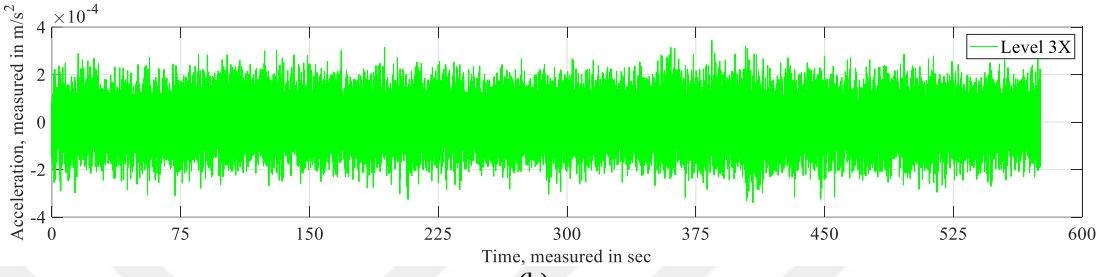
(d)

Figure 5. 1 Temperature, humidity, wind speed and rotor speeds of 80 data sets collected from the Scada system are shown in (a), (b), (c) and (d) respectively

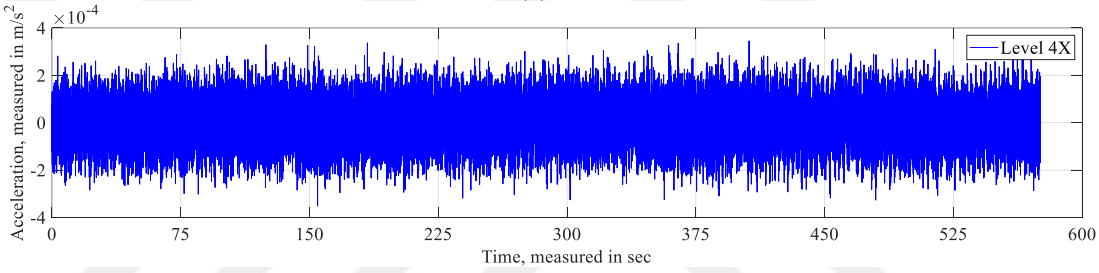
The accelerometers located at the 20th, 40th, 60th and 80th meters respectively are named Levels 1,2,3 and 4. The collected acceleration data (x direction) are presented in Figure 5.2. These data were also recorded just after the Buca earthquake at 04:31 am on 12 December. When the data collected from different levels are compared, it can be interpreted that the vibrations obtained in Level 2 (Figure 5.2 (a)) are relatively less than the other Levels 3-4-5 (Figure 5.2 (a-b-c)).



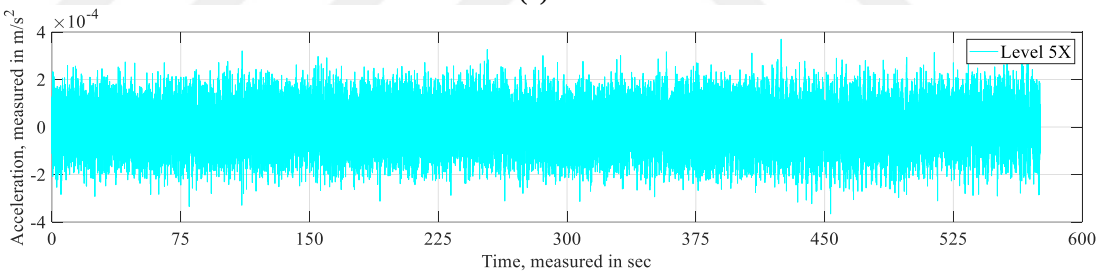
(a)



(b)



(c)



(d)

Figure 5. 2 Vibration data x direction-time graph from data acquisition system on 04.11.2022 at 04:31 am

The monthly averages of temperature, humidity, wind speed and wind direction data from the Scada system are given in Table 5.1. When viewed from a general perspective, this five-month period, which includes seasonal transitions, changes in temperature and humidity have been around fifty percent.

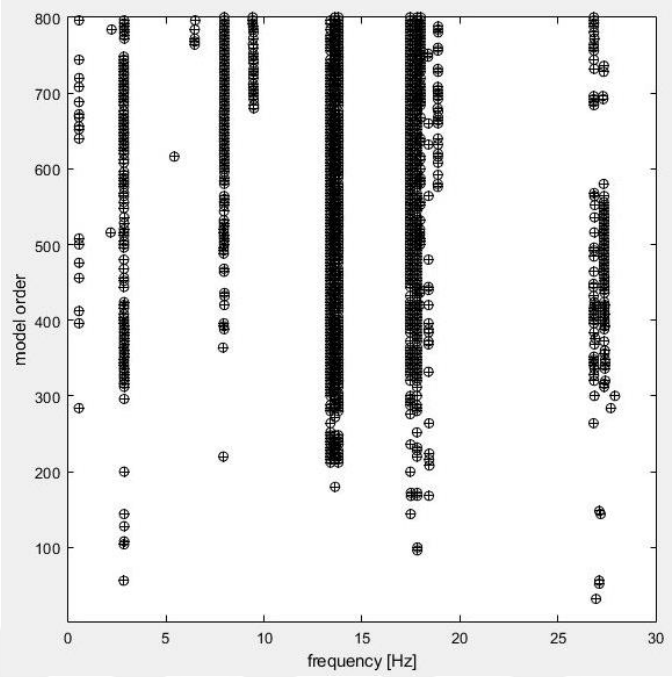
Table 5. 1 The monthly averages of scada data

DATA/ MONTHS	July	August	September	October	November
Temperature (Cº)	26.03	27.30	23.60	14.71	12.26
Humidity (%)	32.11	35.66	37.50	52.49	49.01
Wind Speed (m/sec)	6.96	7.33	7.86	7.17	8.44
Rotor Speed (rpm)	12.66	11.58	10.91	11.25	13.23

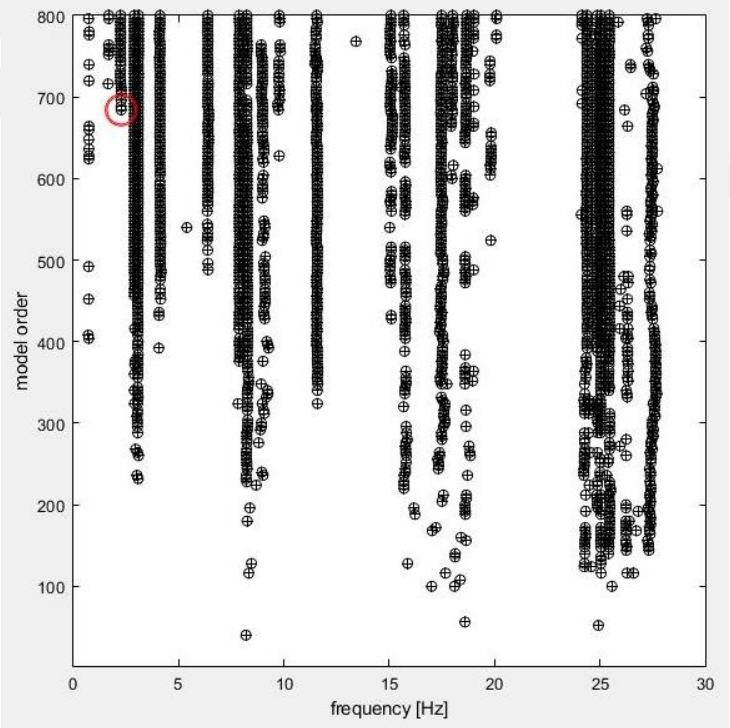
5.2 Experimental Wind Turbine Modal Parameter Obtained by p-LSCF Methods

In July, August, September, October and November of 2022, 4 days have been determined to represent each month. The designated days were determined to be the first day of the first week of the relevant month, the first day of the second week, the first day of the third week and the last day of the last week. Each selected day was intended to fully reflect the day examined using data collected at 00:00, 06:00, 12:00 and 18:00. A total of 80 datasets were examined and 160 analyses were performed using MACEC software with p-LSCF method.

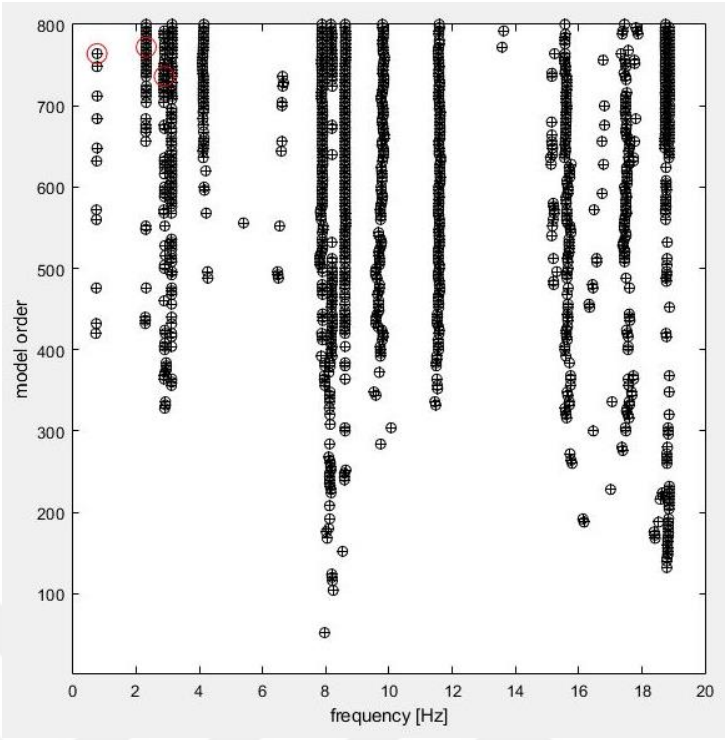
The MACEC program uses the p-LSCF method, allowing users to manually select stable frequencies. Example stabilization diagrams used to obtain stable frequencies from different data sets are shown in Figure 5.3. The results of the 80 analyzes for the x and y directions are given in Figures 5.4 (a) and (b), respectively.


model order
frequency [Hz]
800
700
600
500
400
300
200
100
0
5
10
15
20
25
30

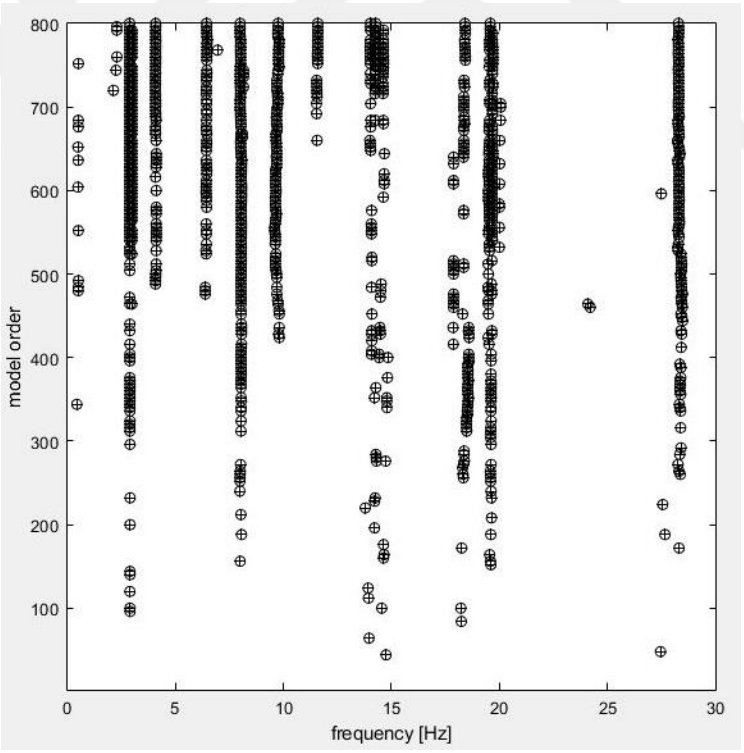
(a)


model order
frequency [Hz]
800
700
600
500
400
300
200
100
0
5
10
15
20
25
30

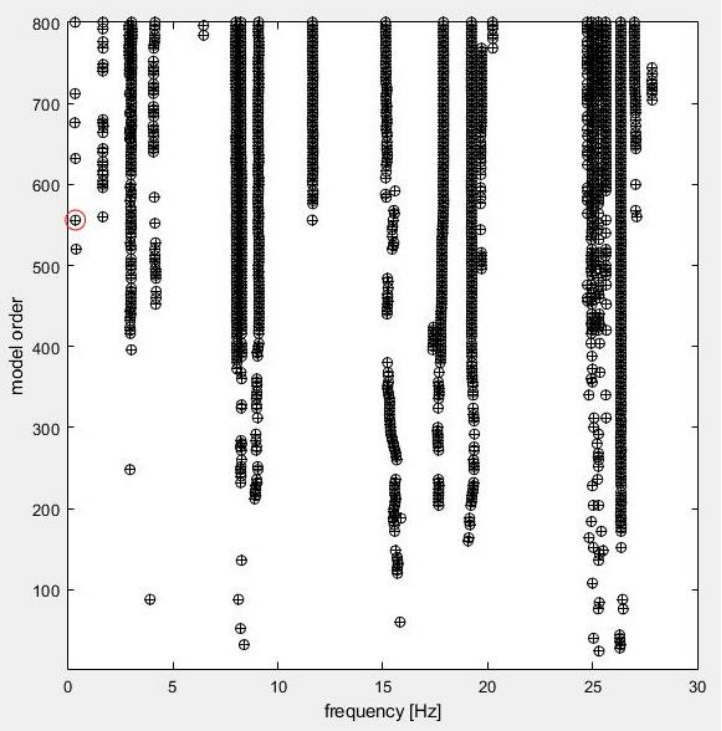
(b)


model order
frequency [Hz]
800
700
600
500
400
300
200
100
0
2
4
6
8
10
12
14
16
18
20

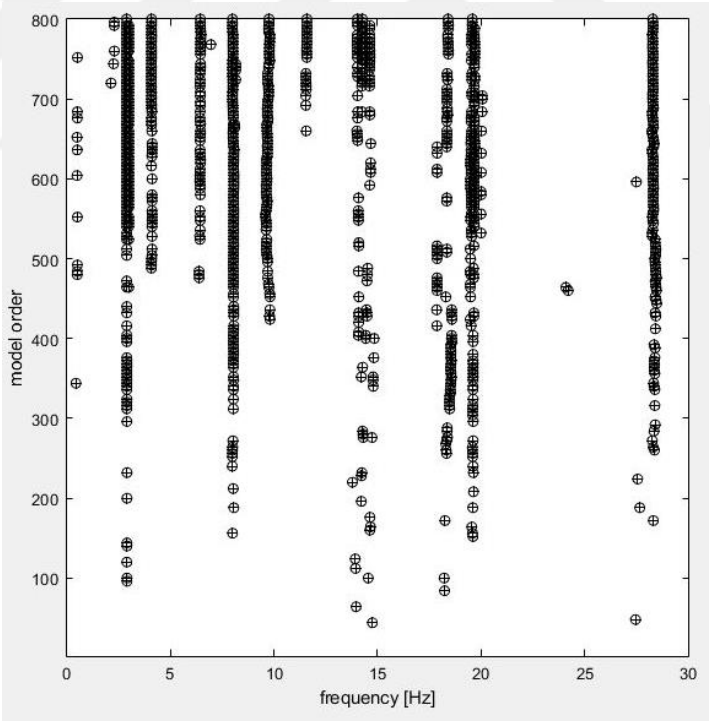
(c)


model order
frequency [Hz]
800
700
600
500
400
300
200
100
0
5
10
15
20
25
30

(d)



(e)



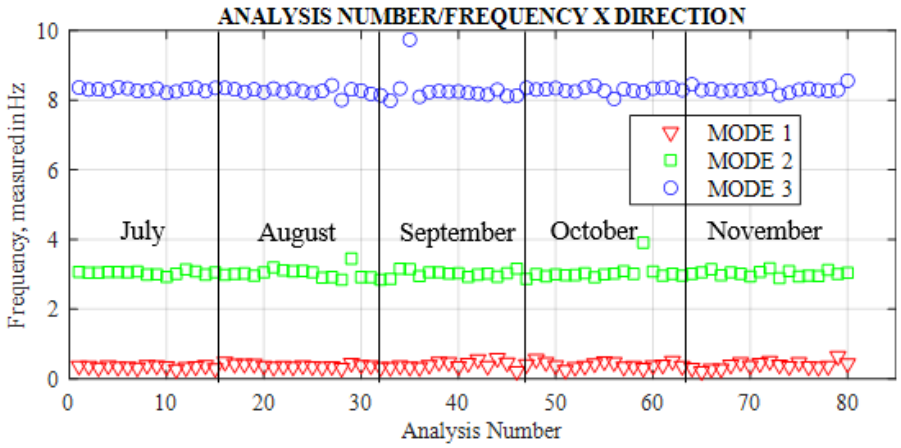
(f)

Figure 5.3 It shows the stabilization diagrams obtained by using (a) the y direction data on Agust 2 at 06:00 am, (b) the y direction data on Agust 11 at 00:38 am, (c) the x direction data on October 14 at 00:58 am, (d) the y direction data on October 14 at 00:58

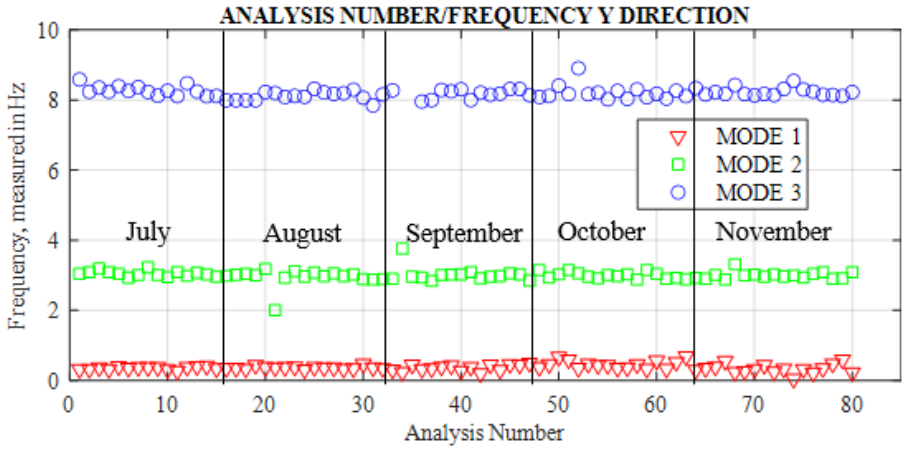
The average of the frequency values of the first three modes obtained using data from the x and y directions is given in Table 5.2. In addition, the frequency values constituting the average values in Table 5.2 are shown periodically in Figure 5.4. When the frequencies found were examined, the standard deviations were calculated as 0.09, 0.15 and 0.46 respectively, and it is understood that the distribution of the 1st mode frequency values was higher than the 2nd and 3rd mode frequency values.

Table 5. 2 Mode frequencies

	First Mode Frequency	**Second Mode Frequency**	**Third Mode Frequency**
x-direction	0.3850	3.0304	8.2957
y-direction	0.3756	2.9993	8.2961



(a)

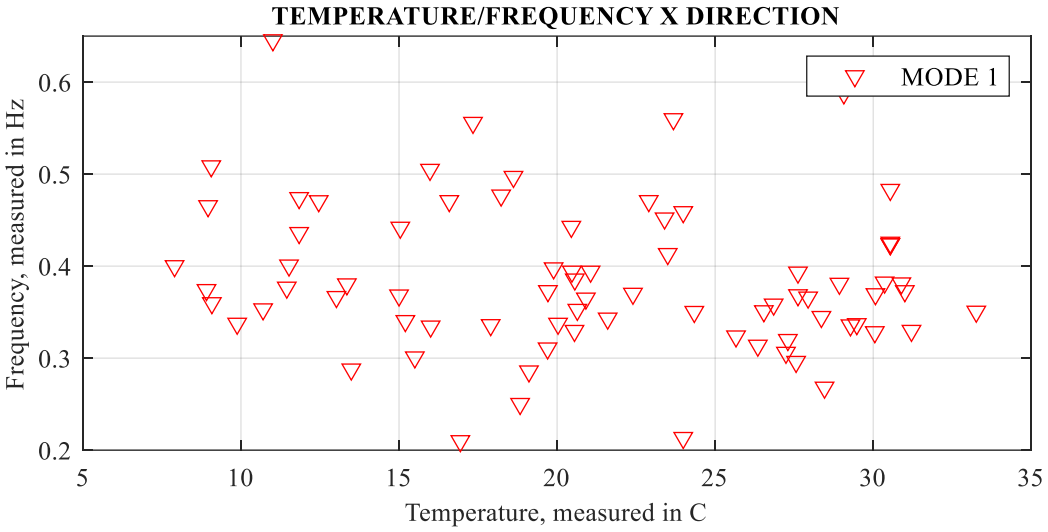


(b)

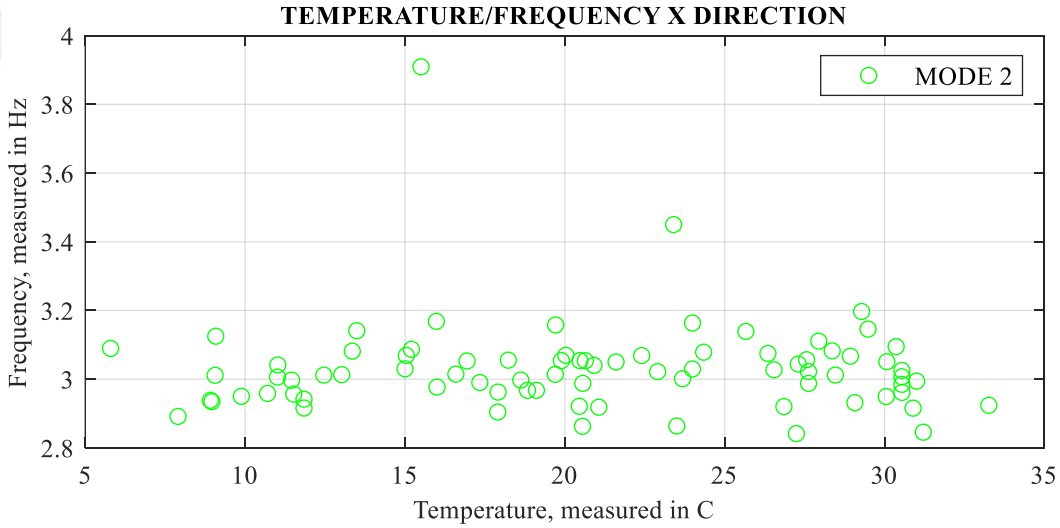
Figure 5. 4 Analysis and frequency (a) x-direction, (b) y- direction

The temperature data collected for 5 months varied between 7-33 degrees Celsius. Considering the temperature change mentioned for the Urla/İzmir location examined, it can be said that it is between the seasonally expected range. The frequency values of the first three modes x and y directions obtained are shown in respectively Figure 5.5 and Figure 5.6.

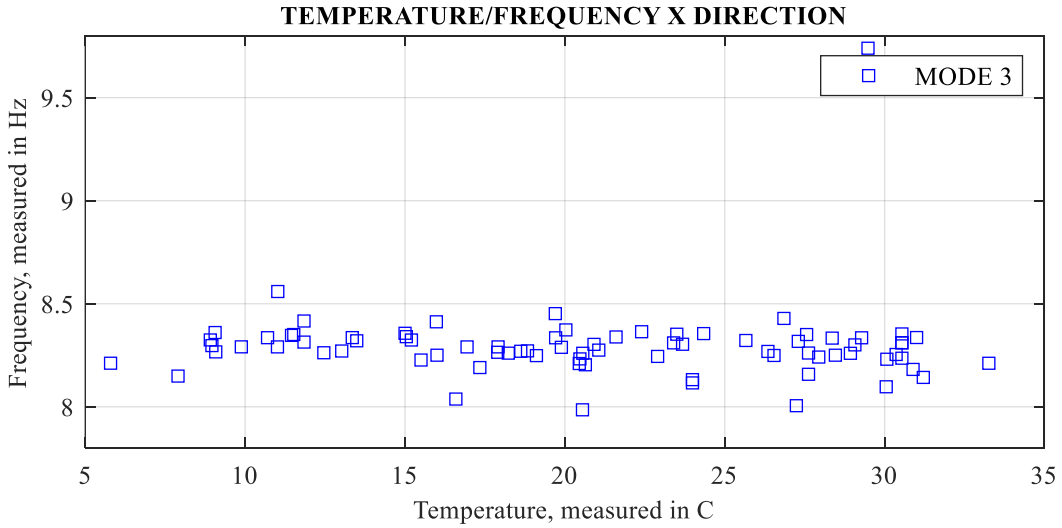
It is understood that the frequency values for the first mode are more random than the other 2nd and 3rd mode frequency values. Considering the clumped frequency values before 10 degrees celsius and after 30 degrees celsius shown in Figure 5.4 (c), when the frequency values obtained for the first three modes and the temperature relationship are examined, it can be said that there is a minimal decrease in the frequency values depending on the temperature increase.


TEMPERATURE/FREQUENCY X DIRECTION
MODE 1
Frequency, measured in Hz
0.2
0.3
0.4
0.5
0.6
5
10
15
20
25
30
35
Temperature, measured in C

(a)


TEMPERATURE/FREQUENCY X DIRECTION
MODE 2
Frequency, measured in Hz
2.8
3
3.2
3.4
3.6
3.8
4
5
10
15
20
25
30
35
Temperature, measured in C

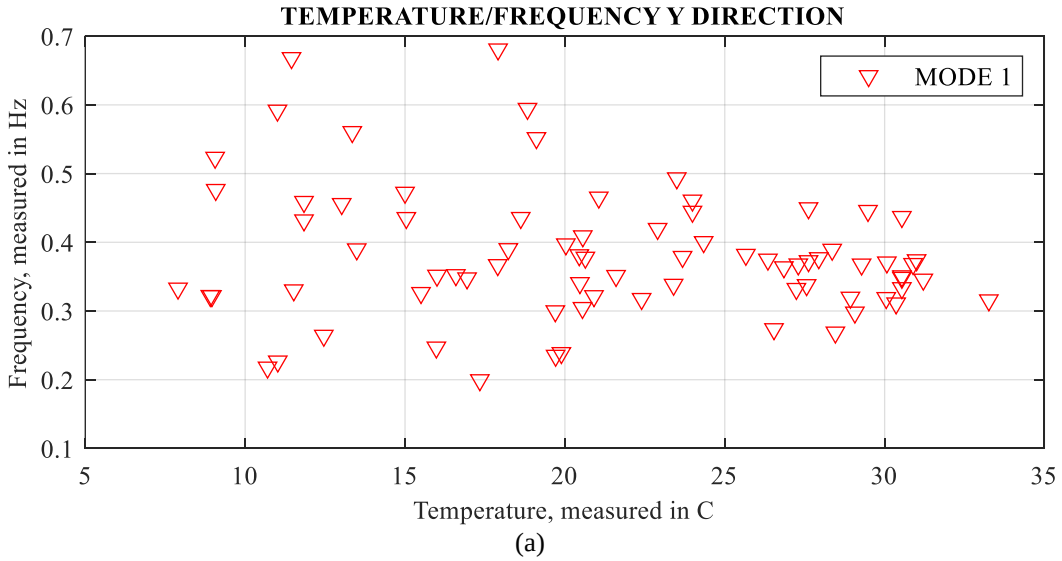
(b)



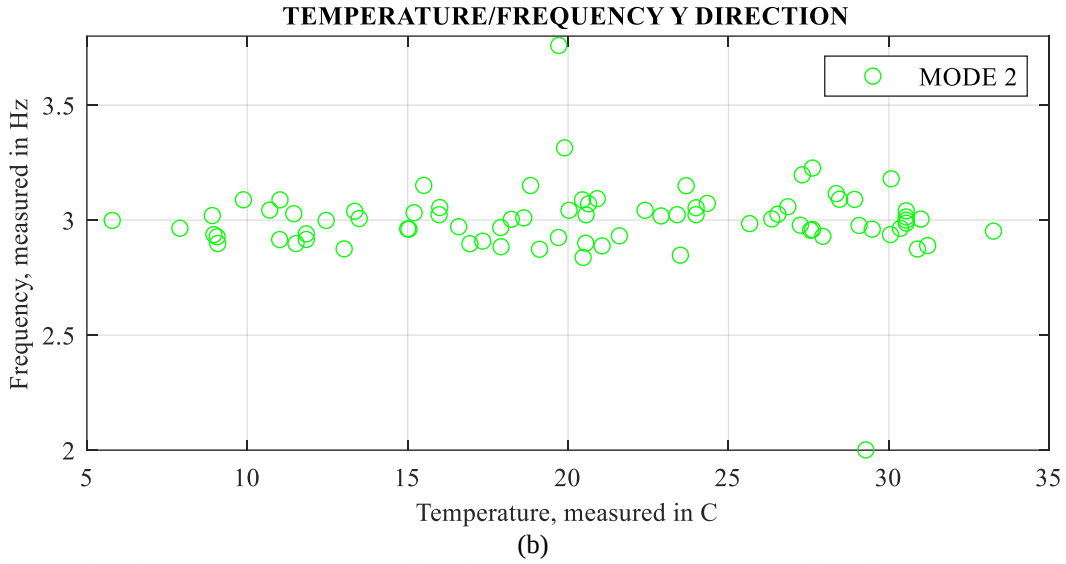
(c)

Figure 5. 5 The vibration data in the x direction collected from accelerometers at four different levels (Level 2-3-4-5) were found to be frequency values using the p-LSCF method. The frequency values of the first, second, and third modes are shown in (a), (b), and (c) respectively

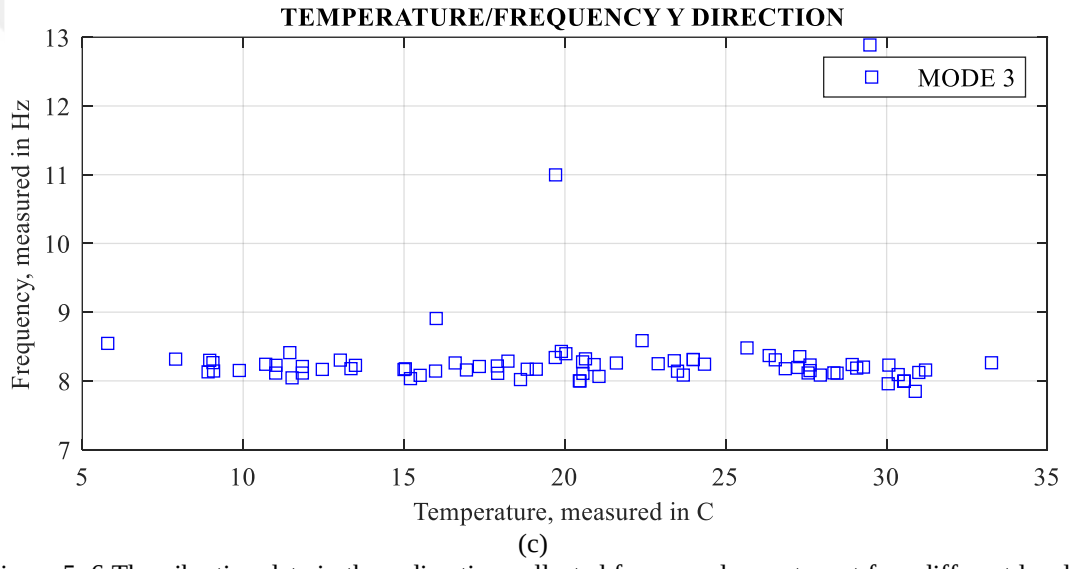
Modal frequency estimations using y-direction vibration data yielded the same results as x-direction. As can be seen in Table 5.2, there are insignificant differences. Figure 5.6 (a-b-c) shows the first three mode frequency values versus temperature values for the y direction.



(a)



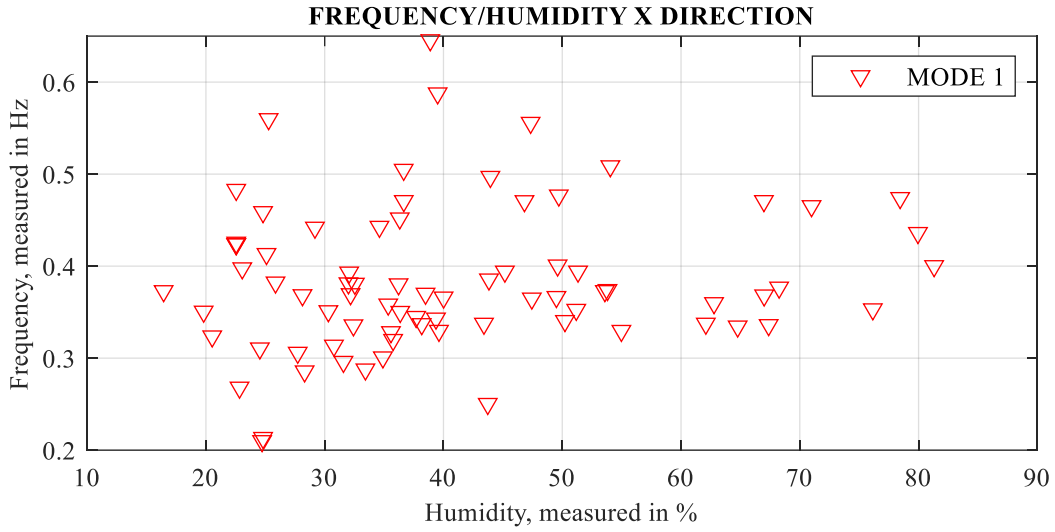
(b)



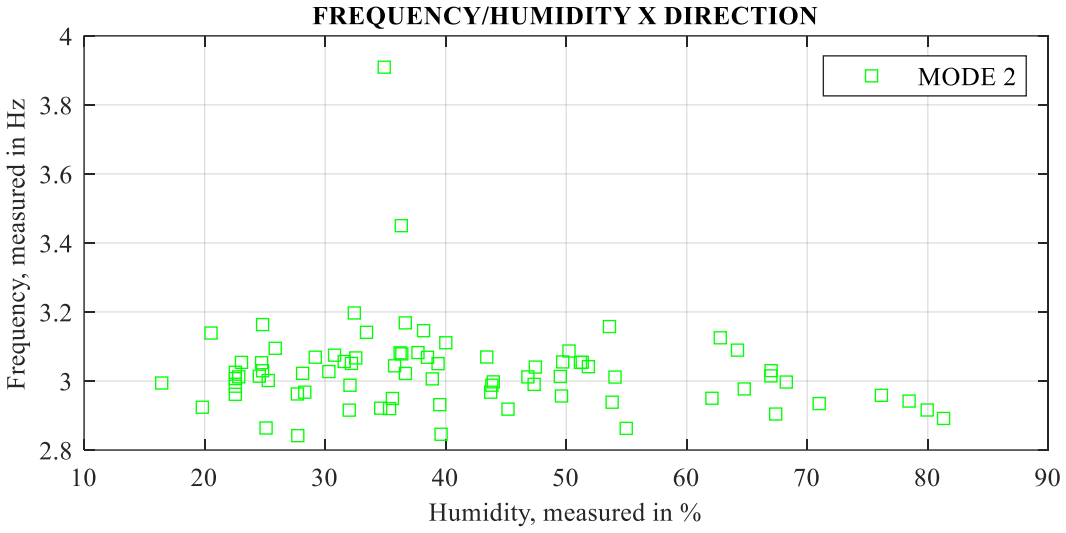
(c)

Figure 5. 6 The vibration data in the y direction collected from accelerometers at four different levels (Level 2-3-4-5) were found to be frequency values using the p-LSCF method. The frequency values of the first, second, and third modes are shown in (a), (b), and (c) respectively

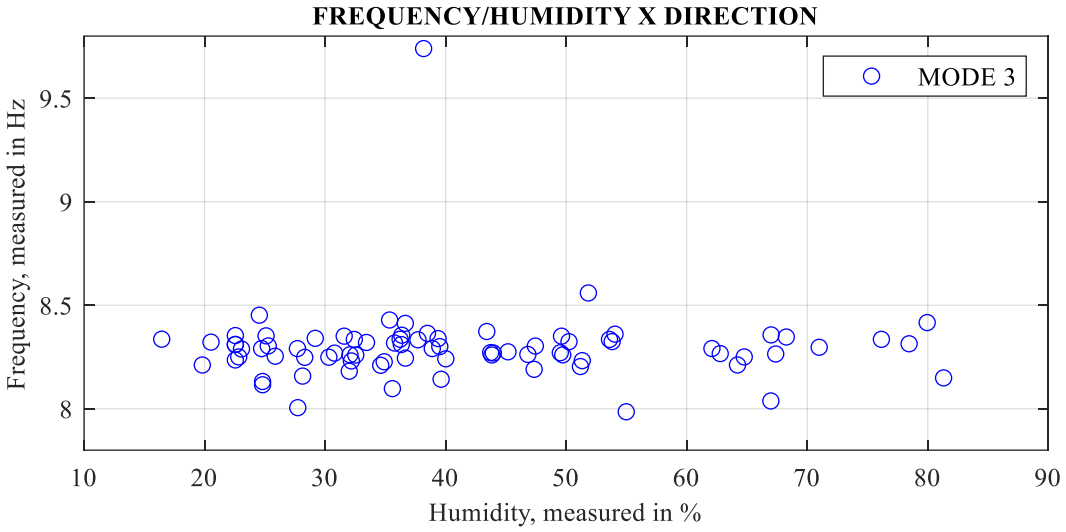
Frequency values versus humidity values obtained using the data collected in the x and y directions are shown in Figure 5.7 and Figure 5.8, respectively. When a period of 5 months was examined, no direct relationship was seen between humidity and frequency.


FREQUENCY/HUMIDITY X DIRECTION
MODE 1
Frequency, measured in Hz
0.2
0.3
0.4
0.5
0.6
10
20
30
40
50
60
70
80
90
Humidity, measured in %

(a)

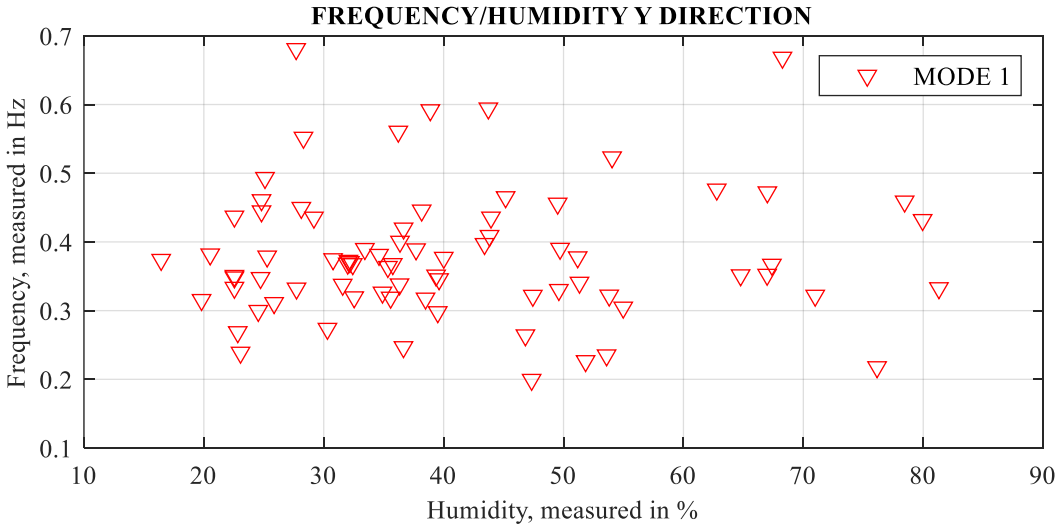

FREQUENCY/HUMIDITY X DIRECTION
MODE 2
Frequency, measured in Hz
2.8
3
3.2
3.4
3.6
3.8
4
10
20
30
40
50
60
70
80
90
Humidity, measured in %

(b)

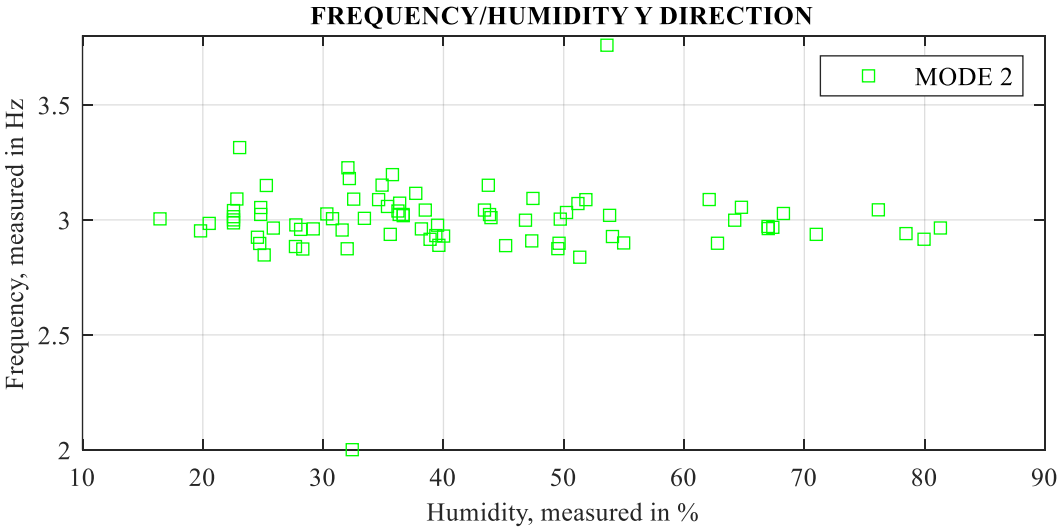


(c)

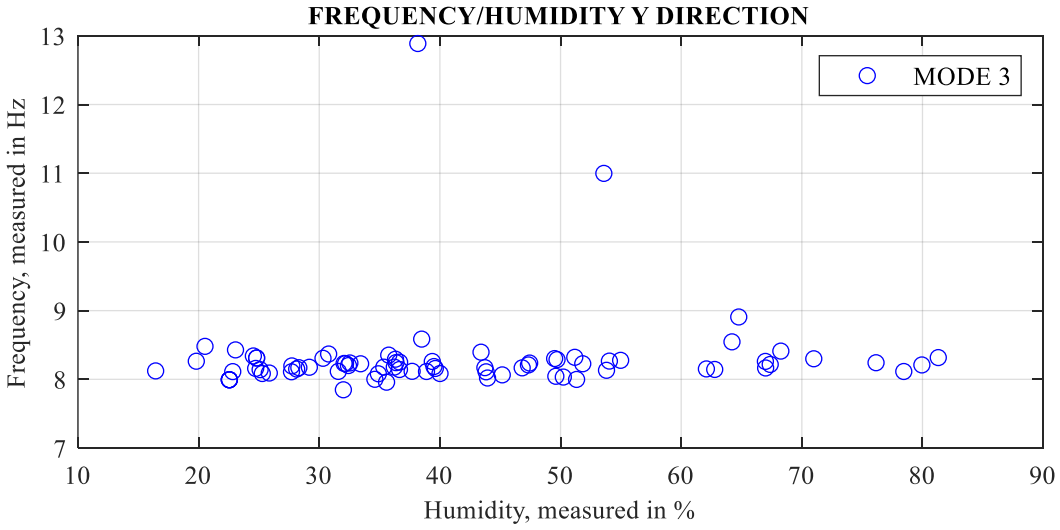
Figure 5. 7 The values of the first three modes obteined by the p-LSCF method using the x-direction data, corresponding to the frequencies and variable humidity ratios are shown in (a), (b), and (c) respectively


FREQUENCY/HUMIDITY Y DIRECTION
MODE 1
Frequency, measured in Hz
Humidity, measured in %
0.7
0.6
0.5
0.4
0.3
0.2
0.1
10
20
30
40
50
60
70
80
90

(a)


FREQUENCY/HUMIDITY Y DIRECTION
MODE 2
Frequency, measured in Hz
Humidity, measured in %
3.5
3
2.5
2
10
20
30
40
50
60
70
80
90

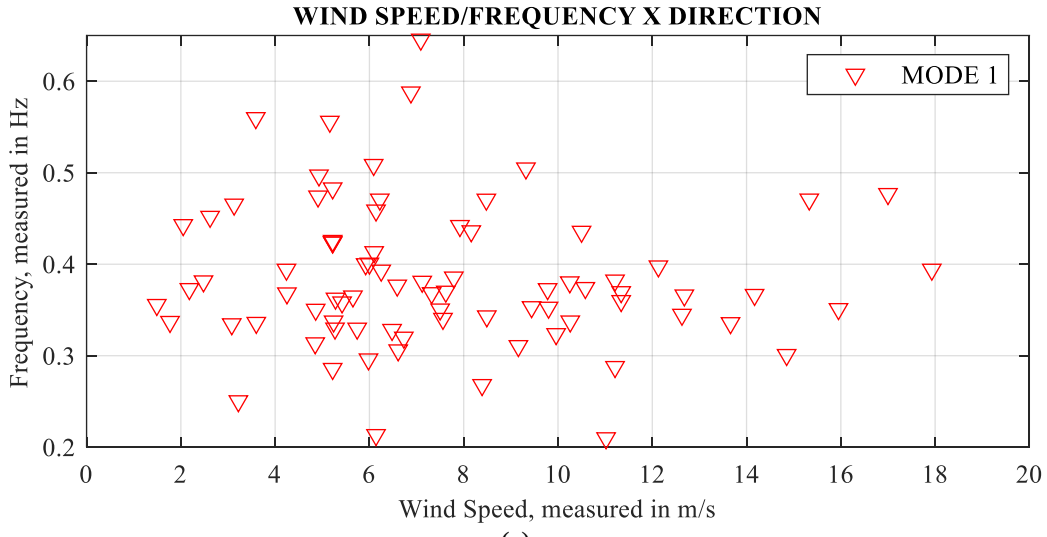
(b)



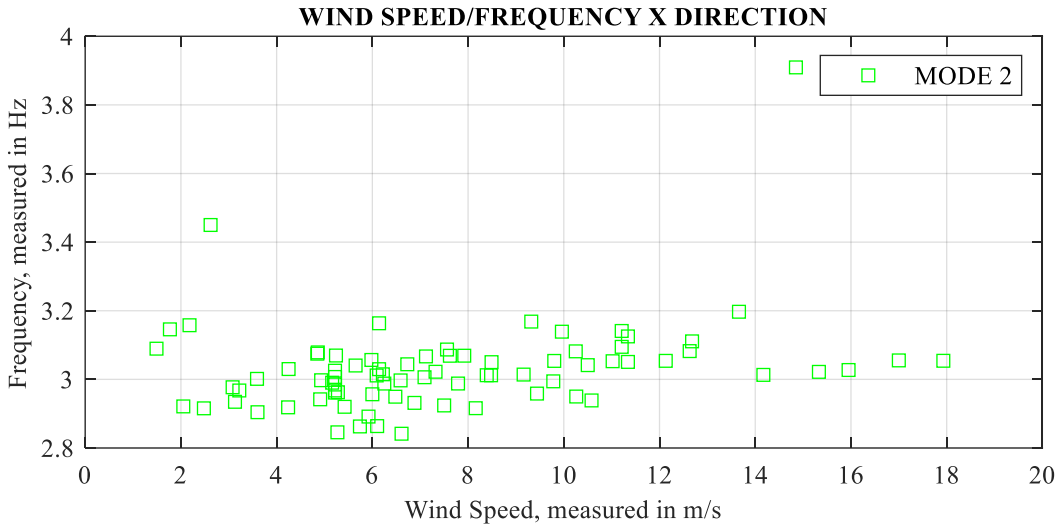
(c)

Figure 5.8 The values of the first three modes obteined by the p-LSCF method using the x-direction data, corresponding to the frequencies and variable humidity ratios are shown in (a), (b), and (c) respectively

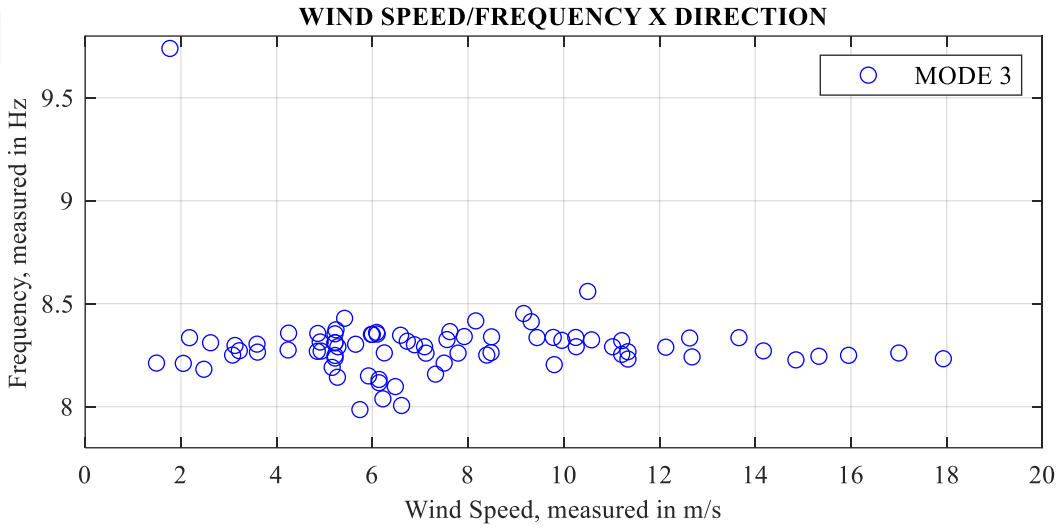
As can be seen in Figure 5.9, the x-direction wind speed was measured between 1.5 and 18 m/sec. Considering the relationship between 1st mode, 2nd mode and 3rd mode frequency values and wind speed, no significant trend could be detected. The frequency value could not be found at speeds less than approximately 2 m/sec wind speed, because the turbine cannot recover the energy to operate at speeds below 3 m/sec.



(a)



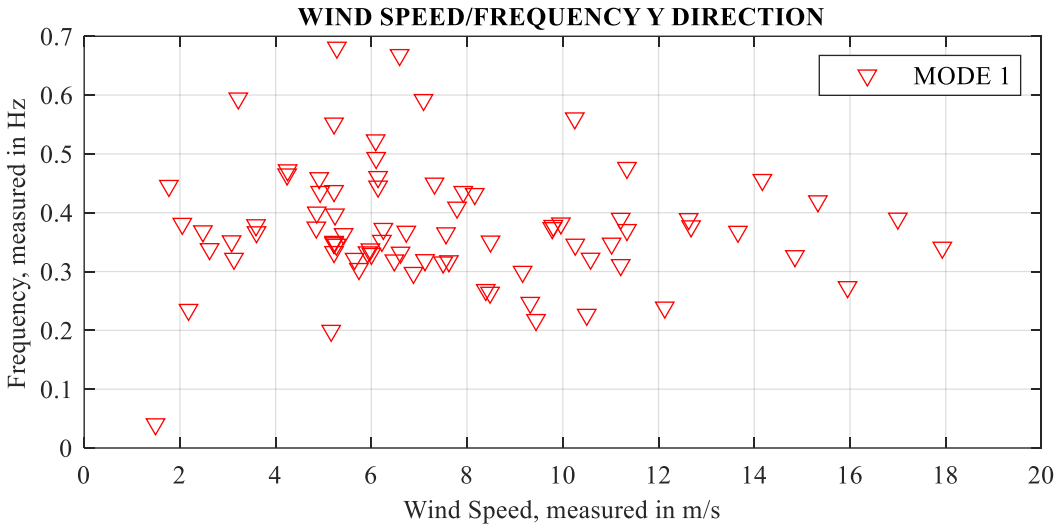
(b)



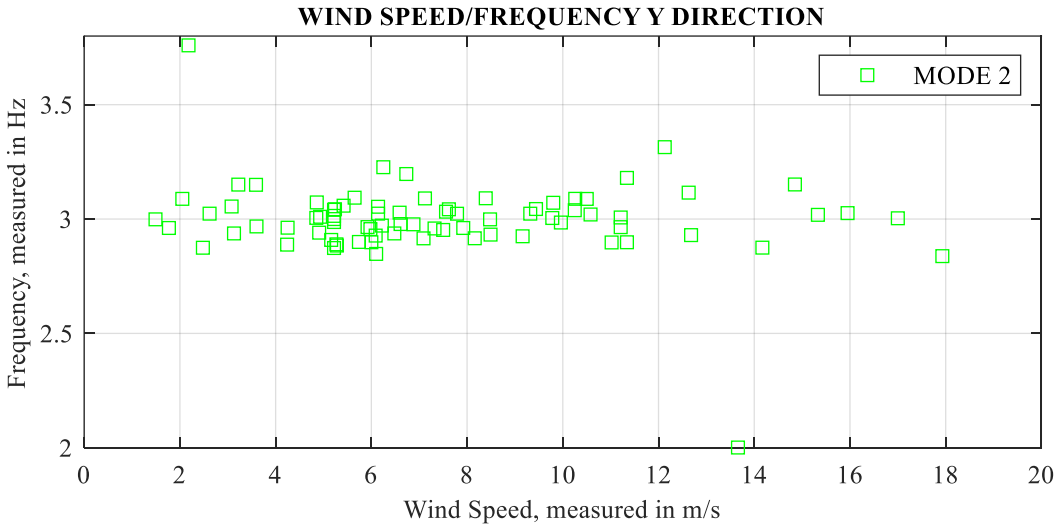
(c)

Figure 5. 9 The values of the first three modes obteined by the p-LSCF method using the x-direction data, corresponding to the frequencies and variable wind speed are shown in (a), (b), and (c) respectively

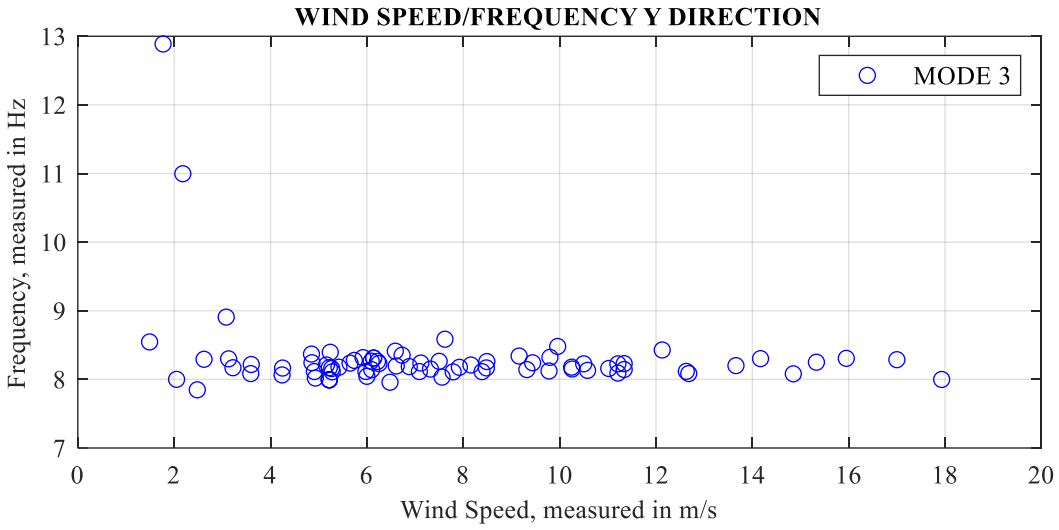
As the frequency values obtained for the x and y directions (given in Table 5.2) are quite close to each other as expected, no significant trend was found in the y direction wind speed-frequency relationship, as in the x direction.


WIND SPEED/FREQUENCY Y DIRECTION
MODE 1
Frequency, measured in Hz
Wind Speed, measured in m/s
0
0.1
0.2
0.3
0.4
0.5
0.6
0.7
0
2
4
6
8
10
12
14
16
18
20

(a)


WIND SPEED/FREQUENCY Y DIRECTION
MODE 2
Frequency, measured in Hz
Wind Speed, measured in m/s
2
2.5
3
3.5
0
2
4
6
8
10
12
14
16
18
20

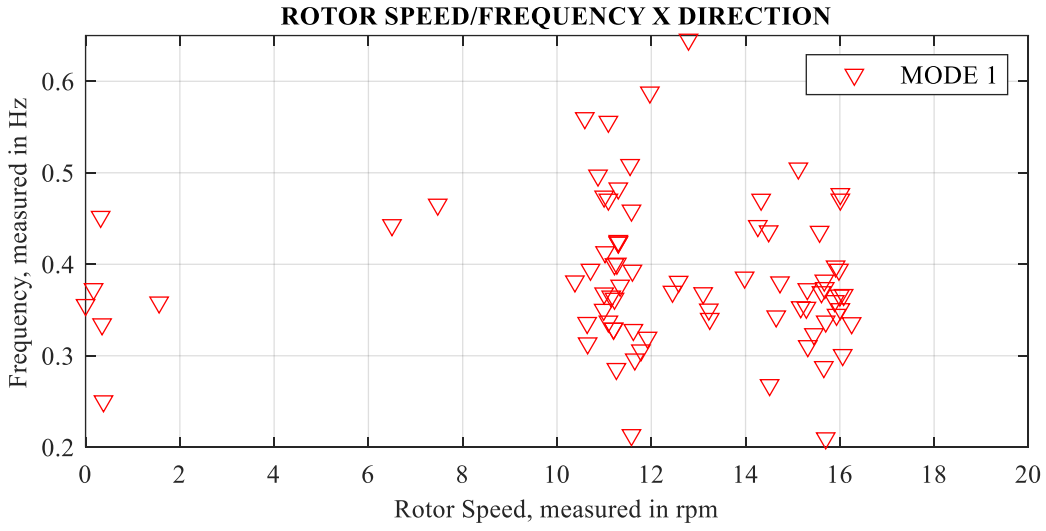
(b)



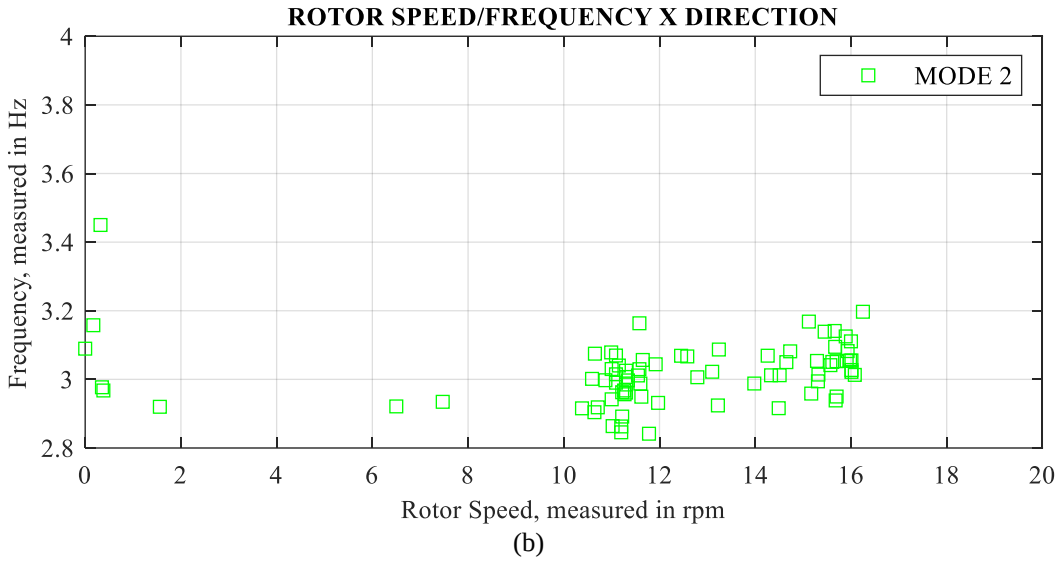
(c)

Figure 5. 10 The values of the first three modes obteined by the p-LSCF method using the y-direction data, corresponding to the frequencies and variable wind speed are shown in (a), (b), and (c) respectively

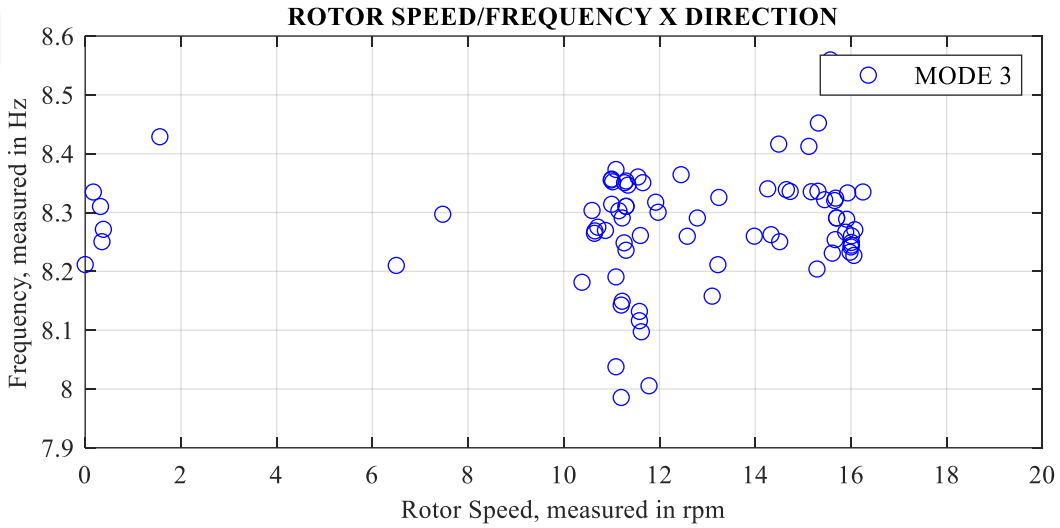
In Figure 5.11, the rotor speed-frequency relationship for the x direction is given. It was observed that the analyzes became more frequent after 10 rpm rotor speed. This can be explained as follows. The investigated wind turbine was designed to produce energy at speeds greater than 10 rpm rotor speed.



(a)



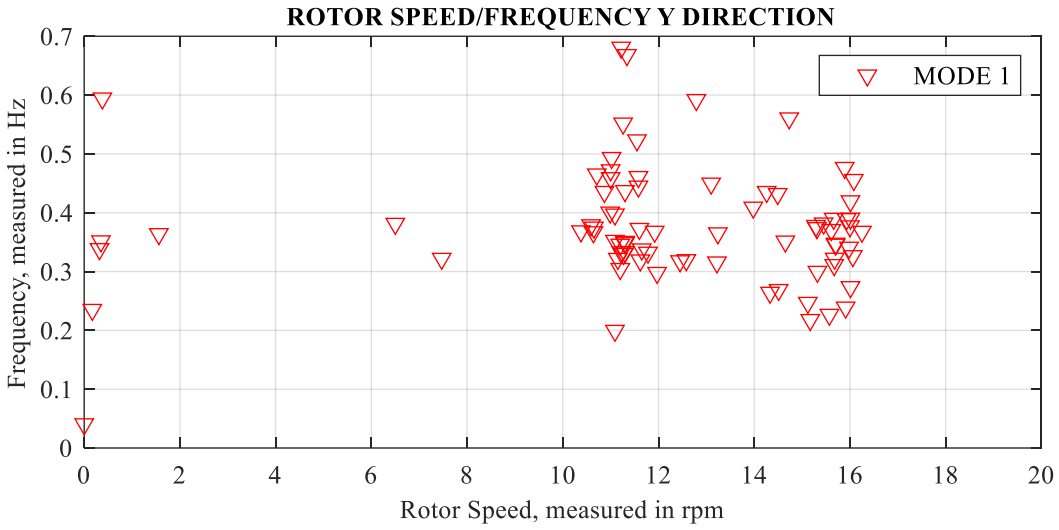
(b)



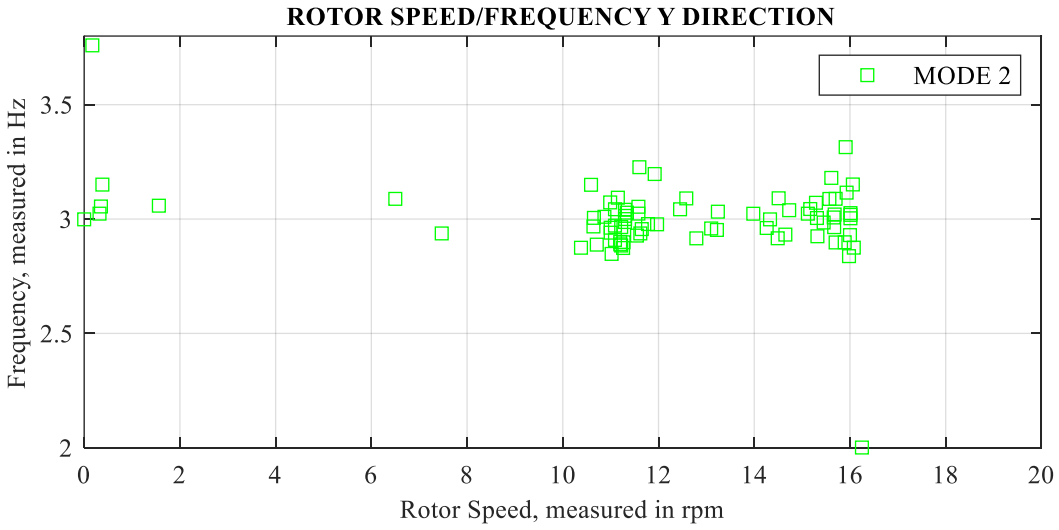
(c)

Figure 5. 11 The values of the first three modes obteined by the p-LSCF method using the x-direction data, corresponding to the frequencies and variable rotor speed are shown in (a), (b), and (c) respectively

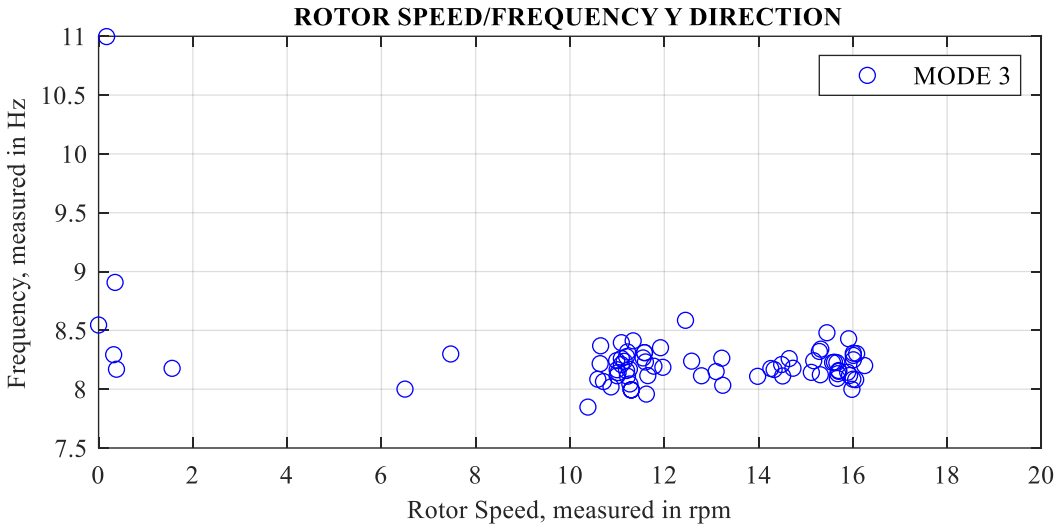
In Figure 5.12, the rotor speed-frequency relationship for the y direction is given. Since the findings for both directions (x and y directions) are quite close, the comments given for the x direction rotor speed-frequency relationship (in Figure 5.11) can be said in the y direction.


ROTOR SPEED/FREQUENCY Y DIRECTION
MODE 1
Frequency, measured in Hz
Rotor Speed, measured in rpm
0
0.1
0.2
0.3
0.4
0.5
0.6
0.7
0
2
4
6
8
10
12
14
16
18
20

(a)


ROTOR SPEED/FREQUENCY Y DIRECTION
MODE 2
Frequency, measured in Hz
Rotor Speed, measured in rpm
2
2.5
3
3.5
0
2
4
6
8
10
12
14
16
18
20

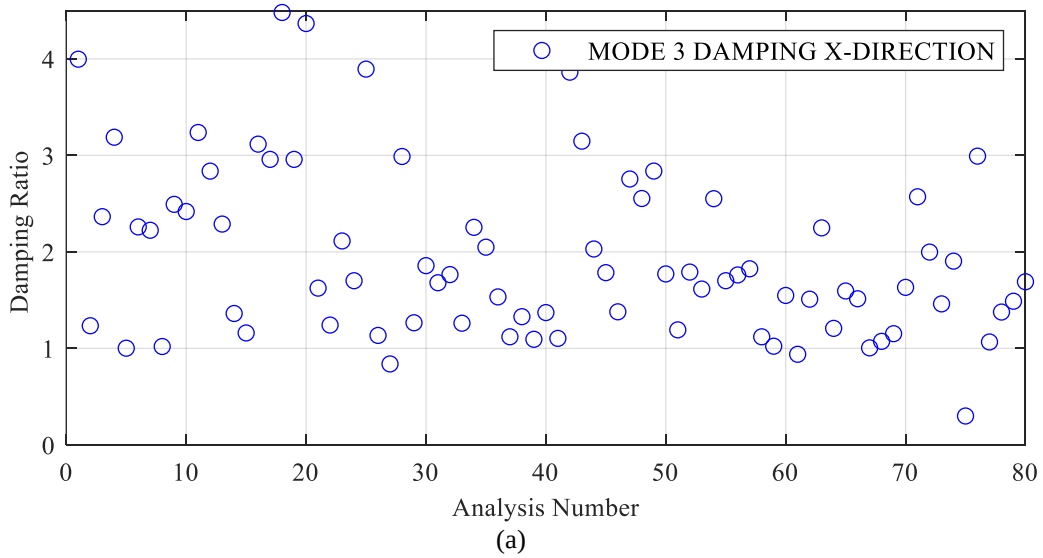
(b)



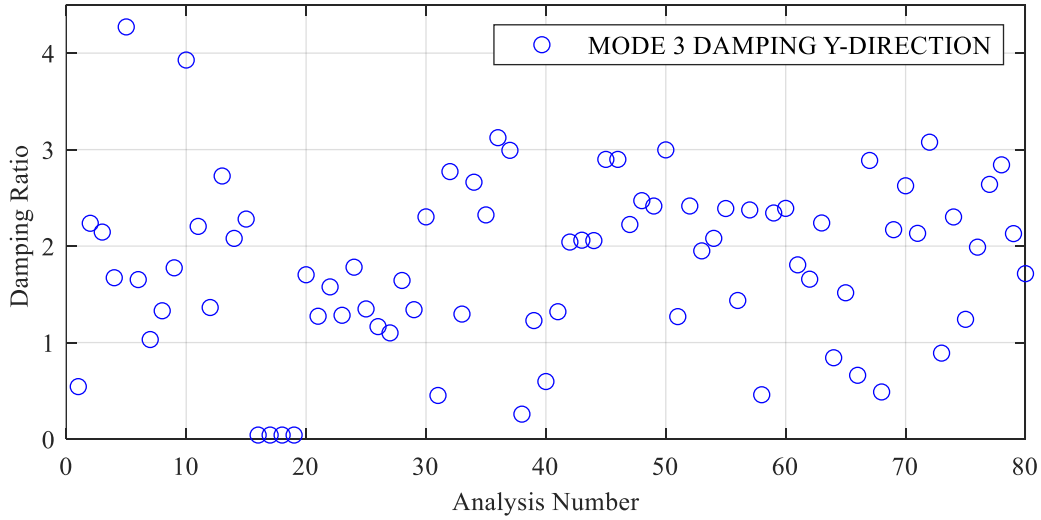
(c)

Figure 5. 12 The values of the first three modes obteined by the p-LSCF method using the y-direction data, corresponding to the frequencies and variable rotor speed are shown in (a), (b), and (c) respectively

In studies carried out under many uncertainties and acceptances, it is very difficult to determine the damping rate, which is one of the modal parameters. In the datasets we used in the MACEC program, which we used to predict modal parameters by p-LSCF method, there were problems in finding the relevant mode damping rates due to filtrations. The damping ratio and the x and y directions for mode 3 are shown in Figure 5.13 (a) and (b).



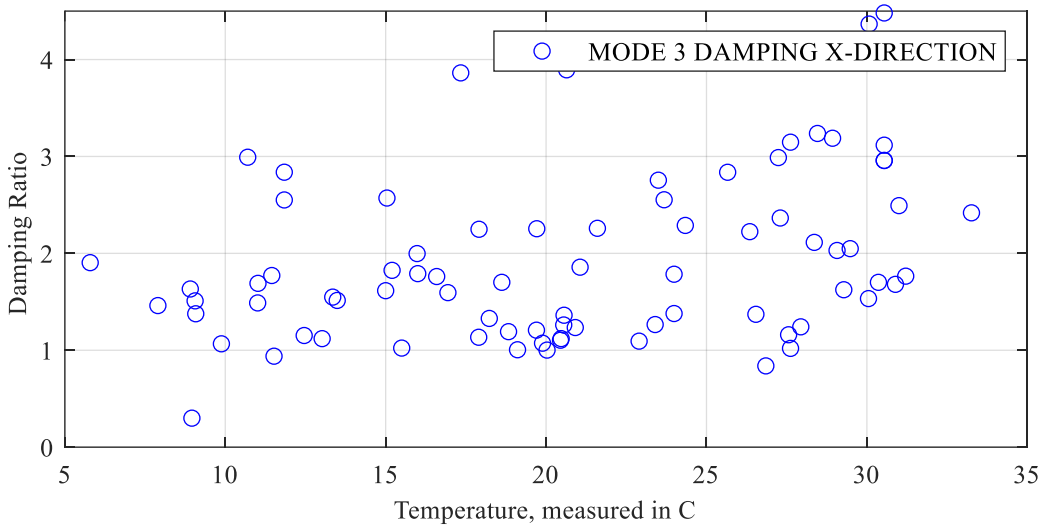
(a)



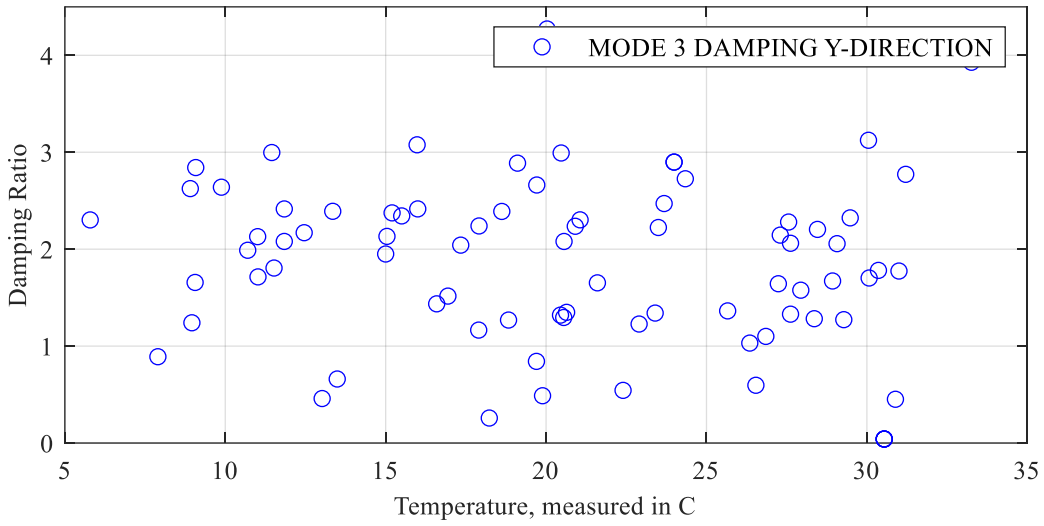
(b)

Figure 5.13 80 analyses for x and y directions respectively (a) and (b), obtained from the damping ratio. The average damping ratio for the x direction was 1.9394 and for the y direction it was 1.8245.

The temperature, humidity, wind speed and rotor speed changes corresponding to the damping rates are given in Figure 5.14, Figure 5.15, Figure 5.16 and Figure 5.17 respectively.

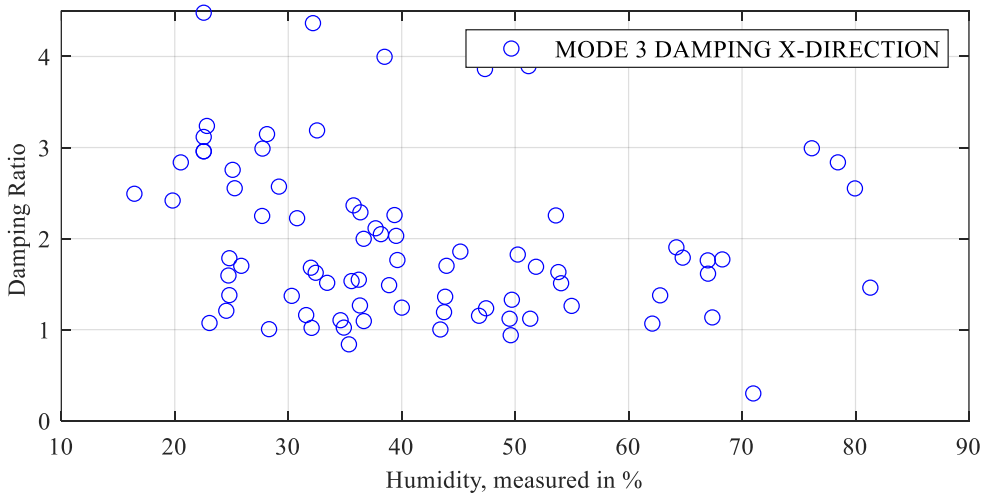


(a)

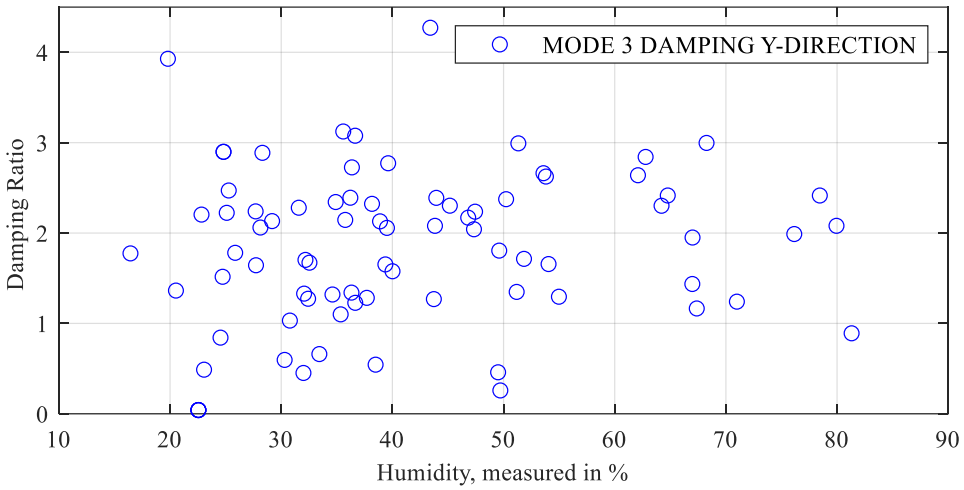


(b)

Figure 5.14 The temperature changes corresponding to the damping rates (a) x direction and (b) y direction

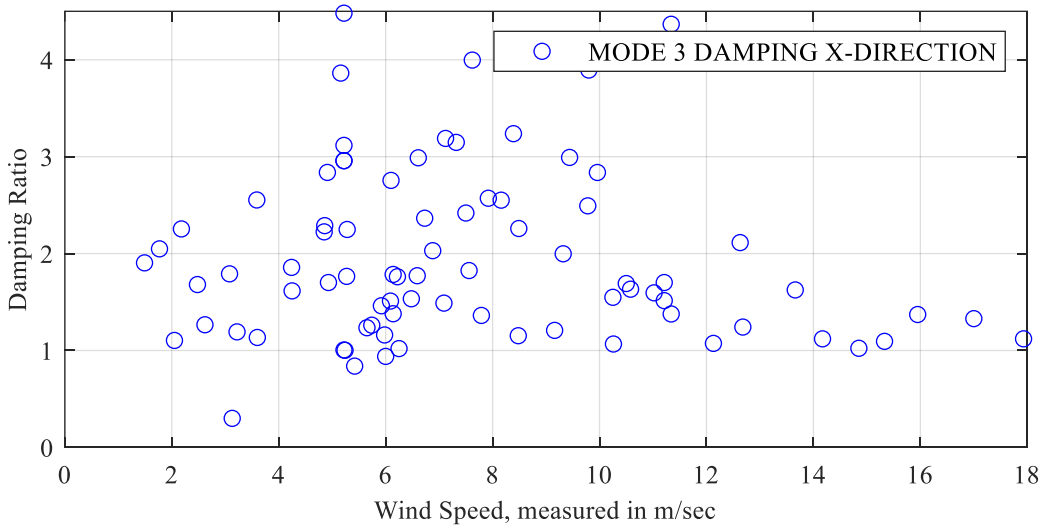


(a)

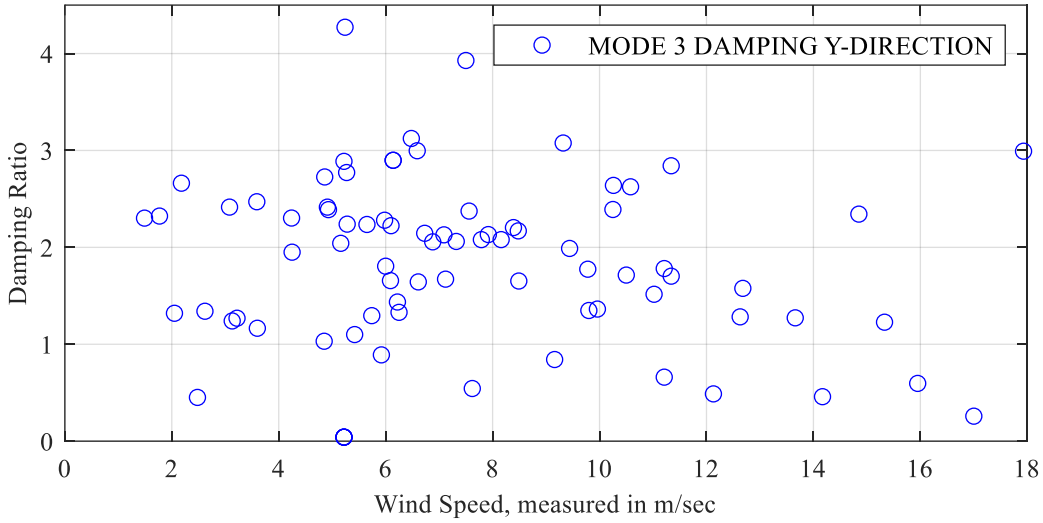


(b)

Figure 5.15 The humidity changes corresponding to the damping rates (a) x direction and (b) y direction

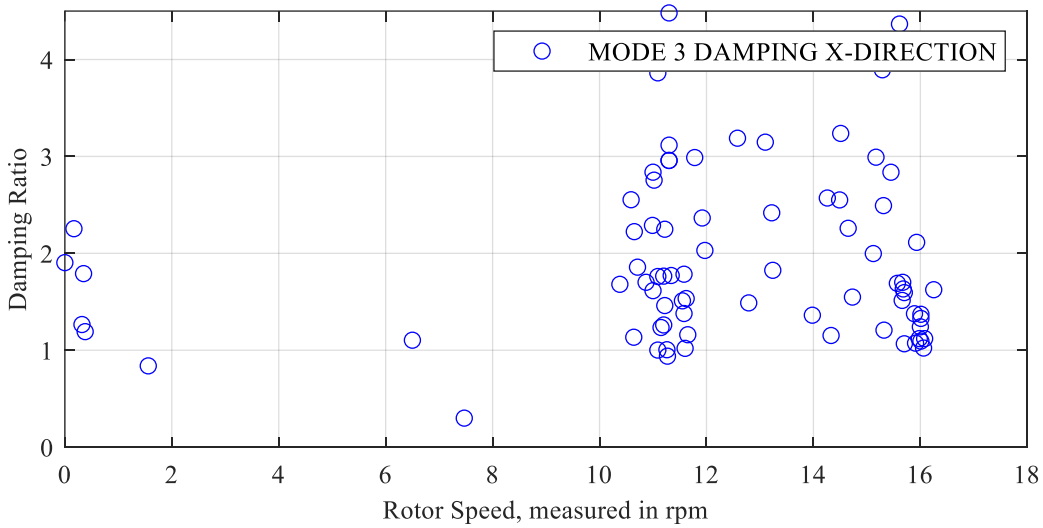


(a)

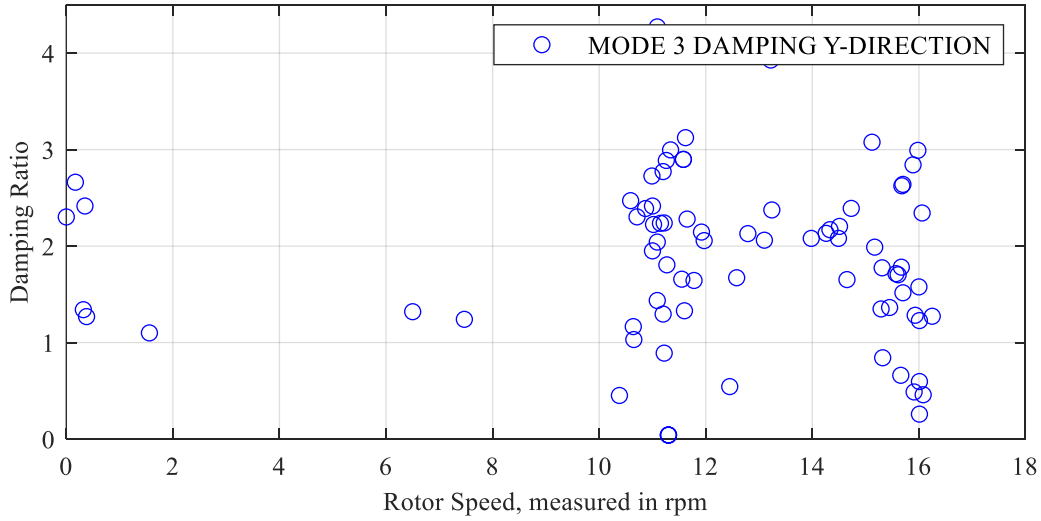


(b)

Figure 5.16 The wind speed changes corresponding to the damping rates (a) x direction and (b) y direction



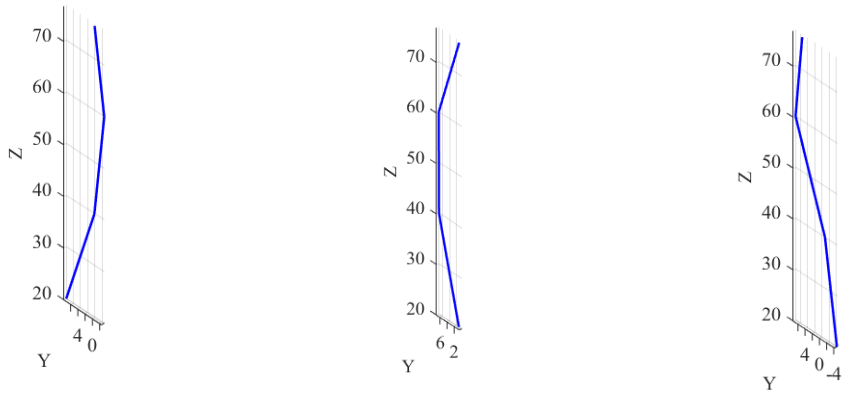
(a)



(b)

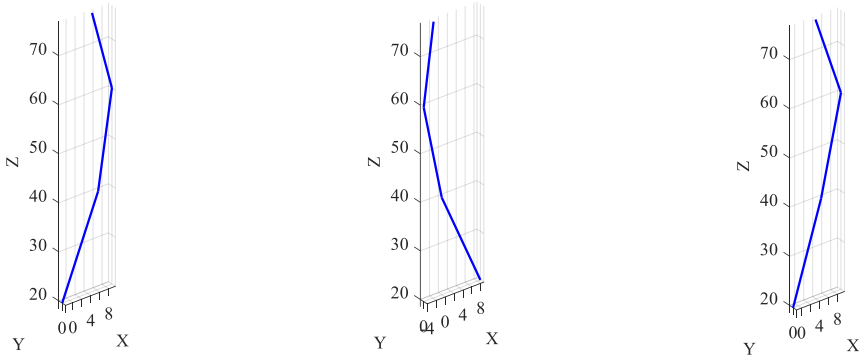
Figure 5.17 The rotor speed changes corresponding to the damping rates (a) x direction and (b) y direction

Another of the modal parameters obtained is the mode shapes. The mode shapes of the first three modes obtained using the data of July 20 and July 25 are shown in Figure 5.13 and Figure 5.14, respectively.



(a) (b) (c)

Figure 5.18 Mode figures for (a) Mode 1, (b) Mode 2 and (c) Mode 3 obtained using data collected at 06:15 pm on October 19, 2022

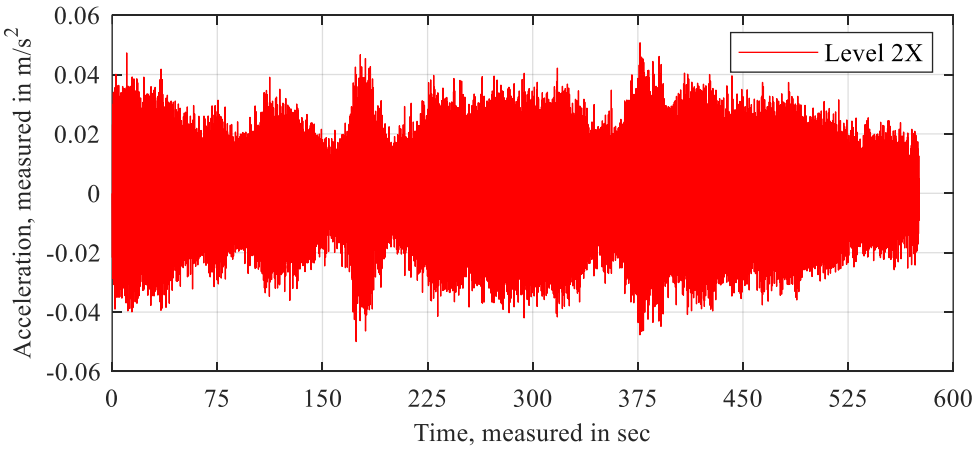


(a) (b) (c)

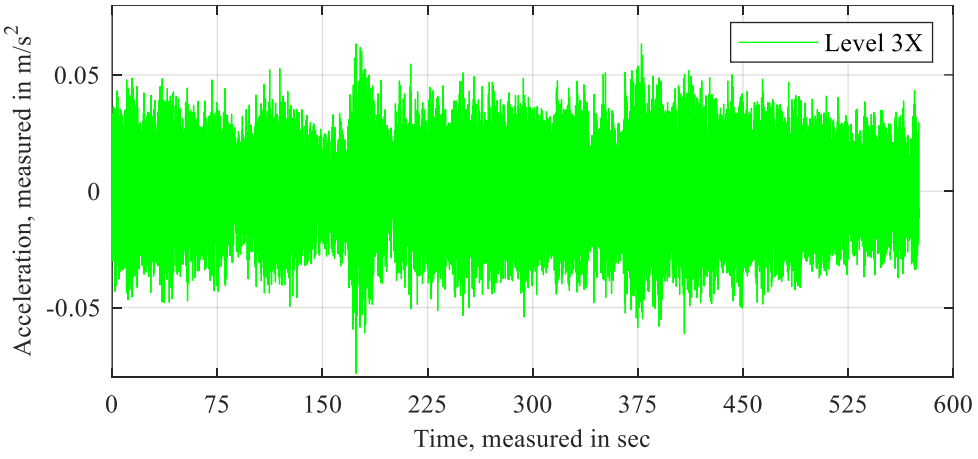
Figure 5.19 Mode figures for (a) Mode 1, (b) Mode 2 and (c) Mode 3 obtained using data collected at 23:50 pm on November 26, 2022

5.3. Damage Scenorios

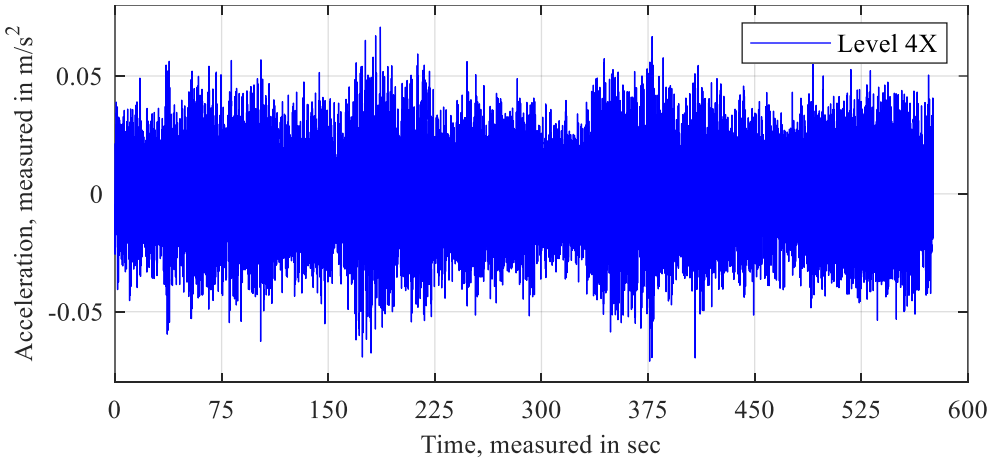
The data collected in different seasons and conditions were processed and frequency values were obtained by p-LSCF method. The data collection system created recorded 2 earthquakes. In Figure 5.15 the records of the 10 October 2022 03:29 am Kusadası Earthquake presented.



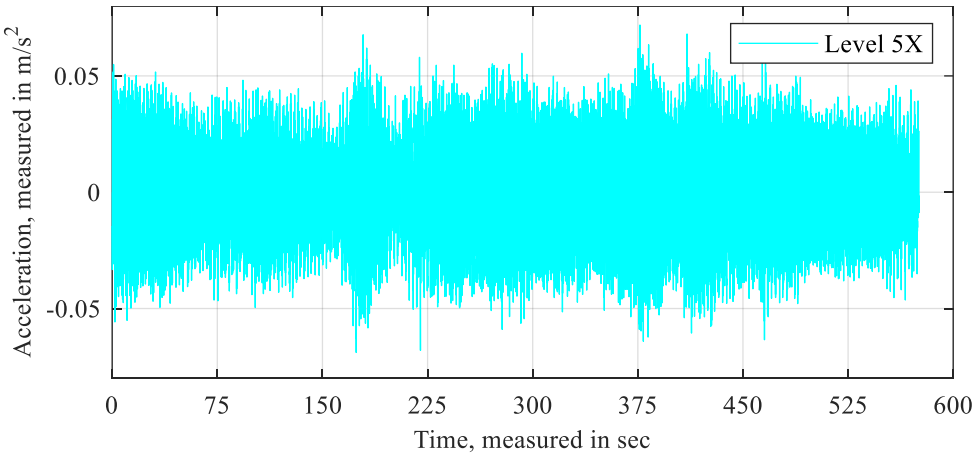
(a)



(b)



(c)

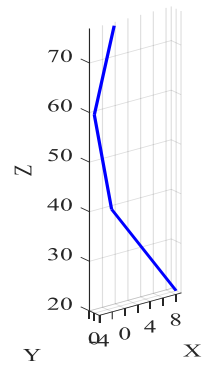
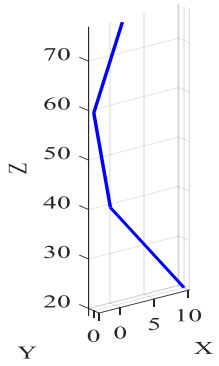
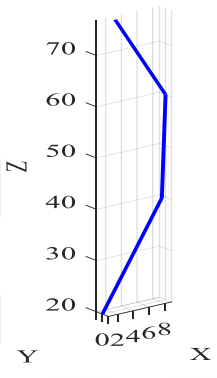
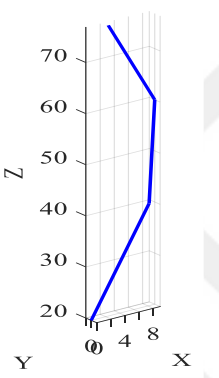
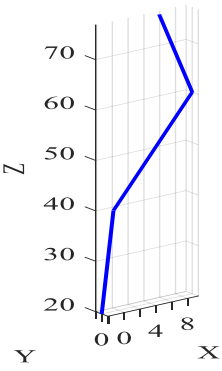
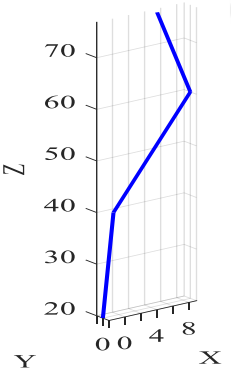


(d)

Figure 5.20 Eartquake record x direction

Before and after the Kusadası Earthquake, two different datasets were analyzed and the mode shapes before and after the earthquake are shown in Table 5.3.

Table 5. 3 Mode shapes obtained using earthquake data

MODES	Earthquake Kusadası	
	Before	After
1. Mode		
2. Mode		
3. Mode		

The records before and after the earthquake were examined and the frequency values shown in Table 5.4 were obtained. As can be understood from the table, it can be said that there is no change when the frequency values before and after the earthquake are taken into consideration.

Table 5. 4 Analysis reasults of earthquakes

Direction	Frequency	Earthquake 1 Kusadası		Earthquake 2 Buca	
		Before	After	Before	After
X	1.mode frequency (Hz)	0.36	0.36	0.35	0.37
	2.mode frequency (Hz)	3.04	3.04	3.06	3.04
	3.mode frequency (Hz)	8.26	8.26	8.27	8.30
Y	1.mode frequency (Hz)	0.34	0.35	0.37	0.37
	2.mode frequency (Hz)	3.06	3.05	3.06	3.06
	3.mode frequency (Hz)	8.27	8.27	8.28	8.27

The absence of a change in frequency values can be associated with the interpretation that there is no damage, and thus it can be interpreted that the earthquakes that occur do not cause any damage to the turbine tower. In addition to these evaluations, visual inspections on site have shown that there is no damage to the turbine tower.

CHAPTER 6
CONCLUSIONS

To estimate the modal characteristics of the wind turbine, 600 seconds of acceleration data sampled at 2048 Hz under environmental and operating conditions were recorded. Data collected from the SCADA system (Rotor speed, nacelle direction, pitch angle, real power, outside temperature values) and data acquisition system (acceleration, humidity and temperature data) were transferred to the workstation located on the campus. Communication and lossless data transfer between turbine-switchyard-campus, a special code was developed for this project using LabVIEW.

It has been observed that the average temperatures between 12.26 and 26.03 degrees Celsius, humidity between 32.11 and 52.49 percent, wind speed between 6.96 and 8.44 m/s and rotor speed between 10.91 and 13.23 rpm during the examined period. Considering these data obtained, it cannot be said that the operational and environmental changes remain in a very wide range. With a 256 Hz sampling rate, the filtered data is cropped to achieve a more manageable file size. A total of 160 analyzes were performed with the p-LSCF method by selecting data with equal day and hour intervals from five different months. As shown in Table 4.1.2, the frequencies of the first three structural modes of the turbine tower were found in the range of 0 to 10 Hz. It is very difficult to determine the damping ratio, which is one of the modal parameters, in studies conducted under many uncertainties and acceptances. In the data sets we used in the MACEC program, which we used to estimate the modal parameters with the p-LSCF method, there were problems in finding the relevant mode damping ratios due to filtrations, therefore, the damping ratio of only the 3rd mode was found to be around 1.5-2 percent.

The frequency and mode shapes of the wind turbine were found by examining two different earthquake records recorded during the observation period. Investigations were made for two cases, before and after the earthquake. When the first three structural frequency values and mode shapes were compared, the values before and

after the earthquake gave similar results. Considering these results, no earthquake-related damage was observed.

Data will be recorded under different environmental and operational conditions and a comprehensive correlation study can be performed to determine their effects on the predicted modal parameters. Within the scope of this study, no direct relationship was observed between the frequency values versus the temperature, humidity, rotor speed and wind speed values obtained using the data collected in the x and y directions.

Long-scale observations, including unusual conditions such as sudden closures, storms, and severe earthquakes that represent operational and environmental conditions, will provide stronger data for understanding the relationship between modal parameters and operational and environmental conditions.

REFERENCES

Allemang, Randall, James De Clerck, Christopher Niezrecki, and Alfred Wicks. 2014. "Topics in Modal Analysis, Volume 7: Proceedings of the 31st IMAC, A Conference on Structural Dynamics, 2013." Conference Proceedings of the Society for Experimental Mechanics Series 45(7). doi: 10.1007/978-1-4614-6585-0.

Bazeos, N., G. D. Hatzigeorgiou, I. D. Hondros, H. Karamaneas, D. L. Karabalis, and D. E. Beskos. 2002. "Static, Seismic and Stability Analyses of a Prototype Wind Turbine Steel Tower." Engineering Structures 24(8):1015–25. doi: 10.1016/S0141-0296(02)00021-4.

Begg, Robert D., Alexander C. Mackenzie, Colin J. Dodds, and Olaf Loland. 1976. "Structural Integrity Monitoring Using Digital Processing Of Vibration Siqnals." Proceedings of the Annual Offshore Technology Conference 1976-May:305–12. doi: 10.4043/2549-MS.

Bendat, J. S., & Piersol, A. G. (2010*). Random data: Analysis and measurement procedures* (4th ed). USA: John Wiley and Sons.

Bogoevska, Simona, Minas Spiridonakos, Eleni Chatzi, Elena Dumova-Jovanoska, and Rudiger Höffer. 2017. "A Data-Driven Diagnostic Framework for Wind Turbine Structures: A Holistic Approach." Sensors (Switzerland) 17(4). doi: 10.3390/s17040720.

Brincker, R., & Zhang, L., & Andersen, P. (2001). Modal identification of output-only systems using frequency domain decomposition. Smart Materials and Structures, 10, 441-445.

Carne, Thomas G., and George H. James. 2010. "The Inception of OMA in the Development of Modal Testing Technology for Wind Turbines." Mechanical Systems and Signal Processing 24(5):1213–26. doi: 10.1016/j.ymssp.2010.03.006.

Chauhan, S., D. Tcherniak, Jon Basurko, Oscar Salgado, Iker Urresti, Carlo E. Carcangiu, and Michele Rossetti. 2011. “Operational Modal Analysis of Operating Wind Turbines: Application to Measured Data.” Conference Proceedings of the Society for Experimental Mechanics Series 5:65–81. doi: 10.1007/978-1-4419-9428-8_6.

Crohas, H., and P. Lepert. 1982. “Damage-Detection Monitoring Method for Offshore Platforms Is Field-Tested.” Oil Gas J.; (United States) 80:8(5):172–75. doi: 10.1115/1.3120328.

Culla, Antonio, Walter D. ’. Ambrogio, Annalisa Fregolent, A Culla, W. D’ambrogio, and A Fregolent. 2012. “Getting a Symmetric Residue Matrix Fromthe Poly-Reference Least Square Complex Frequency Domain Technique Getting a Symmetric Residue Matrix from the Poly-Reference Least Square Complex Frequency Domain Technique.”

Devriendt, Christof, Filipe Magalhães, Wout Weijtjens, Gert De Sitter, Álvaro Cunha, and Patrick Guillaume. 2014. “Structural Health Monitoring of Offshore Wind Turbines Using Automated Operational Modal Analysis.” Structural Health Monitoring 13(6):644–59. doi: 10.1177/1475921714556568.

Guillaume, P., P. Verboven, and S. Vanlanduit. 1998. “Frequency-Domain Maximum Likelihood Identification of Modal Parameters with Confidence Intervals.” Proceedings of the 23rd International Conference on Noise and Vibration Engineering, ISMA 955–62.

Guillaume, Patrick, Peter Verboven, Steve Vanlanduit, Herman Van Der Auweraer, and Bart Peeters. n.d. “A Poly-Reference Implementation of the Least-Squares Complex Frequency-Domain Estimator.” (2).

Hansen, M. H., K. Thomsen, P. Fuglsang, and T. Knudsen. 2006. “Two Methods for Estimating Aeroelastic Damping of Operational Wind Turbine Modes from Experiments.” Wind Energy 9(1–2):179–91. doi: 10.1002/we.187.

Heylen, Ward, Stefan Lammens, and Paul Sas. n.d. “MODAL ANALYSIS THEORY AND TESTING.”

Liu, Caiwei, Jinzhi Wu, and Yigang Zhang. 2011. “Review and Prospect on Modal Parameter Identification of Spatial Lattice Structure Based on Ambient Excitation.” Applied Mechanics and Materials 94–96:1271–77. doi: 10.4028/www.scientific.net/AMM.94-96.1271.

Loland, Olaf, and Colin J. Dodds. 1976. “Experiences in Developing Monitoring Systems and Operating Integrity In the North Sea.” Offshore Technology Conference. doi: 10.4043/2551-MS.

Maes, K., A. Iliopoulos, W. Weijtjens, C. Devriendt, and G. Lombaert. 2016. “Dynamic Strain Estimation for Fatigue Assessment of an Offshore Monopile Wind Turbine Using Fi Ltering and Modal Expansion Algorithms.” Mechanical Systems and Signal Processing 76–77:592–611. doi: 10.1016/j.ymssp.2016.01.004.

Manolakis, G. M., & Ingle, V. K., & Kogon, S. M. (2000). *Statistical and adaptive signal processing*. New York: McGraw Hill.

Manzato, S., B. Peeters, R. Osgood, and M. Luczak. 2010. “Wind Turbine Model Validation by Full-Scale Vibration Test.” European Wind Energy Conference and Exhibition 2010, EWEC 2010 5(December):3710–20.

Moaveni, Babak, Joel P. Conte, and François M. Hemez. 2009. “Uncertainty and Sensitivity Analysis of Damage Identification Results Obtained Using Finite Element Model Updating.” Computer-Aided Civil and Infrastructure Engineering 24(5):320–34. doi: 10.1111/J.1467-8667.2008.00589.X.

Oliveira, Gustavo, Filipe Magalhães, Álvaro Cunha, and Elsa Caetano. 2015. "Automated Modal Tracking and Fatigue Assessment of a Wind Turbine." 5:1–8.

Ozbek, Muammer, and Daniel J. Rixen. 2011. "Optical Measurements and Operational Modal Analysis on a Large Wind Turbine: Lessons Learned." Conference Proceedings of the Society for Experimental Mechanics Series 5(1):257–76. doi: 10.1007/978-1-4419-9428-8_21.

Pandey, A. K., M. Biswas, and M. M. Samman. 1991. "Damage Detection from Changes in Curvature Mode Shapes." Journal of Sound and Vibration 145(2):321–32. doi: 10.1016/0022-460X(91)90595-B.

Peeters, B., and Herman Van der Auweraer. 2005. "PolyMAX: A Revolution in Operational Modal Analysis." Proceedings of the 1st International Operational Modal Analysis Conference, IOMAC 2005 (January 2005).

Peeters, Bart, Herman Van Der Auweraer, Patrick Guillaume, and Jan Leuridan. 2004. "The PolyMAX Frequency-Domain Method: A New Standard for Modal Parameter Estimation?" Shock and Vibration 11(3–4):395–409. doi: 10.1155/2004/523692.

Peeters, Bart, and Guido De Roeck. 1999. "REFERENCE-BASED STOCHASTIC SUBSPACE IDENTIFICATION FOR OUTPUT-ONLY MODAL ANALYSIS." Mechanical Systems and Signal Processing 13(6):855–78. doi: 10.1006/MSSP.1999.1249.

Proulx, Tom. 2015. Structural Health Monitoring and Damage Detection, Volume 7. Vol. 7.

Rackwitz, Rüdiger, and Bernd Flessler. 1978. "Structural Reliability under Combined Random Load Sequences." Computers & Structures 9(5):489–94. doi: 10.1016/0045-7949(78)90046-9.

Rainieri, Carlo, and Giovanni Fabbrocino. 2014. Operational Modal Analysis of Civil Engineering Structures: An Introduction and Guide for Applications.

Reynders, Edwin. 2012. “System Identification Methods for (Operational) Modal Analysis: Review and Comparison.” Archives of Computational Methods in Engineering 19(1):51–124. doi: 10.1007/S11831-012-9069-X/FIGURES/42.

Reynders, Edwin, Daan Degrauwe, Guido De Roeck, Filipe Magalhães, and Elsa Caetano. 2010. “Combined Experimental-Operational Modal Testing of Footbridges.” Journal of Engineering Mechanics 136(6):687–96. doi: 10.1061/(ASCE)EM.1943-7889.0000119.

Reynders, Edwin, Kristof Maes, Geert Lombaert, and Guido De Roeck. 2016. “Uncertainty Quantification in Operational Modal Analysis with Stochastic Subspace Identification: Validation and Applications.” Mechanical Systems and Signal Processing 66–67:13–30. doi: 10.1016/J.YMSSP.2015.04.018.

Reynders, Edwin P. B. 2021. “Uncertainty Quantification in Data-Driven Stochastic Subspace Identification.” Mechanical Systems and Signal Processing 151:107338. doi: 10.1016/J.YMSSP.2020.107338.

Reynders, Edwin, Rik Pintelon, and Guido De Roeck. 2008. “Uncertainty Bounds on Modal Parameters Obtained from Stochastic Subspace Identification.” Mechanical Systems and Signal Processing 22(4):948–69. doi: 10.1016/J.YMSSP.2007.10.009.

Reynders, Edwin, and Guido De Roeck. 2008. “Reference-Based Combined Deterministic–Stochastic Subspace Identification for Experimental and Operational Modal Analysis.” Mechanical Systems and Signal Processing 22(3):617–37. doi: 10.1016/J.YMSSP.2007.09.004.

Stubbs, N., S. Park, C. Sikorsky, S. Choi, N. Stubbsy, S. Parky, C. Sikorskyz, and S. Choiy. 2000. “International Journal of Systems Science A Global Non-Destructive

Damage Assessment Methodology for Civil Engineering Structures A Global Non-Destructive Damage Assessment Methodology for Civil Engineering Structures." International Journal of Systems Science 31(11):1361–73. doi: 10.1080/00207720050197758.

Stubbs, Norris, Taft H. Broome, and Roberto Osegueda. 2012. "Nondestructive Construction Error Detection in Large Space Structures." Https://Doi.Org/10.2514/3.10365 28(1):146–52. doi: 10.2514/3.10365.

Tcherniak, D., S. Chauhan, and M. H. Hansen. 2011. "Applicability Limits of Operational Modal Analysis to Operational Wind Turbines." Conference Proceedings of the Society for Experimental Mechanics Series 1:317–27. doi: 10.1007/978-1-4419-9716-6_29.

Tcherniak, Dmitri, Shashank Chauhan, Michele Rossetti, Iciar Font, Jon Basurko, and Oscar Salgado. 2010. "Output-Only Modal Analysis on Operating Wind Turbines: Application to Simulated Data." European Wind Energy Conference and Exhibition 2010, EWEC 2010 5(April):3550–60.

Vandiver, J. Kim. 1975. "Detection of Structural Failure on Fixed Platforms By Measurement of Dynamic Response." Proceedings of the Annual Offshore Technology Conference 1975-May:243–51. doi: 10.4043/2267-MS.

Wind, G. L. 2010. "GL Guidelines-2010." Guidelines & Rules.

Zhang, Lingmi, Rune Brincker, and Palle Andersen. 2005. "An Overview of Operational Modal Analysis: Major Development and Issues." Proceedings of the 1st International Operational Modal Analysis Conference, IOMAC 2005.